INSTITUTO TECNONÓLOGICO Y DE ESTUDIOS
SUPERIORES DE MONTERREY

Campus Estado de México
School of Engineering and Sciences

Search for high-molecular weight linear polymers for the formulation of novel solutions for the fabrication of micro fibers by electromechanical spinning

A thesis presented by:
Antonio Osamu Katagiri Tanaka

Submitted to the
School of Engineering and Sciences
in partial fulfillment of the requirements for the degree of

Master of Science

in

Nanotechnology

Estado de México, Atizapan de Zaragoza, December 02, 2020

"Carbon is a simple element but .....

one branch of chemistry is devoted to its compounds!

... one branch of science is devoted to the many forms of the element as a solid material.

The best of this is that although most carbon materials are grey or black to the naked eye and the uninitiated. A closer examination reveals the form, beauty and even color of carbon science."

Marsh, Harry
Universitat d'Alacant, Alicante, Spain
scopus.com

Dedication

To my parents, who believed in me no matter the outcome. Mom, dad, this work is possible because of you, for always telling me to believe in my dreams.

Thanks for all your unconditional confidence, support, patience, and encouragement. You were my main motivation for pushing through this work.

Acknowledgements

There are a number of people without whom this thesis might not have been written, and to whom I am greatly indebted.

I offer my gratitude and appreciation to my supervisors, Dr. Héctor Alán Aguirre Soto and Dra. Dora Iliana Medina Medina, for the deft ways in which you fondly challenged and supported me through out the whole of this work - knowing when to push and when to let up. I offer special thanks to those who supported me in the mechanics of producing this thesis. Dr. Héctor Alán Aguirre Soto, for reading and rereading drafts, editing and proofing, typing and helping me get 'unstuck' with this thesis on many occasions. And Braulio and Arnoldo for 'rescuing' me at those times when I was almost defeated by the laboratory equipment.

I would also like to acknowledge the support from Tecnológico de Monterrey and CONACyT (tuiton and living expenses). I also thank Regina Elizabeth Vargas from CIDyT, for the countless hours she helped me with sample characterization.

Finally, I would like to thank my family, who always believed in me. I am grateful for their love, caring and patience even in the hardest and restless days. They always encourage me to following my dreams, and that feeling will always be dear to me.

Search for high-molecular weight linear polymers for the formulation of novel solutions for the fabrication of micro fibers by electromechanical spinning

by Antonio Osamu Katagiri Tanaka

Abstract

Carbon nano-wires are versatile structures composed of carbon chains with a wide range of applications due to their high chemical resistance and electric properties. Regardless of the high interest in the implementation of carbon nano-wires in energy, environmental and health-care applications, no feasible processes have been developed to fabricate carbon nano-wires with spatial control at a reasonable cost. Carbon nano-wires have been fabricated with the use of a photoresist, but little is known about polymers that can produce conductive carbon nano-wires after pyrolysis. Various polymer solutions have been tested in near field electrospinning (NFES) and photopolymerization separately, however, few have been tested for nano-wire fabrication purposes through the process of spatio-temporal deposition with NFES, photo-polymerization for cross-linking and pyrolysis. The intention behind the thesis proposal is to use rheological analyses of different polymer solutions to determine if they can be easily electrospun at low voltages and then fabricate nano-wires with them. This thesis work arises from the need to test a greater variety of polymer-solvent combinations with the goal of designing a polymer solution to fabricate carbon nano-wires with higher conductivity than the current SU-8 polymeric nano-fibers. The present work includes the design of polymer solutions that can be electrospun, with the hope that the selected high molecular weight polymers can be photo-polymerized, and then pyrolyzed into conducting carbon nanowires. The overarching goal is to contribute towards the development of novel designed polymer solutions to achieve mass scale manufacturing of conductive carbon nano-wires in an inexpensive, continuous, simple and reproducible manner as central components for nano-sensors.

keywords: nanotechnology, carbon, nano-wires, Near-Field Electrospinning, NFES

List of Figures

List of Tables

Contents

Chapter 1

Introduction

Carbon nano-materials are subjected of great interest for research purposes due to their various potential applications in diverse areas that take advantage of the nano-scale properties. Carbon nano-materials are suitable for catalysis, adsorption, carbon capture, energy and hydrogen storage, drug delivery, bio-sensing, and cancer detection. [1, 2] Some matchless properties that allow carbon nano-materials to be utilized within multiple functionalities include high porosity, distinguished structures, uniform morphologies, high stability, high magnetic properties, and high conductivity. [3–10]

This document bestows a thesis project to perform research to engineer a polymer solution to contribute towards the long-term goal of achieving mass scale manufacturing of high conductive glass-like carbon nano-wires with a control of the jet diameter in an inexpensive, continuous, simple and reproducible manner. This thesis discusses several manufacturing processes such as near field electrospinning, photo-polymerization, pyrolization, and carbonization, as they have shown to be promising methods for the fabrication of carbon nano-materials. [11] See Figure 1.1. A number of processes have been developed for specific purposes of polymeric nano-fibres, some include surface deposition, composites, and chemical adjustments. Polymeric nano-fibers must be also pyrolyzed to generate carbon nano-wires with conductive capabilities [12] for electrochemical sensing and energy storage purposes.

Nanotechnology has led to the study of different polymer patterning techniques to integrate carbon nano-wires structures. One technique is known as far-field electrospinning (FFES), a process in which electrified jets

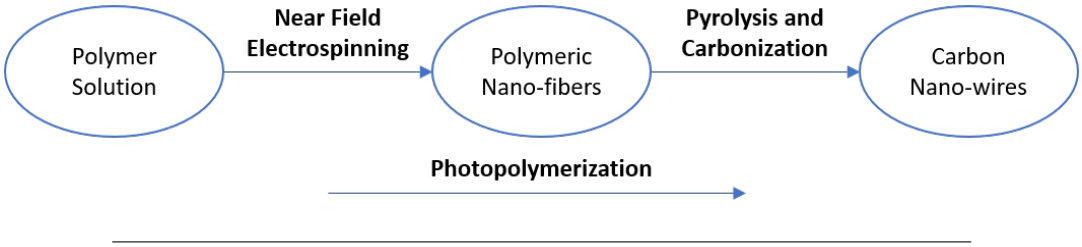

FIGURE 1.1: Fabrication process and characterization techniques of conductive carbon nano-wires to achieve through the dissertation.

of polymer solution are dispensed to synthesize nano-fibres which can then be pyrolyzed. One sub-technique derived from electrospinning is near-field electromechanical spinning or NFEMS. Unlike FFES, NFEMS has proved to deliver sufficient spatial control for patterning polymeric nano-fibres. [11]

The present work was proposed to continue the work done by others [11, 13] in regards to the synthesis of carbon nano-wires. Previous work includes the fabrication of suspended carbon nano-wires by two methods: electro-mechanical spinning and two-photon polymerization with a photoresist. [11, 13] This work is intended to focus on electro-mechanical spinning processes only, to bring off polymer solutions that can be electrospun by NFEMS to yield polymer fibers than can hopefully be crosslinked by UV light and the pyrolyzed and pyrolyzed into conducting carbon nano-wires. The polymer solutions described by Cárdenas and Flores [11, 13] were used as benchmarks and starting points for the present studies.

Traditional near-field electrospinning or NFES allows large-scale manufacturing combined with spatial control of material deposition. [12] However, the reported efforts required the use of electric fields in excess of 200 kV/m for continuous operation, this seems to contradict the previous sentence. [12] concluded that the state-of-the-art fabrication processes for polymer nano-fibers are still lacking in terms of precision, cost, speed and throughput.

1.1 Carbon Nanowires Research Developments in Terms of Published Papers, Synthesis and Fabrication

Nanotechnology's ability to control and piece together materials at the nano-scale has enabled the development of various carbon nano-materials and carbon nano-structures, such as nano-dots, nano-fibres, nano-tubes

and nano-wires. [14–17] This section focuses on the applications at the micro-scale and nano-scale levels, as well as the current research of carbon-based nano-materials (CBNs).

1.1.1 Carbon and carbon-based nanomaterials

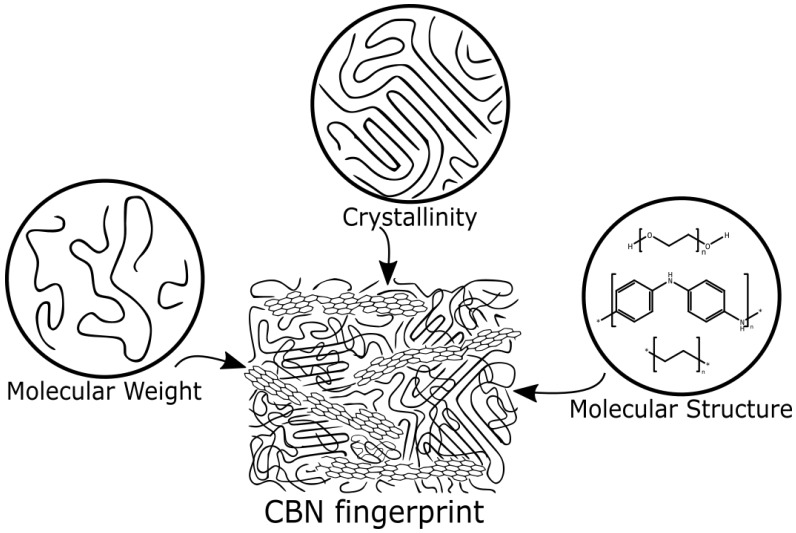

FIGURE 1.2: Molecular to meso-scale structural features of synthetic polymers influence the emergence of specific micro-structural features in polymer-derived carbon materials after pyrolysis.

Carbon is a versatile element capable of forming a number of bonds with other elements or with itself. Cabon-based nano-materials (CBNs) exist in diverse forms, depending on the precise values of each degree of freedom that specify the material properties at multiple scales. Hybridization, crystallization, percolation, anisotropy, porosity, impurities and imperfections are some of the relevant features that determine the CBN set of properties. The combination of these features at the micro- and meso-scale burst a variety of macro-scale properties that comprise the CBN fingerprint (1.2). The interminable collection of possible CBN fingerprints range from soft, conductive lubricants to very hard, low conductivity solids [18]; and from black colour, bulks to transparent, disordered thin films. [3] Figures 1.3 and 1.4 show the existence of different allotropes based on carbon orbitals which have the ability to hybridize in sp1, sp2 and sp3 configurations, assembling different carbon allotropes.

In terms of porosity, CBNs exhibit different properties according to the degree of 'open' and 'closed' pores. A 'closed pore' is a void or empty space in solid materials where a discontinuity is present within the array of atoms and molecules. On the other hand, an 'open pore' refers to a void which is

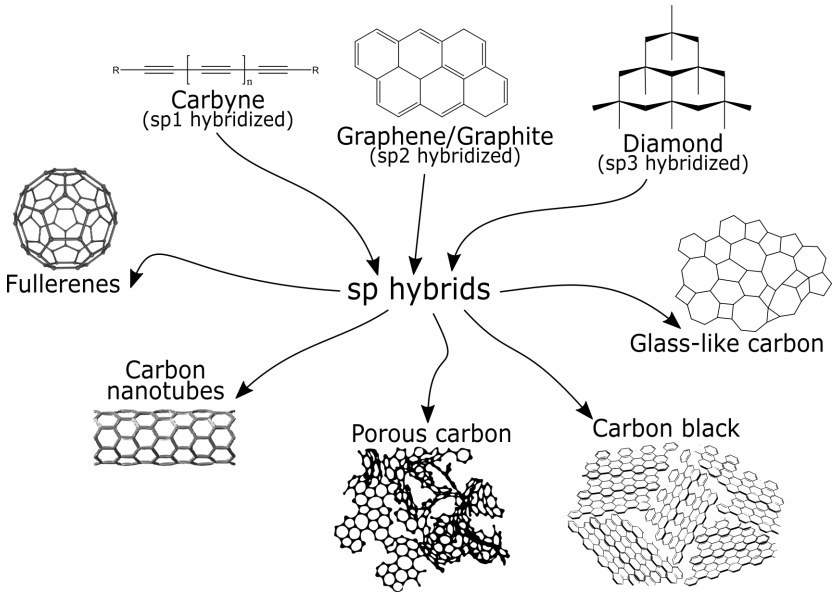

FIGURE 1.3: Three carbon allotropes (diamond, carbyne and graphene) are the building blocks of additional deriving carbon-based materials such as fullerenes, porous carbon and glass-like carbon.

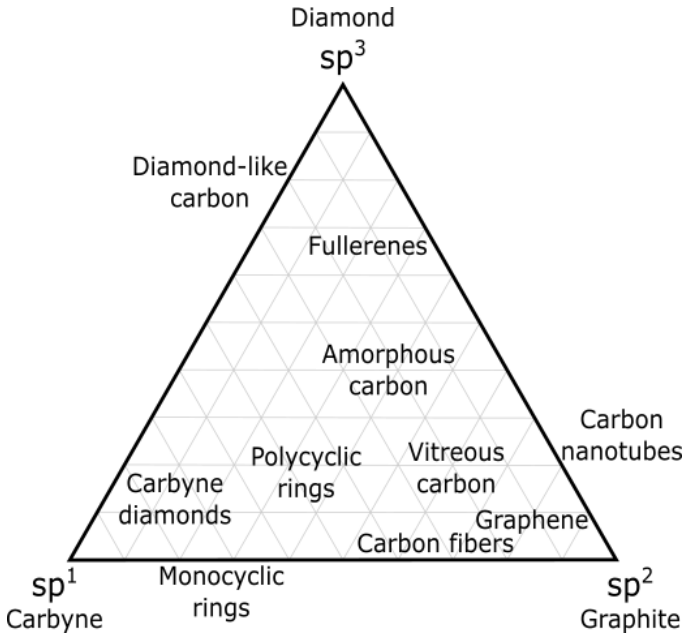

FIGURE 1.4: Ternary phase diagram of amorphous carbon regions based on hybridization degree. Adapted from [19–25].

connected to the outer surface of the solid, in other words a 'open pore' is a 'closed pore' with an opening to the external surface. [26] Figure 1.5 shows a classification of carbon allotropes according to their porosity.

Thermal conductivity and electrical conductivity decrease with increasing

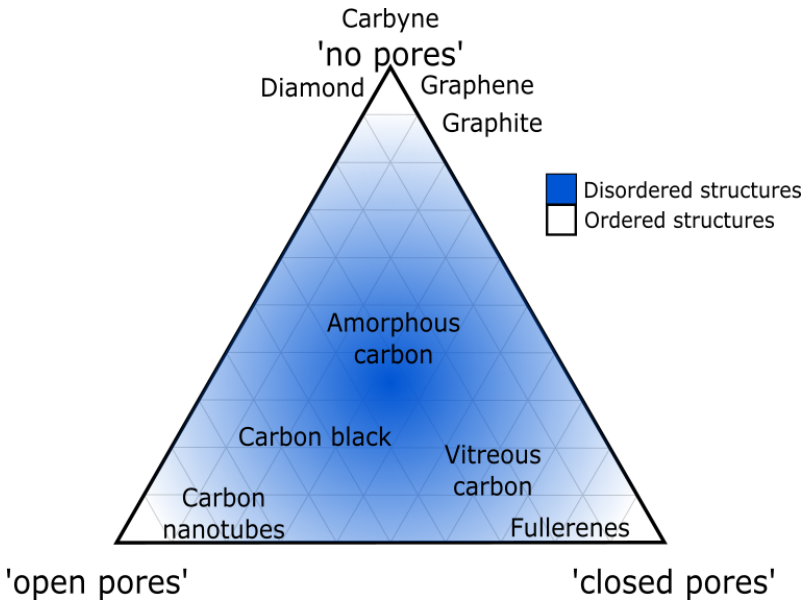

FIGURE 1.5: Ternary phase diagram of amorphous carbon regions based on structure order and porosity. Regions are colored by the degree of crystalline order within the carbon structure. White represents highly ordered structures, whereas white represents disordered structures. [18, 26]

porosity due to the reduced amount of material to conduct electrons and energy. Furthermore, porosity negatively affects the mechanical properties like strength and elastic modulus as it reduces the volume in which stresses are distributed. [18] Moreover, stresses are concentrated at the pores which makes the material prone to mechanical failure. [18, 26]

Due to the versatility and variety of CBNs, CBNs have been fabricated and implemented for various purposes. [4, 6–10]. For instance, field effect transistors (FET) have been studied by Novoselov [27] and Heersche et. al. [19]. Carbon FET devices have reported field-effect mobility one order of magnitude higher than that of silicon FETs. Other literature suggests CBNs to be favorable to detect a variety of gases and bio-molecules. [28, 29] As molecules are absorbed by the CBN, the carrier density and electrical resistivity of the carbon material changes. Moreover, CBNs have showed good performance in applications in energy (prevent wastage of energy), water (purification) and diagnostics (lab-on-chip systems and nano-sensors). [17, 30] As mentioned above, the morphology of CBNs has an impact on the electrochemical and mechanical properties. [18, 26, 31] In this regard, carbon nano-structures, such as nano-wires [32, 33], have been fabricated to achieve improved electrochemical characteristics.

1.1.2 Carbon Nano-wires

As depicted in Figure 1.4, carbon nano-wires (CNFs) have been classified as linear, sp2-rich structures. [19–25] Nano-fibers own good electrical, optical and mechanical characteristics, however those properties are highly dependent on the morphology of the fibers. [34] The material properties of 1D nano-structures depend on fiber diameter, porosity, crystallinity degree and crystallite orientation. Consequently, the fabrication parameters and environment conditions have an impact on the reproducibility of high quality fibers. [34] Carbon nano-fibers (CNFs) have diameters of several micrometers (Figure 1.8) and are different from carbon nano-tubes (CNT). [35–39] Unlike carbon nano-tubes with hollow cores, carbon nano-fibers can be represented as stacked layers along the thread length. [39–41] The stacked geometry of carbon nano-fibers results in unique electrical, chemical and mechanical properties. [42–44] Unlike CNFs, carbon nano-tubes inherent problems such as high cost and low effective surface area, which limit their practical use. [25]

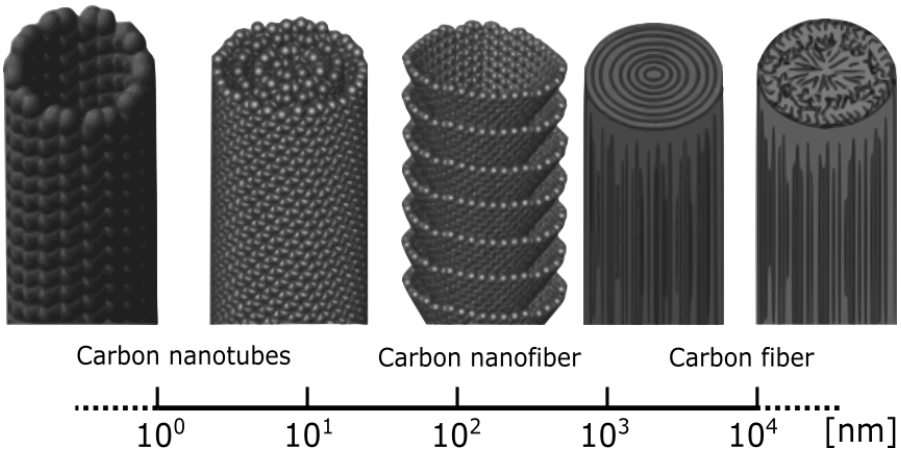

FIGURE 1.6: Various types of fibrous carbon materials bear different characteristics according to their molecular structure. Adapted from [25]

Carbon nano-wires have been used for the improvement of power density and specific energy in lithium-ion batteries. [45–47] Authors posit that the performance and capacity of Li-ion batteries depend on the CNF structure and texture. Through the right combination of electrospinning and carbonization parameters, electrically conductive, mechanically tough and low diameter fibers have been achieved by Yoon et al. [41]. Yoon reported 431 mili-ampere-hour per gram batteries with vitreous carbon nanofibers. Yoon states that the battery capacity highly depends on the

pyrolysis process parameters as the morphology of the fiber develops pores and hence different surface properties. CNFs supercapacitors have been investigated as energy storage devices due to their high power bearability and long lifecycles. [48–51] The studies' authors posit that carbon nano-fibers can be implemented as high-power supercapacitors due to their large surface area and high electrical conductivity.

On the other hand, the low reactivity and unique morphology of CNFs make them promising catalyst supports for metal nano-particles. [52–54] It is well known that the morphology and nano-structure of the supporting material are the main factors that prevent agglomeration of nano-particles. [55, 56] Moreover, in bone tissue scaffold applications, collagen is the most popular scaffold. However, collagen scaffolds bring xenogenicity issues which leads to disease transfer or immunogenic reactions, besides its inhability to preserve its shape once placed in the body. [57–64] Currently, carbon fibers have been studied for bone tissue scaffold, however early attempts yield too thick fibers for cell cultivation and tissue regeneration. [65, 66] As depicted in previous research of CNFs for different applications, fiber morphology seems to have a significant impact on their performance.

Typically, carbon nano-fibers (CNFs) are synthesized by a combination of a patterning process and a pyrolysis process. Electrospun CNFs have characteristics such as high surface area, thin morphology with nano-scale diameters. The properties of electrospun fibers allow CNFs to be implemented in nano-sensing devices, energy storage applications, and tissue scafflods. [30, 67–72] Several patterning techniques have been attempted to achieve the desired fiber morphology. In addition to electrospinning, CNFs have been also fabricated by two-photon polymerization (TPP) and photo-lithography techniques. [73] Cardenas et al. implemented TPP and conventional UV lithography to study the fabrication of CNFs within carbon micro-electromechanical systems (C-MEMS). The fabrication of these kind of carbon devices has been previously reported for techniques, such as electrospinning and photoresist patterning by photolithography using SU-8. The typical fabrication process of C-MEMS begins with a spin-coating of a photoresist unto a substrate (typically SU-8), followed by patterning techniques with UV-exposure by photolithography. Followed by the development of the desired features. Finally, the device is carbonized in a pyrolysis furnace in an inert environment. [74]

Near-field electrospinning can be regarded as a complementary technique, by which polymeric nanofibers can be produced, since the structural geometries created by photolithography are restricted by the diffraction limit. [74, 75] SU-8 is designed to produce vitrous carbon structure via photolithography, it is not design for electrospinning procedures as it lacks the right viscosity and solution conductivity. Cardenas [11] and Flores [13] have adapted the SU-8 formulation by the addition of tetrabutylammonium tetrafluoroborate (TBF) and poly(ethylene oxide) (PEO). TBF was added to increase the solution conductivity and PEO provides the required viscosity. Both additives are required to yield smooth solution flow during electrospinning. Figure 1.7 illustrates the ingredients that comprise the SU-8 formulation.

TABLE 1.1: Polymer Solutions from Previous Work [11, 13]

Sample	**Concentration** $wt\%$		
	SU-8	**PEO**	**TBF**
1	99.25	0.25	0.50
2	99.00	0.50	0.50
3	98.75	0.75	0.50
4	98.50	1.00	0.50

The thinnest fibers fabricated by Cardenas [11] were achieved with sample 1 of Table 1.1, with the following characteristics: a) Fiber yield rate of 81%; b) Fiber diameter before pyrolysis of $4.966\mu m$; c) Fiber diameter after pyrolysis of $204nm$; d) Average fiber length of $60.54.3\mu m$; and e) Fiber electrical resistance from $407K\Omega$ to $1.727M\Omega$. Cardenas results have areas of opportunity regarding the fiber yield rate and the high variability on the fiber electrical resistance. These undesirable characteristics could be a consequence of the addition of PEO to the solution. SU-8 based vitreous carbon is obtained after a pyrolysis process in which the oxygen already present in the SU-8 formulation allows the formation of close pores during annealing. However, the further addition of oxygen content present in the PEO molecules may be the cause of the low yield rate and high variability in electric resistivity from sample to sample.

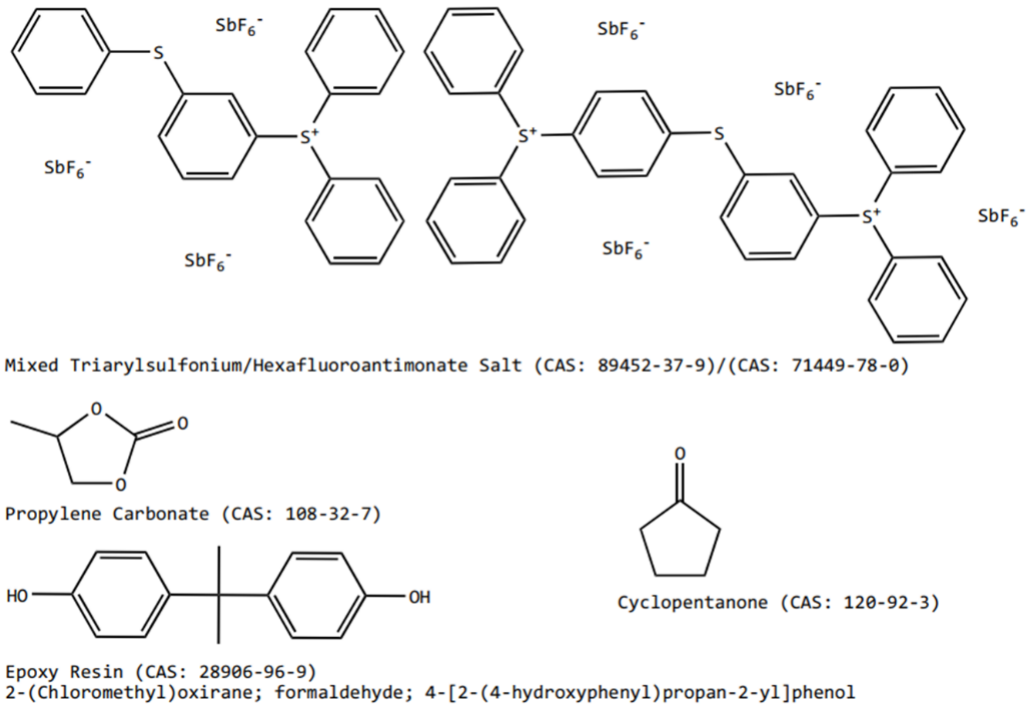

FIGURE 1.7: Components of SU-8 2000 Series Resists. Adapted from [76]

1.2 Problem definition and motivation

The role of carbon nano-wires in nano-sensor devices play an important role, as portable instruments require light-weight and small-sized components. [30] Table 1.2 lists some advantages of nano-sensors that can be accomplished by the fabrication of CNFs via near-field electrospinning and a thermal treatment in an inert environment.

TABLE 1.2: Advantages of Nano-sensors. Adapted from [30]

Advantage	**Description**
High sensitivity	More accuracy, single molecule detection
Small size	Light-weight, portability, low-power consumption, small sample size, reduced sample preparation, and ease of use
Low response time	High-frequency, real time analysis
Low cost	Disposable devices

Sensors of small size require less time to output a stable signal as signals require less time to travel shorter lengths, hence signal noise is also reduced. Nano-sized sensors allow data collection and measurements to be performed in real time at faster speeds. [30] The nano-scale also allows sensors to

increase the active surface area, enabling the absorption and detection of analytes at low concentrations. [30] Conventional sensors are bulky and require higher amounts of power to operate. In gas sensing, neither a large sensing surface or a large sample is required to get a readable output signal from the sensor. Power consumption can be saved by reducing the thermal mass of the sensor. [30] Furthermore, if several gases are to be detected, an array of several gas sensors are to be assembled into an array. A multi-gas sensor array can increase the size and cost, whereas an array of gas nano-sensors (each functionalized to detect a specific analyte) can be implemented into a single device. [30] Nano-sensors can be classified by the kind of energy or physical phenomena that is detected, as depicted in Table 1.3 for instance: biological, mechanical, thermal, chemical, and optical sensors. [2, 30]

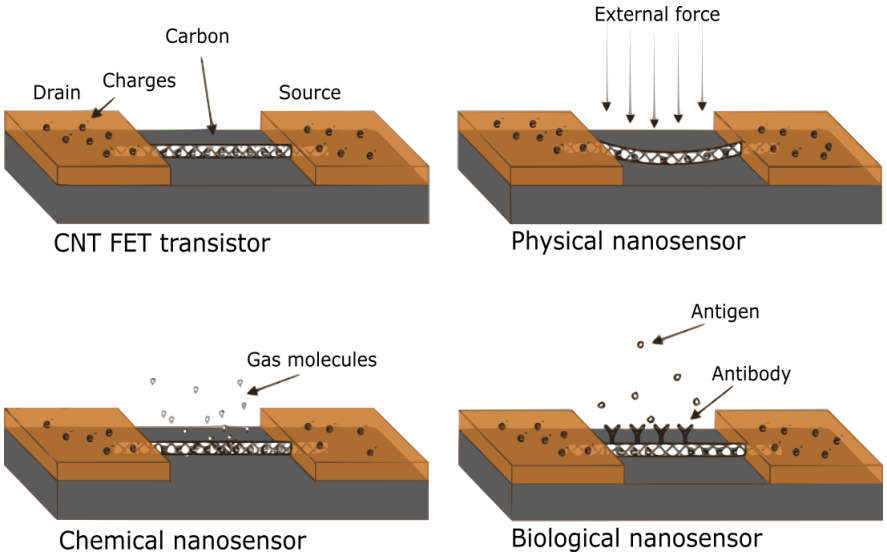

FIGURE 1.8: Diagram examples of carbon-based nano-sensors. Adapted from [2]

Carbon nanowires have been fabricated with a photoresist by two-photon polymerization techniques. However little is known about polymers that can produce conductive carbon nano-wires after pyrolysis, as it is generally believed that most polymers do not form significant amounts of graphitic carbon when carbonized. In the past, photopolymerization processes have been applied to the fabrication of nano-structures with the use of an epoxy based photoresist. [77] Photopolymerization techniques deliver patterning resolutions with nano-scale tolerances through two-photon lithography for the production of highly detailed structures [78].

TABLE 1.3: Classification of Nano-sensors. Adapted from [30]

Classification	**Phenomena / Energy**
Mechanical	Position, acceleration, stress, strain, force, pressure, mass, density, viscosity, moment, torque
Acoustic	Wave amplitude, phase, polarization, velocity
Optical	Absorbance, reflectance, fluorescence, luminescence, refractive index, light scattering
Thermal	Temperature, flux, thermal conductivity, specific heat
Electrical	Charge, current, potential, dielectric constant, conductivity
Magnetic	Magnetic field, flux, permeability
Chemical	Components (identities, concentrations, states)
Biological	Biomass (identities, concentrations, states)

On the other hand, electrospinning has been classified as a process with promising results at nano-structure fabrication [77], yet there is little research regarding the implementation of electrospinning for the fabrication of carbon nano-wires. Electrospinning has the potential to be a more straightforward process for the design and fabrication of nano-structures, as it can achieve mass scale manufacturing in a continuous, simple and reproducible manner. Cardenas [11] showed that electrospinning can be implemented with ease for carbon nano-wire fabrication. Mechano-electrospinning, a new variant of electrospinning shows promising results in the production of ordered carbon nano-wires. As stated in [11], mechano-electrospinning is a recent technology invention and brings new challenges, such as the reproducibility of carbon nano-wire production. Furthermore, the study of a new fabrication process to produce carbon nano-wires that involves mechano-electrospinning will enable spatial control of the fiber deposition.

Since electrospinning seems to be a better alternative for carbon nano-wire fabrication processes; and for that purpose of its implementation, it is required to develop polymer solutions that can be mechano-electrospun, photopolymerized and pyrolyzed into conducting carbon nano-wires. Most applications of carbon-based materials are not currently feasible due to the lack of a continuous, simple and reproducible fabrication method with inexpensive processes. With the newly designed polymer solution, it would be possible to produce carbon nano-wires in large quantities, and therefore more applications will become feasible. On the other hand, the

new technique will overcome some limitations of other methods such as lithography. For instance, patterns created by lithography processes cannot be originated, only replicated, all constituent points of the pattern can only be addressed at the same time, and the process requires the pattern to be encoded into a mask. [79]

1.3 Hypothesis

The viscoelastic properties of polymer solutions along with synthesis parameters can be controlled through rheological analyses to obtain low voltage electrospun-able, photopolymerizable and graphitizable solutions for the fabrication conductive of carbon nano-wires. The viscoelastic properties of polymer solutions along with synthesis parameters can be modified by replacing the PEO (Poly(ethylene) oxide) component within the existing polymer solutions described in Flores [13] and Cardenas [11] work. PEO is to be replaced as its only purpose is to allow the electrospinning process to take place, but no benefit is obtained from it after pyrolysis. The hypothesis is that oxygen-less polymers will yield carbon nano-wires of better quality than those made from PEO blends, therefore the study is to verify the eletrospinnability of high carbon content oxygen-less polymers in solution.

1.4 Research Questions

- Is there any evidence of conductive carbon nano-wire fabrication though electrospun-able and pyrozable polymer solutions?
- What are the process parameters to consider/control for the fabrication processes of carbon nano-wires?
- What viscoelastic properties are to be controlled/tested to deliver an electrospun-able and pyrozable polymer solution?
- What are the optimal fabrication parameters for the synthesis of carbon nano-wires through near-field electromechanical spinning?
- What materials can be used to ease the electrospinning process and favor the carbon nano-wire properties after pyrolysis?

1.5 Objectives

1.5.1 General objective

Formulate polymer solutions by selection of linear high-molecular weight polymers and solvents and then match their viscoelastic properties to those of the benchmark SU-8/PEO solution to select the polymer/solvent combinations that have the greatest protential to replace or modify the SU-8/PEO formulation for the fabrication of microscopic polymer fibers that may be converted to conductive suspended carbon nano-wires.

1.5.2 Specific objectives

- Propose polymer solutions that can be electrospun by Near-Field Electrospinning.
- Through rheological analyses, determine if polymer solutions can have comparative viscoelastic properties to those of the SU-8/PEO benchmark.
- Learn how the diameter of the electrospun polymer fiber can be controlled by appropriate tuning of the NFES parameters and solution properties.
- Propose alternatives to the SU-8/PEO benchmark formulation for the production of microscopic polymer fibers with potential for the fabrication of carbon nano-wires.

1.6 Dissertation Outline

The dissertation is organized as follows. Chapter 1, an introduction to carbon-based nanomaterials is presented. The applications and characteristics of carbon structures are listed with an emphasis on carbon nano-wires. Chapter 2 is comprised by a review of the electrospinning process. The process parameters such as process variables, ambient parameters and solution properties and their influence in fibers formation are studied. Data collection of near-field electrospinning publications was done to execute an adimensional analysis to describe and predict the fiber diameterfrom the process parameters. Chapter 3 focuses on the selection of candidate polymer-solvent combinations to replace the

PEO-SU-8 formulation. Rheological tests (frequency sweeps) were done to study the visoelasticity of polymer solutions. Chapter 3 estimates the optimal polymer concentrations to fabricate continuous fibers through NFES. Chapter 4 presents the fabrication of polymeric fibers. The near-filed process parameters, materials and methods are discussed, where a replicate of experiments of PEO solutions from literature is used as an experimental control. The last chapter shows the results of the fiber characterization of different sets of polymer solutions, though an optical microscope. Finally, the conclusions of this work and the considerations to future works are presented.

Chapter 2

Near-Field Electrospinning as an Affordable Way to Gain Spatial Control

2.1 Review of Polymer Solutions for NFES with Spatial Control

Near-field electrospinning (NFES) is identified to be a technique able to fabricate polymer nano and micro fibers with accurate placement. [80] In the past years (2006-2020) [11–13, 81–159], several polymer solutions have been successfully electrospun into fibers through several variants of the conventional NFES process. Each NFES variant intended to tailor the process parameters in order to improve the fibers' properties.

Near-field electrospinning (NFES) is known as a versatile nano-fabrication technique, suitable for several applications such as tissue engineering, chemical sensing, filtration, energy storage, besides others (see Figure 2.1). Fast developments in electrospinning has been observed in recent years. However, this process is limited by the electric field wiping instability effects during polymer deposition. This leads to a major challenge: how to surpass this limitation of planar two-dimensional prints. The current trend in this area lies on the research of new materials, techniques to increase precision patterning in NFES systems.

Even though electrospinning is an old invention [160], it is currently a trending topic among researchers [161–163]. One of the reasons electrospinning is to be studied is its potential to fabricate polymer nano fibers from a variety of polymers. The technique allows the production of thin continuous fibers with ease, with micro and sub-micrometer diameters,

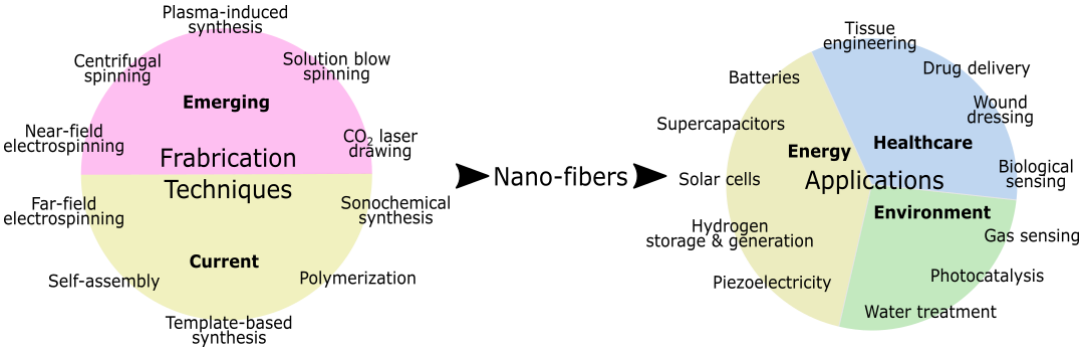

FIGURE 2.1: Syntheses and Applications of Nanofibers. Adapted from [1]

which is something difficult to achieve by other techniques. Furthermore, the basic setup can be modified with ease to fabricate different fibers with diversified functionalities from different materials. The produced fibers can be aligned or unaligned. Besides, the electrospinning equipment is inexpensive and of small size, compared to the equipment of standard spinning techniques [164]. On the other hand, the understanding of the electrospinning process has improved in the last years.

Current literature dictates the typical spinning setup is comprised by three main components: a polymer reservoir, a fiber collector, and some way to dispense the fibers onto the collector. The spinning process is an electro-hydrodynamic (EHD) technique that yields continuous polymer fibers. Other EHD techniques are spraying and atomization which produce polymer droplets and polymer particles respectively, seeFigure 2.2.

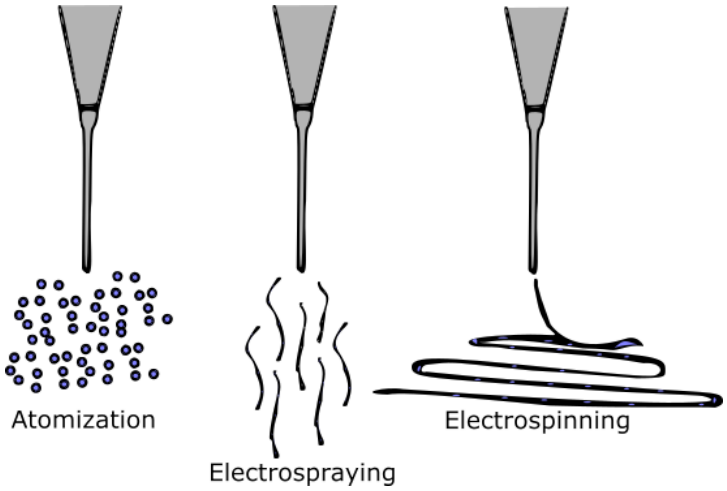

FIGURE 2.2: Electrohydro-dynamic techniques

2.1.1 Stretching forces

Electric Field

Electrospinning (electrostatic fiber spinning) is a fiber fabrication approach that implements an electric field to produce fibers by applying an electrical potential difference between the syringe needle and the collector. With the influence of high electric fields, the fibers are prone to brake into separate layers due to the whipping instabilities as the jet travels to the substrate. The instability can be mitigated by adding additional ring electrodes between the spinneret and the grounded collector. [165]

The typical electrospinning setup applies an electrostatic charge to the polymer fluid at the tip of the needle nozzle, which results in the formation of the Taylor cone [166], from which a single polymer jet is ejected to the grounded collector. From the Taylor cone, the supplied polymer jet (typically a polymer solution) accelerates and reduces in diameter. The fiber finally develops upon complete solvent evaporation. Electrospun fibers are prone to splitting with the increase in acceleration due to high applied voltages, where multiple fibers are produced in a process known as electrospraying [167].

The electrospinning process starts with charging a polymer solution droplet. When a polymer solution is administrated with a syringe pump, solution droplets will fall under the influence of gravity. The solution dripping stops when the electric field is strong enough to break the solution's surface tension, causing the droplet to change shape forming a jet [168].

Shin et al. [169] reported that the growth of the whipping instability is one important element within the electrospinning technique. As detailed in Shin's work, weak electric fields produce a single uniformly thinning jet, and at strong electric fields the jet becomes unstable after traveling a short distance.

High voltage power supply: DC & AC - Direct current (DC) is typically used in electrospinning with the electrons flowing in one direction. Alternate current (AC) implementations are also studied as the AC creates a change in the direction of the current flow. Kessick et al. [170] demonstrated the implementation of AC power supplies in the production of polymer fibers.

The AC electrospinning setup is similar to that for the DC variant. AC

electrospinning apparatus do not require a grounded collector as the current alternates. In AC, the produced fibers are prone to carry an electric charge, while those generated shortly after have an opposite charge. The difference in charges lead the fibers to discharge on each other, creating an aerogel plume of fibers [171]. The optimal AC frequency depends on the materials used and is typically within $50Hz$ and $1kHz$ [172].

The AC technique has been studied for drug loaded related applications. Balogh et al. [173] compared fibers fabricated by DC and AC spinning techniques. Their work reports that AC and DC electrospinning can produce fibers with all three polymers, where the AC process allowed the implementation of faster flow rates than in the DC setup. The DC electrospinning technique generated fibers with a maximum flow rate of 5 ml/h; on the other hand, the AC setup allowed an increase in flow rate up to 40 ml/h.

Centrifugal force

The spinning processes require the implementation of a force to break the polymer source into a polymer jet. Centrifugal spinning intends to produce fibers by the use of a rotating polymer source. The centrifugal force generated from typical rotatory speeds above 2000 rpm, results in fiber formation. [174, 175].

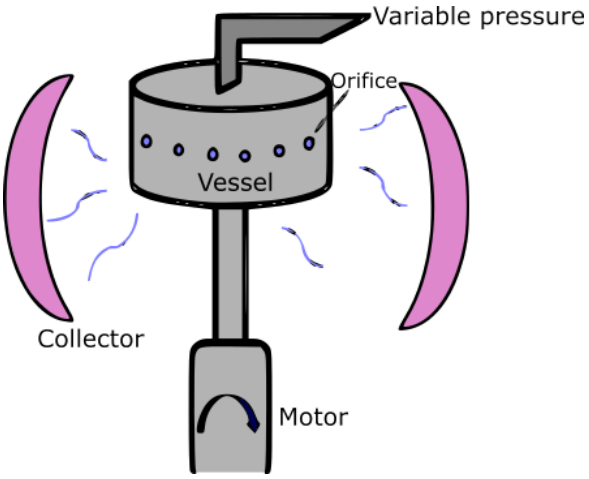

FIGURE 2.3: Typical setup used in pressurized gyration processes

The centrifugal force technique has been applied to polymer solutions and melts. This approach is used in applications were the precise deposition of the fibers is not relevant and production rate is to be maximized [176]. Efforts in centrifugal spinning are focused on drug delivery applications.

Zander [177] fabricated polycaprolactone (PCL) fibers using the solution and melt variants of the centrifugal approach. Zander's fibers were produced with rotatory speed between 3000 and 18000 rpm obtaining $10\mu m$ diameters.

On the other hand, PCL and PVP fibers were generated by Amalorpava et al. [178]. Amalorpava achieved sub micron/size fiber diameters for drug release purposes and bacteria growth inhibition properties. Literature [179] has shown that centrifugal approach has a simple setup that promises a large scale fabrication of fibers.

In some cases the centrifugal force implementations and pressurized gyration can be combined with an electric field. The implementation of two stretching forces (centrifugal and electrical forces), can help solvent evaporation [180]. Centrifugal electrospinning implements the same setup as the standard centrifugal spinning with the addition of a high voltage power supply between the rotating dispensing nozzle and the collector. The combined method has been proven to yield parallel fibers [181–184] at a higher rate [181, 182] than the standard electrospinning approach.

Blowing forces

Nano-fibers can be produced with the implementation of pressurized gas with a polymer solution. The setup used for blow spinning is similar to the one used in coaxial electrospinning, where the polymer precursor is dispensed at a controlled rate. Unlike traditional electrospinning, in the solution blow spinning setup the needle nozzle applies pressurized gas to the polymer solution through an outer spinneret [185], see Figure 2.4.

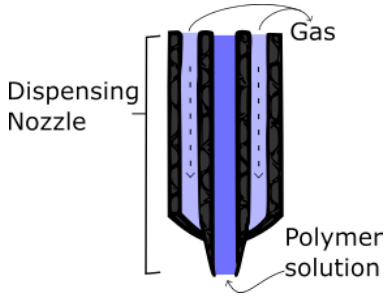

FIGURE 2.4: Dispensing nozzle used for solution blow spinning or melt blowing. [185]

Poly(lactic acid) (PLA) fibers have been produced by solution blow spinning. Oliveira et al. [186] fabricated fibers from $6wt\%$ PLA solutions with progesterone for live stock reproductive cycle regulation applications.

On the other hand, Souza et al. [185] conducted a study to compare the standard electrospinning and the solution blow spinning techniques. Poly(3-hydroxybutyrate-co-3-hydroxyvalerate) were fabricated by both methods. The fibers produced by traditional electrospinning had thicker diameters and the size uniformity was higher in the fibers produced by solution blow spinning. The experimental setup requires a coaxial needle nozzle with a pressurized gas flow along with a potential difference between the dispensing needle and the grounded collector.

Mechanical force

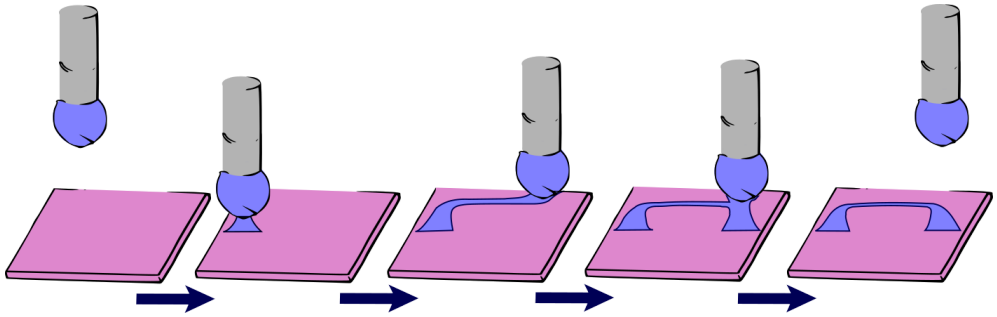

FIGURE 2.5: Typical mechanical fiber drawing process

Mechanical drawing comprises the simple technique to produce fibers by stretching the polymer solution with a glass pipette. [187] Nevertheless, the drawing technique is not scalable or with practical complications. [188] Touch-spinning methods have been developed to introduce a scalable technique for the production of nano fibers where the fiber is created by stretching the polymer precursor with a moving collector, as depicted in Figure 2.5. Touch-spinning is another mechanical technique that comprises a moving stage with an embedded glass rod (Figure 2.6), where a polymer solution is supplied from a syringe needle such that the tip of the glass rod makes contact with the polymer solution as it rotates, creating fibers. The rotation stretches the fiber, causing the fiber to increase in length and decrease in diameter. The increase in length causes the fiber surface are to increase and therefore making the polymer solution solvent to volatilize, ending with a dry fiber within the collector.

The touch spinning technique implies that the fiber diameter can be controlled by the moving collector's speed and the polymer solution concentration. The main difference lies on the fact that the touch spinning method implements mechanical control to manipulate and stretch the fibers

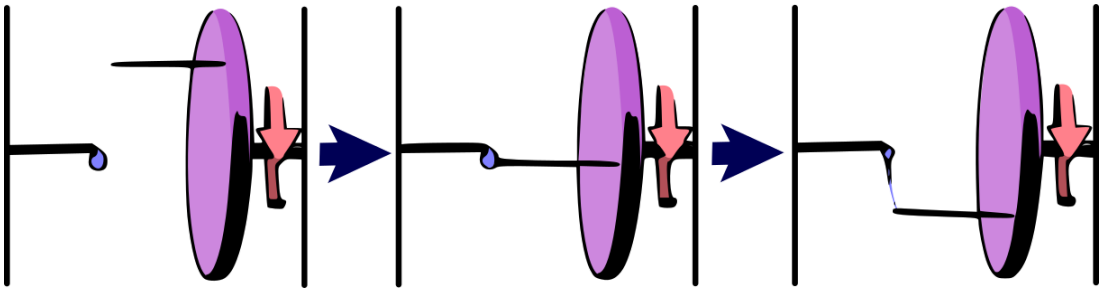

FIGURE 2.6: Touch-spinning technique.

during the fabrication process, guiding the fiber in the collector enabling better control over fiber alignment. [189]

Microfluidic forces

The microfluidic spinning technique manipulates and controls the polymer solution in networks of micrometer channels. The channel network are typically embedded in a microfluidic chip, where the solution deposition rate is controlled by active components (pumps and valves) with a computer. Cheng et al. [190] compared and combined the microfluidic spinning and electrospinning techniques. Heterogeneous materials and cell patterning within a single microfiber can be designed by the integration of microfluidic channels. Therefore, microfluidic spinning is more suitable for cell encapsulation and tissue regeneration and tissue engineering [190].

On the other hand, Kang et al. [191] managed to fabricate micro fibers by imitating the "silk spinning" process of spiders. Kang's micro fibers properties were modified using a microfluidic system with a programmable flow control (See Figure 2.7). The current microfluidic spinning approach is not scalable to a large fiber production, however it enables the fabrication of high-complex fibers that are not easily achieved by other methods.

Microfluidic techniques offer the possibility to embed several components into a single fiber, where each component can be released at different parts of the fiber.

2.1.2 Dispensing nozzle

Unlike traditional electrospinning, coaxial electrospinning (co-electrospinning) requires de implementation of a dual needle nozzle, where one needle is nested concentrically inside another needle, see

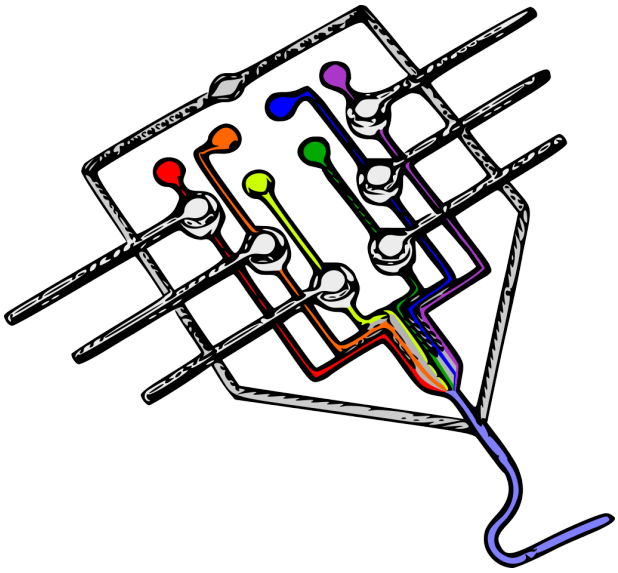

FIGURE 2.7: Microfluidic device used by Kang et al. [191]

Figure 2.8 [192, 193]. The purpose of the co-electrospinning setup is to produce core/shell fibers, unlike mono axial electrospinning that yields monolithic fibers. Sun et al. [194]. Addressed electrospinning setups, where both the core and shell are comprised by PEO (poly(ethylene oxide)) and for a PEO shell with a poly(dode-cylthiophene) core. Sun et al. state that co-electrospinning has the potential to extend the range of materials that can be used for electrospinning. The shell solution can be modified to make the core solution spunable. It was also discovered that non-spunable solutions can by implemented as shell solutions in conjunction with a spunable core solution. [195]

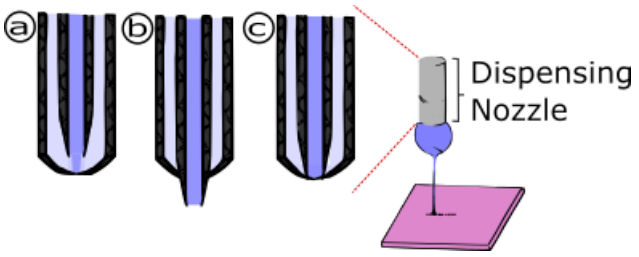

FIGURE 2.8: Needle configurations in coaxial electrospinning. (a) the outer needle encasing the inner; (b) the inner needle protruding from the outer; (c) both needles inline with each other;

Some advantages of co-electrospinning setups are the breaking of the polymer drop surface tension, initiating the jet burst from the spinneret nozzle. On the other hand, as the morphology and shape of the fibers depend on the polymer solution properties, the use of a co-axial nozzle allows the modification of the material properties by producing bubbles, scaffolds and

particles. [196, 197]. As in conventional NFES, in co-electrospinning, the needle tip is connected to a high voltage power supply with a grounded collector.

2.1.3 Polymer Reservoir (Polymer Melt & Polymer Solution)

Electrospinning processes can be classified based on the type of polymer reservoir. As Brown et al. [198] discussed, the polymer melt is equivalent to the polymer solution electrospinning. The use of a polymer melt increases the complexity of the process, because the nozzle syringe and spinneret required to be heated to maintain the polymer in a liquid state. The fibers produced in melt spinning are typically found to have larger diameters than those from the polymer solutions due to the higher viscosity of a polymer melt. The apparatus used by Brown et al. [198] is depicted in Figure 2.9.

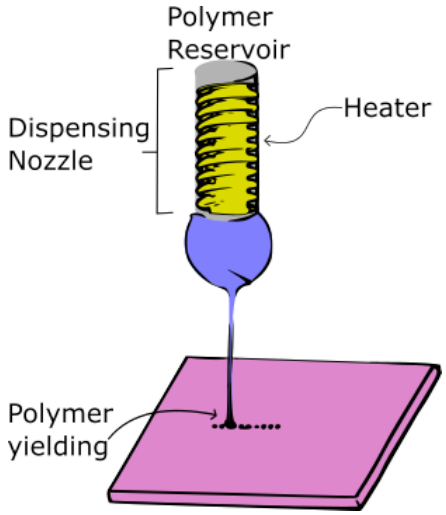

FIGURE 2.9: Typical Melt Electrospinning Setup

Despite the added complexity and thicker diameters, the melt electrospinning technique is safer to be performed on larger scales as it does not have the need to handle volatile solvents. Therefore, polymer melt reservoirs get rid of any solvent contamination. The first report of a melt electrospun drug delivery system came from Nagy et al. [199], who prepared fibers by melt electrospinning of Eudragit EPO with carvedilol. The drug and polymer were melted and mixed to form a homogeneous solid mixture prior to spinning. The melt-spun fibers reached diameters of 5–30 μm, compared to 300–1000 nm diameters produced from solution-spun fibers [199].

Balogh et al.'s work has built on this idea by blending plasticizes with the polymer Eudragit EPO and carvedilol active ingredient. [200] The plasticizes Triacetin, Tween 80 and Polyethylene Glycol were investigated in order to reduce the melting point of the polymer-drug mixture. A lower temperature is desirable to minimize the degradation of the drug.

Lian and Meng [201] performed a comparison of poly(ε-caprolactone) (PCL) fibers fabricated by the melt and solution electrospinning techniques. They arrived to the conclusion that melt spinning is preferable when the polymer presents a low solubility. On the other hand, the melt fibers were produced in a slower release rate. Gernot et al. [202] demonstrated that submicron-size fibers are possible through melt electrospinning. In their effort, they achieved a precise deposition of PCL fibers with diameters of $817 \pm 165nm$.

In literature, melt electrospinning has less evidence than the solution approach. However, melt electrospinning promises to be as flexible as its solution counterpart in handling multiple polymers, as reported in McCann's work [203]. Currently, the melt electrospinning setup is harder to analyze or study and the lack of research on this technique explains its unexplored potential.

2.1.4 Polymer Solution

In electrospinning, it is typically agreed that the diameter of the fibers increases as the polymer concentration increases due to greater viscosity, which resists the forces pulling on the solution. In near field electrospinning, similar observations have been reported where concentration increases, fiber diameter appears to increase proportionally [204, 205], seeFigure 2.20.

TABLE 2.1: Approximation process to estimate the critical polymer concentration.

Observation	Concentration Adjustment
Dripping, no stream	Increase
Splitting small droplets	Increase slightly
Steady stream	No concentration adjustment
Splitting large globs	Decrease slightly
Nozzle clogging	Decrease

Polymers

The polymer selection is typically guided by the intended final application of the fibers produced therefrom. For example, a fast dissolving hydrophilic polymer such as poly(ethylene oxide) (PEO) is used for fast drug delivery systems. Otherwise, slow dissolving polymers such as poly(ε-caprolactone) (PCL) or poly(lactic-co-glycolic acid) (PLGA) are implemented. [206]

The polymer molecular weight along with the polymer concentration and solvent selection have a direct effect on the solution viscosity, conductivity and surface tension, hence the solution behavior in the electrospinning process. The spinnable viscosity range varies with the polymer and solvent.

Solutions with low viscosity result in insufficient polymer chain entanglements to produce fibers. [206] If the solution is too viscous, then the surface tension cannot easily be overcome by the electric field. In both cases, the result can be droplets or particles forming rather than fibers as described in Table 2.1.

Solvents

The solvent used must be capable of dissolving the polymer of interest at an appropriate concentration to form fibers, and must posses a suitable volatility. A low-volatility solvent like water may fail to evaporate completely over the distance between the spinneret and the collector. Hence, when the fibers form, they will contain residual water owing to this incomplete evaporation. The solvent will subsequently evaporate from the fibers upon storage, resulting in ribbon-like (flattened) fibers, wrinkles on the fiber surface or fused fibers. On the other hand, a high-volatility solvent may evaporate very quickly, leading to larger fiber diameters (less time for elongation before solidification) and clogging of the spinneret (due to drying of the liquid at the spinneret before jetting, or drying of the Taylor cone during jetting). Solvents commonly used for electrospinning include ethanol, chloroform, trichloroethane and hexafluoroisopropanol [162, 207, 208].

Mixtures of miscible solvents can be used to ensure that sufficient polymer can be dissolved to give a solution of appropriate viscosity and volatility with suitable dielectric constant range to allow fiber formation. However, care must be taken because using a mixture of solvents with very different volatilities can result in porous fiber structures, as reported by Katsogiannis

et al. for organic solvent mixtures with dimethyl sulfoxide (DMSO). [209] DMSO evaporates much more slowly than the organic solvents used, which results in its incorporation into the fibers. The DMSO will eventually evaporate, yielding porous fibers.

It is also important to take into account the surface tension of the solution. Solvents with very high surface tensions (e.g. water) can result in instability arising during the spinning process, and a broad range of fiber diameters in the products. If necessary, a surfactant can be added to reduce the surface tension, but this will be incorporated into the fibers produced.

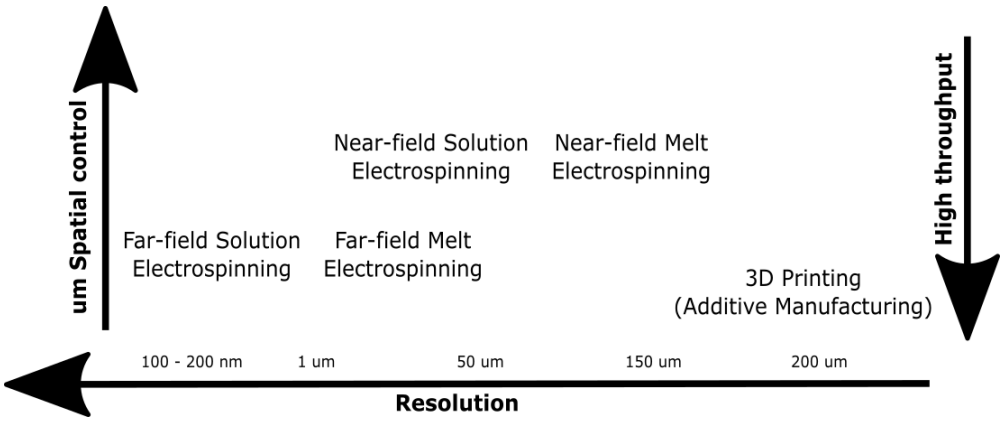

FIGURE 2.10: Different Electrospinning Methods in Terms of Spatial Control, Fiber Throughput and Resolution. Adapted from [210]

As depicted in Figure 2.10, solution electrospinning yields fibers with higher resolution than melt electrospinning techniques, and near-field electrospinning offers greater spatial control of the deposition of fibers than the far-field technique. Moreover, solution electrospinning often involves the use of toxic solvents, whereas melt electrospinning is a solvent free process but with the additional complexity as a heater needs to be installed. [210]

2.2 Properties that Improve Accuracy of Nano-Fiber Deposition

Near-field electrospinning is considered to be an outstanding technique to fabricate polymer fibers with spatial control and it has evolved through several modifications to improve the precision and accuracy of the fiber deposition. This work is intended to collect the NFES variants of electrospunable polymer solutions with spatial control in recent research.

Appendix E is a collection of the relevant NFES process parameters and achieved fiber morphology.

Some differences have been discovered between Low-Voltage Near-Field Electrospinning (LV-NFES) and conventional NFES. Low voltage near field electrospinning produces thinner fibers with lower voltages; as shown in Figure 2.23. Moreover, when implementing a moving stage, the fibers are affected by the mechanical stretching. Bisht et al. and Chang et al. [211, 212] reported that thinner diameters are obtained with the increase of the x-y stage velocity, and larger diameters by decreasing the stage velocity.

Bisht and Chang's work [211, 212] reports a controlled technique to fabricate polymeric nano fibers in a continuous manner, using a low-voltage setup. Their purpose is to find a workaround to the drawbacks of traditional NFES by using a superelastic polymer precursor, which allows continuous patterning without breaking. In low voltage near-field electrospinning (LV NFES), a visco-elastic polymer is used to allow continuous spinning at about $200V$.

Kim et al. [212] experimented with a NFES variation where the fiber deposition is guided by conductive rails, see Figure 2.11. As stated by the authors, the induced electric field is enhanced by the conductive pattern, which allows the fibers to follow the desired deposition path. As the fibers are prone to follow the conductive pattern, additional fibers can be stacked on top of the previously deposited fibers. The stacking process was successfully achieved in high electric field conditions at: $750\mu m$ substrate to collector distance, and a 600 μm needle to rail (offset) distance, see Figure 2.11.

Gupta et al. [213] introduced a new technique to fabricate polymer scaffolds for tissue engineering applications and organ development. As described by Gupta et al. [213], the fiber deposition equipment is comprised by a stainless steel needle with a internal diameter of 750 μm , connected to a high voltage power supply of up to 30 kV with a deposition rate of about $\geq 1\mu L min^{-1}$. The setup was embedded to a motorized collector capable of controlled programmable motions The proposed technique was able to produce fibers of $150\mu m$ in diameter with pre-designed patterns.

Wang, et al., Huang, et al., and Chen, et al. [214–216] experimented with

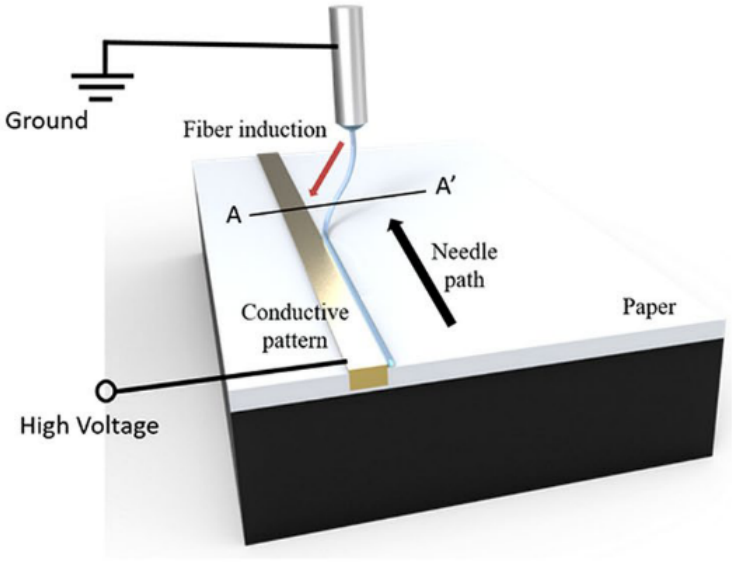

FIGURE 2.11: NFES setup for controlled fiber deposition on pre-patterned conductive electrodes. Adapted from [212]

several multi-nozzle near-field electrospinning of aligned nano fibers. The multi-nozzle NFES apparatus is similar to the one used in conventional NFES with some modifications to the needle, see Figure 2.12. The authors implemented similar NFES setups where the installed linear array of nozzles is supplied with a constant flow rate of solution.

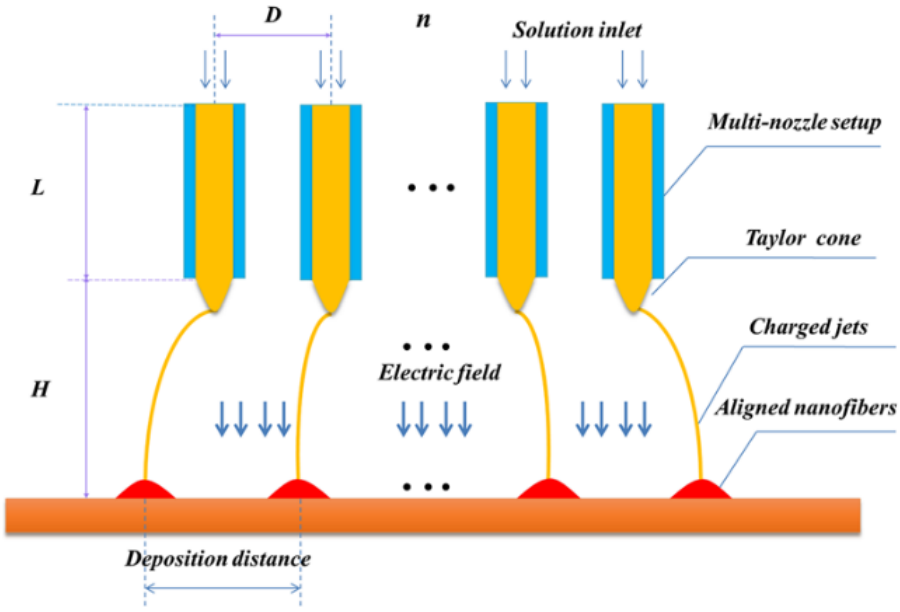

FIGURE 2.12: The geometry distribution of linear array multi-nozzle system. Adapted from [215].

The authors came to the conclusion that the distance between the deposited fibers increased as the needle-to-collector distance increased, due to the influence of the applied voltage dissipates.

Huang, et al. [217] studied the mechanoelectrospinning (MES) technique for the fabrication of nano-fibers. The MES technique tries to improve deposition accuracy by the introduction of a mechanical drawing force. The MES is predominantly controlled by the collector stage velocity, the nozzle-to-collector distance, and the applied voltage. The authors believe that MES can compete as a low-cost, high precision fabrication of electronics and enable the direct writing of structures for nano-scale lithography. Figure 2.13 shows the polymer jet behavior when a mechanical force is implemented within the NFES process.

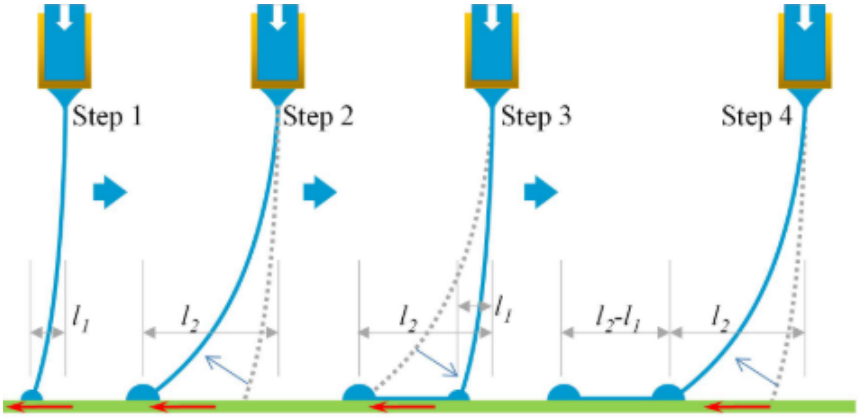

FIGURE 2.13: Schematic diagram of leap direct-writing. Adapted from [217]

Micro and nano-fibers have been written using AC pulse-modulated electrospinning by Bu et al. with polyethylene terephthalate (PET) as substrate [218]. The AC electrical field influences the electrospinning jet. The alternate current tends to decrease the repulsive electrical force allowing a stable straight jet between the dispensing nozzle and the insulating PET substrate. Bu et al. varied the stage velocity; faster stage velocities enable the deposition of straighter fibers [218].

A mechano-electrospinning technique was presented by Nagle et al. [219]. With the implementation of a mechanical drawing force, a higher resolution nano fibrous pattern can be produced with lower voltages as the Taylor cone becomes more stable. Nagle et al. studied PEO fibers at different nozzle-to-collector distances. Evidence suggests that better patterning accuracy increases with increasing nozzle to collector distance as the solution is effectively dried [219]. Near field mechano-electrospinning enables the collection of non-woven fibers over large areas.

To spin nano-fibers at close distances, the initial diameter of the jet is required

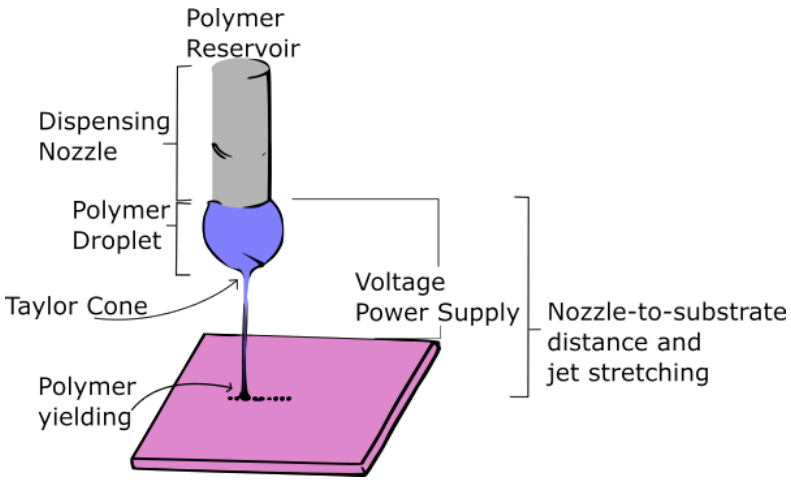

FIGURE 2.14: Near-Field ES Process Parameters

to be as small as possible since stretching of the thread is limited. Kameoka et al. [220] demonstrated that a small initial spinning radius can be achieved using an atomic force microscope tip with a small polymer solution drop at the tip.

Near-field electrospinning, has been shown to enable the fabrication of nano-fibers and nano-fibrous patterns [221]. Nevertheless, having a small polymer solution drop at the nozzle tip limits the length of the fibers that can be fabricated in a continuous manner. Using a spinneret with a reservoir (e.g. syringe) of solution generally produces fibers with diameter of a few micrometers [213, 222], since it creates a limit to which the nozzle inner diameter can be reduced to allow the solution to flow through. The implementation of thicker needle nozzles translates into an increase in diameter of the deposited polymer fibers.

Coppola et al. [223] have showed a NFES variant that allows polymer nano-fibers to be deposited directly from a polymer drop, averting the issue of nozzle clogging. The fibers are also prone to soaking after deposition thus giving the fibers a semi-circular cross-section as shown by Xue and coworkers [222].

2.2.1 Nozzle spinneret

The thinnest nozzles in literature so far are about 50 nm in diameter, by Chang et al. [204] who used a 100 μm inner diameter needle tip to electrospin poly(ethylene oxide) (PEO). Camillo et al. [224] used a micro-diameter-tip Tungsten spinneret in a 26G needle to electrospin

co-polymer, poly[2-methoxy-5-(2-ethylhexyloxy)-1,4-phenylenevinylene] (MEH-PPV) with poly(ethylene oxide) (PEO). The nozzle most commonly comprises a simple narrow-bore, blunt-end metal needle. The diameter of the needle can vary, but most commonly researches work with internal diameters below 1 mm . This translates to needles of gauge 18–22. In general, this simple spinneret design can be used to achieve successful spinning. A blunt-end rather than a tapered-end for the needle exit is important as the size distribution of the products increase with an increase in needle tip angle. However, it should be noted that there will be some interactions between the solvent and polymer molecules in the solution and the metal surface of the spinneret. There will exist some attractive forces between the polar groups in the polymer and the electro-positive metal surface, which can act counter to the drawing force of the electric field and can pull the polymer solution back into the spinneret. It has been found that coating the spinneret exterior in a non-conductive and non-stick polymer such as Teflon or epoxy coating can reduce these interactions. [225, 226] As a result, the electrical energy can be more efficiently used to elongate and narrow the polymer jet, and narrower fibers can be produced. In addition, strong attractive forces between the polymer jet and the metal spinneret can result in fibers becoming attracted to the needle, leading to lower yields and potentially to blocking of the exit orifice.

2.2.2 Applied Voltage

In recent literature, near field electrospinning has been studied to reduce the fiber diameter and to improve the control over fiber deposition. Madou et al. [211] and Chang et al. [204] came to the conclusion that higher voltages yield thicker micro-fibers with a loss in jet stability. This relationship between the applied voltage and resulting fiber diameter is influenced by other variables such as nozzle-to-substrate distance and solution deposition rate. For instance, if a high voltage is applied at a low deposition rate then electrospraying is achieved, meaning the formation of several non-continuous fibers. The applied voltage shall be sufficient to break the surface tension and initiate the jet, but low enough to avoid multiple jets at the nozzle tip.

Madou et al. [211] achieved the fabrication of thinner fibers with spatial control by reducing the applied voltage to 200-600 V at a nozzle-to-substrate distance of 0.5-1 mm. The low voltage setting alone does not create

enough charge to break the polymer solution surface tension to initiate the electrospinning process. Madou et al. [211] and Chang et al. [204] initiated the electrospun fibers by mechanically pulling the polymer solution at the nozzle tip using a micro-probe tip. Chang and coworkers reduced the applied voltage from 1.5 kV to 600 V with a nozzle-to-substrate distance of 500 μm to yield a fiber diameter between 3 μm and 50 nm . With an applied voltage of 200 V and a nozzle-to-substrate distance of 1 mm.

In near-field electrospinning, the applied voltage has an impact on the morphology of the fiber. For instance, a voltage higher or lower to the optimum voltage will translate into an increase in fiber diameter. Song et al. [227] demonstrated that an increase in voltage from 400 to 500 V can reduce the fiber diameter from 160 to about 60 $nm$with a nozzle-to-substrate distance of 20 μm. A workaround to break the polymer solution surface tension is to initialize the NFES process with a higher voltage and then lower the voltage once the jet is created. Huang et al. [217] implemented the previous and obtained ordered fibers with a distance between adjacent fibers of 50 μm.

2.2.3 Nozzle-to-substrate distance

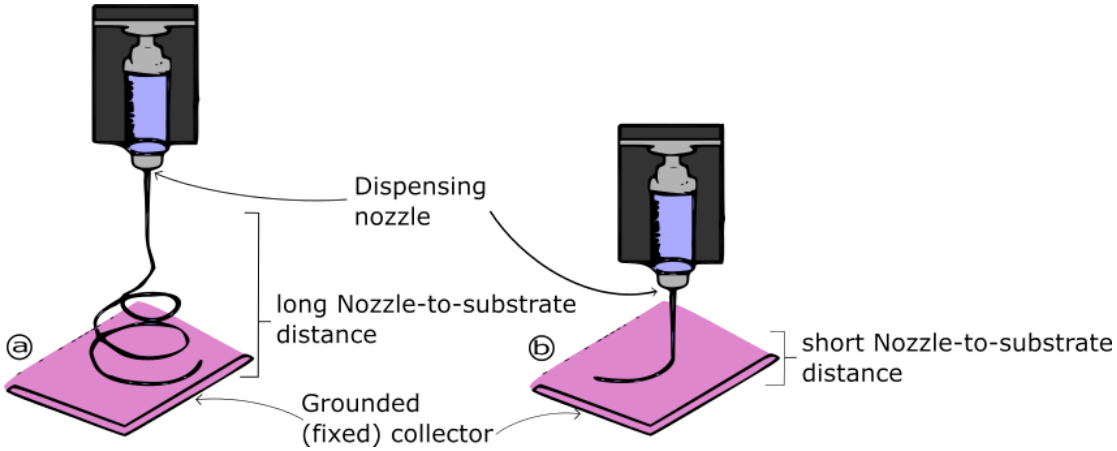

FIGURE 2.15: a) Typical Far-field Electrospinning (FFES) Setup. b) Typical Near-field Electrospinning (NFES) Setup.

Figure 2.15.a, depicts the typical setup for the conventional far-field electrospinning (FFES). As stated in previous sections, the precursor polymer droplet becomes charged with the employment of an electric field between the polymer solution and the collector [228]. When the polymer solution surface tension is overcome by the electric field potential difference, a jet is formed, starting the electrospinning process. The electrospinning process can be broken down into two steps: i) first the jet travels in a straight line,

and ii) the jet begins to curl due to bending and whipping instabilities [170, 229]. The fiber spatial control in far-field electrospinning is limited due to the instabilities, inhibiting the precise deposition of fibers.

With the goal of achieving controlled fiber deposition, Sun et al. [221] reported an electrospinning variation known as near-field electrospinning (NFES),Figure 2.15.b, describes the near-field electrospinning setup, where the distance between the dispensing nozzle and the collector is reduced to write fibers while the jet travels in a straight line. Moreover, some mechanical influence is required to deposit fibers with higher precision. The mechanical force is introduced by moving collector. If the polymer solution jet speed is faster than the speed of the moving collector, the written fiber will curl; on the other hand, if the collector moves faster than the polymer jet, the fiber will gradually diminish [222, 230]. Currently, due to the lack of theoretical models, the near-field electrospinning process parameters (such as the collector speed) are typically tuned by experience and experimentation only. Adimensional analyses have been done [81, 210, 231–238] and can be used as a guide to design and prepare electrospinning setups, however these analyses are recently developed and hence their little appearance in literature publications.

The main difference between NFES and FFES is the distance between the needle and the collector which is higher in FFES (about 10 cm) compared to NFES, which ranges in the mm scale. The short distance allows the production of well-aligned fibers within particular designs. In NFES, the fiber morphology can be altered by the control of the distance between the nozzle and the substrate (collector). With the decrease of the nozzle-to-substrate distance, the electric field strength increases; however it can cause incomplete solvent volatilisation and possible short circuits between the collector and the nozzle tip.

An optimal nozzle-to-substrate distance shall be defined to ensure the fabrication of dry continuous fibers. If the solvent is not well evaporated, the produced fibers are prone to defects; on the other hand, if solidification happens too fast, the solids can block the spinneret which can prevent a continuous fiber yield. Furthermore, the polymer jet will discharge itself as soon as possible, therefore long distances can result in low yields.

2.2.4 Substrate

Due to the close distance between the grounded substrate and the charged spinneret in NFES, the set up is prone to electrical shorts. In NFES, when a short circuit takes place, the electrospinning process is interrupted resulting in the fabrication of discontinuous fibers. Two workarounds to avoid electrical shorts is to lower the applied voltage and to use less conductive substrates [239, 240].

Liu et al. [239] discovered that the fiber alignment is improved by using a glass-cooper foil substrate, however the alignment of the fibers is spoiled after prolonged depositions due to residual charges. Additionally, the effect of residual charges is amplified when the used collector substrate contains a conductive layer and a non-conductive layer [239].

In contrast, Choi et al. [240] implemented a hydrophilic substrate to deposit the fibers with plasma treatment to increase the conductivity of selected areas. NFES was carried out with precise deposition as the fibers were placed as per the desired design within the hydrophilic substrate.

2.3 Data collection of NFES fiber morphology and process parameters

The near-field electrospinning process parameters and the morphological data (diameters and images) reported in papers reviewed was collected and classified into a single database with the purpose of analyzing and finding correlations between the process parameters and the obtained fiber diameter after a NFES process. The analysis was based from data ranging from the first reported NFES apparatus built in 2003 by J. Kameoka et al. [116] to recent studies conducted in 2020. [11–13, 82–159] The data was divided in three groups depending on the format of the available information, as follows:

1. Case 1 : data is collected as-is from literature. This procedure was implemented when the data is listed within tables and/or as text format.

2. Case 2 : data is only presented in a figure as plots.

3. Case 3 : data is not available in text format or plots, however Scanning

Electron Microscopy (SEM) images are reported from the obtained fibers.

2.3.1 Image Analysis - Data extraction from plots

Most numerical data of NFES process parameters and fiber diameters is available only in the form of plots. The reported figures provide a visual relationship between the variables of interest, however recovering the numerical values of the data is a tedious process prone to errors. To avoid mistakes and accelerate the acquicition of data from the plots, WebPlotDigitizer was used. WebPlotDigitizer is a HTML5 tool that facilitates accurate data extraction with ease of use. Figure 2.16 is a screenshot of the software in use.

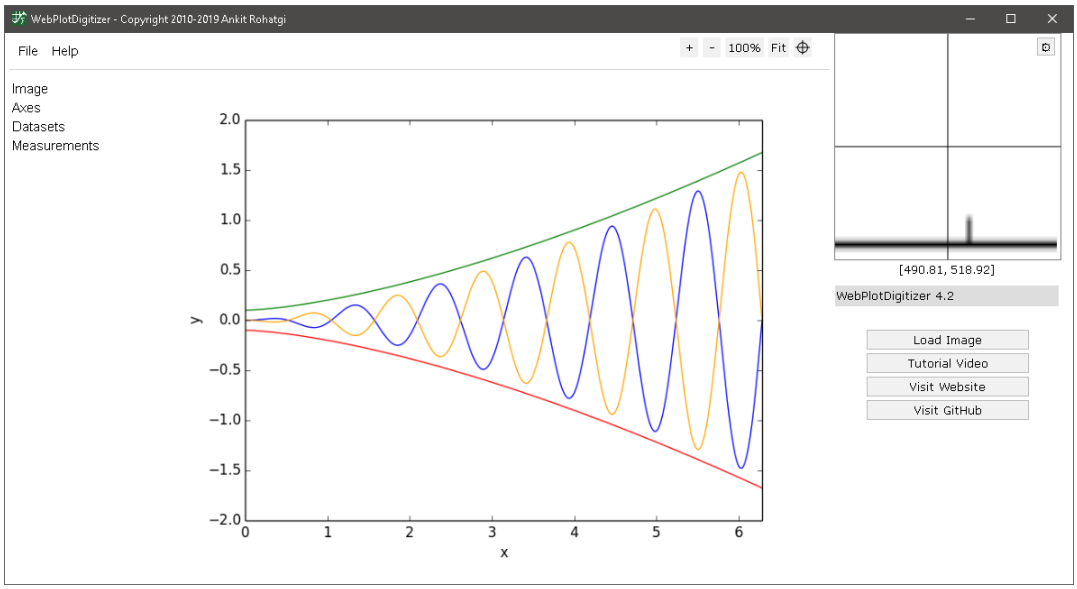

FIGURE 2.16: Open session of WebPlotDigitizer github.com

2.3.2 Image Analysis - Data extraction from Scanning Electron Microscopy Images

Scanning Electron Microscopy Images (SEM) images contain information in a two-dimensional grid that can be extracted using point and line counting techniques, however this can be a laborious process for a large number of images. To decrease the complex and lavorious aspect of the counting process, a *Python* script was developed to measure fiber diameters from the available SEM images. As shown in Figure 2.17, the image analysis algorithm follows three main steps: pre-processing, segmentation, object detection, and data processing.

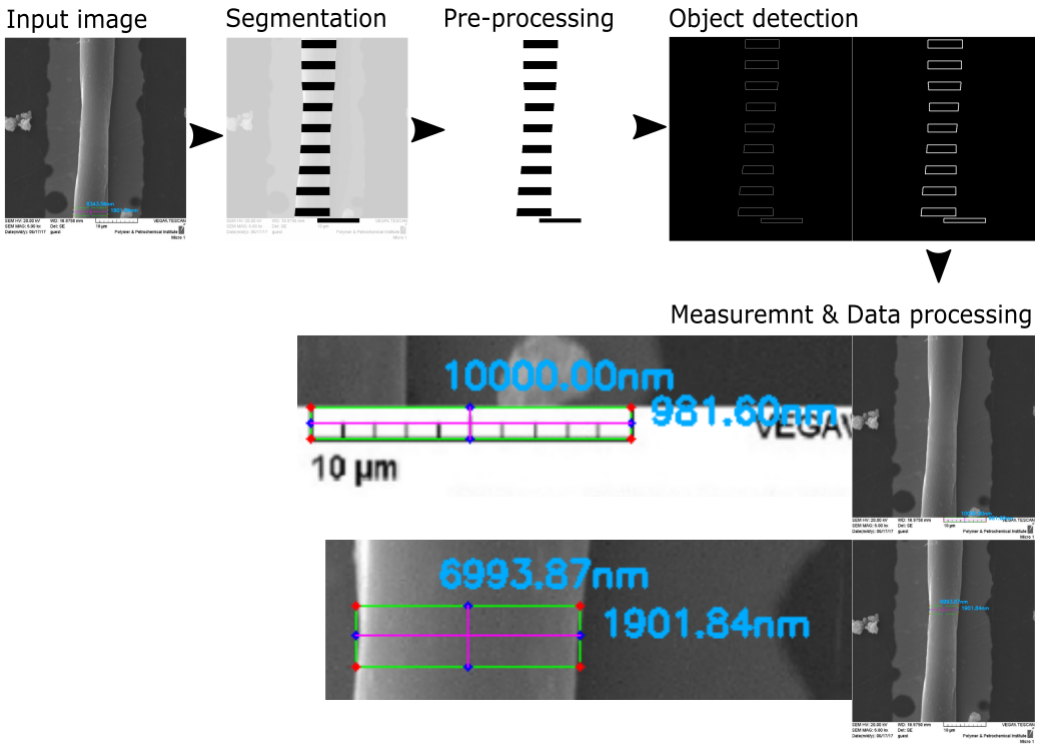

FIGURE 2.17: Image Analysis Algorithm to Measure Fiber Diameters from SEM images. Ilustration uses Yousefi et al.'s work as an example. [158]

The adopted image analysis was implemented with the *Python* package *OpenCV* (Appendix F). First a segmentation procedure is executed over an input image to delimit the objects to be measured (fiber sections and scale-bars). The segmentation step is the only step needed to be done manually in a image processing software, in this case *Inkscape* was used. Next, the segmented image is passed into the *Pyhton* script, which will convert its input image into a binary image. A binary image is a black and white image (with no gray scale) that facilitates the detection of the object edges as the color intensity change between the objects and the background is well-defined. Once the binary image is computed, the *Canny* edge detection algorithm is executed. Once the edges are well-defined, the image is dilated to make the edges more visible. The final step before measurement, the *OpenCV findContours* function is called to store the objects in memory. The first object to be measured is the scale bar as this is needed as a reference to convert the pixel counts to a metric unit. Finally, the objects are located within the image with four edge points, and the reference object is used to compute the metric length as the ratio of counted pixels between two edge points and the scale bar dimension in meters.

Measurements were validaded with Camillo's, Gupta's, Jiang's, Min's, Sun's, Wang's, and Xue's [85, 91, 98, 120, 127, 144, 156] results as those authors reported both, a SEM image and the measured fiber diameter. For instance, Figure 2.18 shows in black the reported diameters by Min and in white the diameters measured by the *Python script* of two samples. The measurement error of the developed script is about 3.2% in average. It is considerable to mention that the reported measurement error is mainly contributed to the fact that most fibers are not of the same diameter along the fiber length. In most cases, measurements at the end of the fibers are thicker than the ones measured in the center.

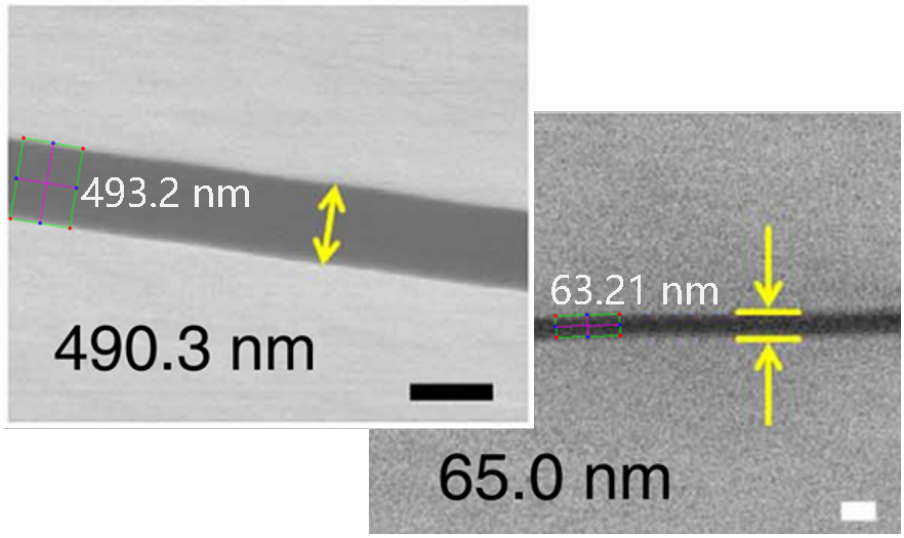

FIGURE 2.18: Validation of the developed image analysis meassurement tool. SEM images of Min's work are used as an example. [156]

2.4 Discussion & NFES Challenges

Helix electrodynamic printing (HE-printing) was presented by Duan et al. [241] with the intention of depositing aligned fibers. The authors fabricated a stretchable piezoelectric device using micro- and nano-fibers to demonstrate the possible applications of HE-printing for electronics manufacturing. Duan et al. concluded that the fiber morphology is mainly affected by: the stage velocity, the applied voltage, and the nozzle-to-collector distance.

Figures 2.20, 2.21, 2.22, 2.23, 2.24 and 2.25 are scatter plots that depict the relationship of various process parameters (polymer concentration $C_{polymer}$, nozzle inner diameter D_{nozzle}, NFES working distance L, NFES applied

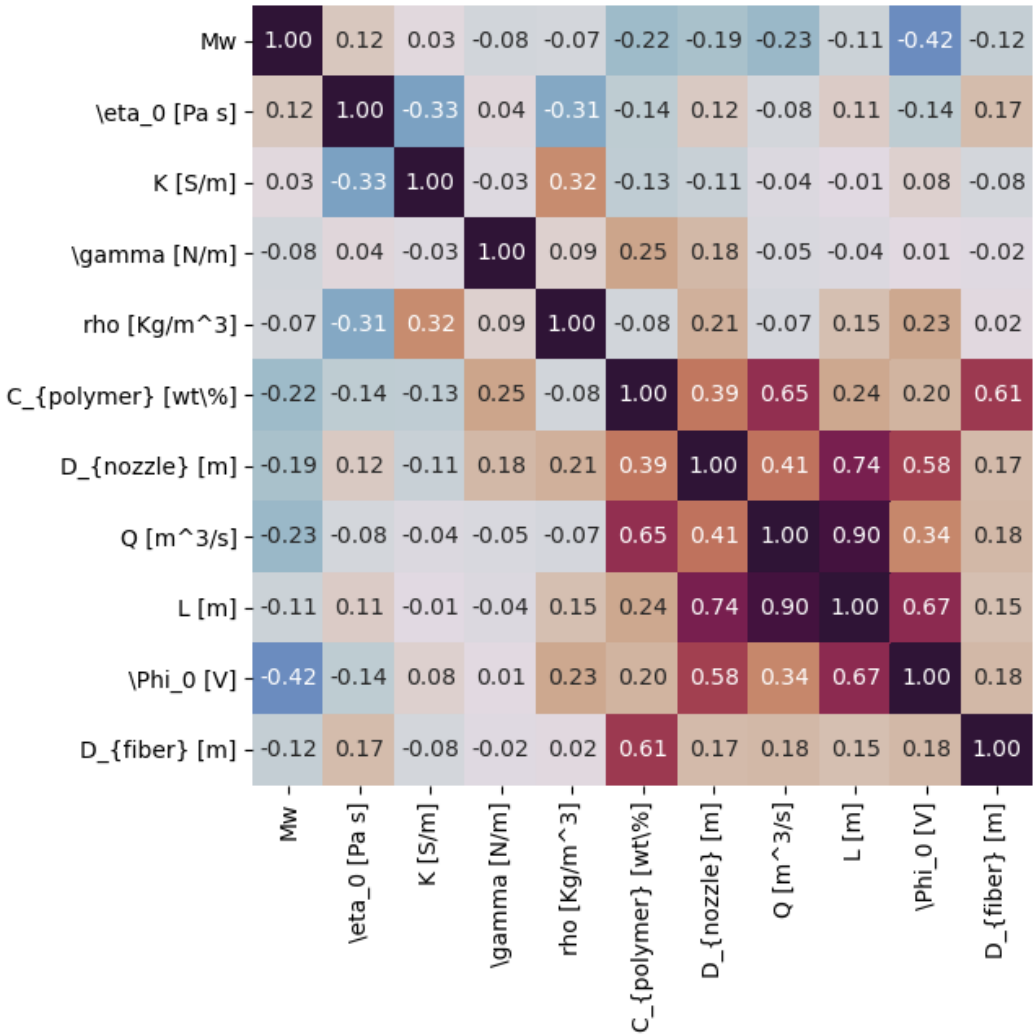

FIGURE 2.19: Correlation matrix comprised by the NFES data from recent literature. [11–13, 82–159] Fiber diameter is highly correlated with polymer solution concentration and slightly correlated with solution flow rate, zero-shear viscosity and nozzle diameter.

voltage Φ_0, flow rate Q, and stage velocity v_{stage}) with the final fiber diameter D_{fiber}. In a generalized summary, these figures suggest that thin fibers are produced with the implementation of low polymer concentrations, small nozzle diameters, short working distances, low applied voltages, low flow rates, and high stage xy velocities. Moreover, based on the degree of dispersion of the data points, polymer concentration $C_{polymer}$ is the most reliable process parameter to describe and predict the behavior of the fiber diameter, as most of the data can be grouped in a single cluster. Unlike $C_{polymer}$ in Figure 2.20, various data clusters can be identified within the other scatter plots. For instance, Song's results [153] deviate from the main cluster in Figures 2.21, 2.22, 2.23, and 2.25, this may be because Song et al. used

Au/Pd coated glass capillary nozzles instead of the traditional stainless steel precision tips. However in the $C_{polymer}$ vs. D_{fiber} figure, Song's results fit within the main cluster.

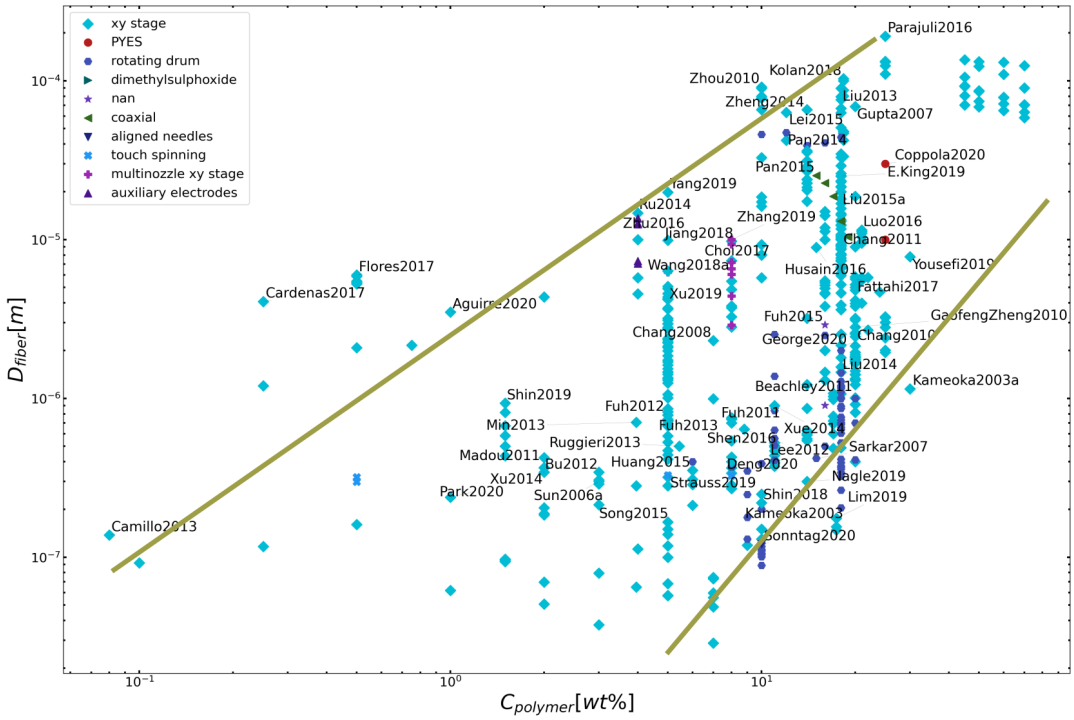

FIGURE 2.20: Scatter Plot of Polymer Concentrations and Fiber Diameters from Literature Experimental Results. [11–13, 82–159]

The trend of Figure 2.21 shows that thicker nozzle diameters yield thicker fibers. However, the final fiber diameter can be reduced without changing the nozzle diameter. For instance Chang et al. [138] achieved the thinnest fibers of about 50 nm in diameter even though Chang implemented nozzle needles of similar diameter as Shin, Min and Xu by the implementation of different settings on the other process parameters. For instance: the glass glass capillary nozzles by Song [153], the melt-NFES setup by [123, 137], the long working distances implemented by Husain [121], the low stage velocities by Shin [84] to fabricate coiled fibers, and the high polymer concentrations by Parajuli [86] are some differences from the traditional NFES setup that are represented as isolated clusters within Figures 2.20, 2.21, 2.22, 2.23, 2.24 and 2.25. It is worth nothing that Chang's thinnest fiber may be a one-time result where, neither the yield rate nor the reproducibility of their technique was not reported.

The relationship between the fiber diameter, the working distance L and applied voltage Φ_0 can be depicted in Figures 2.22 and 2.23. The near-field

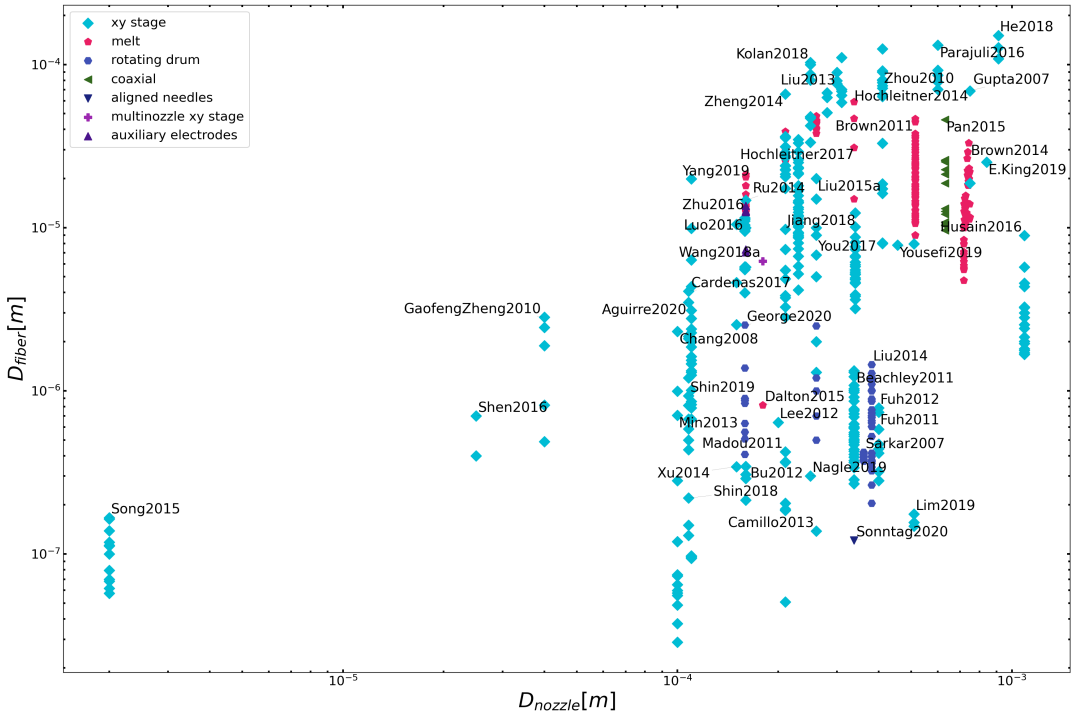

FIGURE 2.21: Scatter Plot of Nozzle Inner Diameters and Fiber Diameters from Literature Experimental Results. [11–13, 82–159]

electrospinning jet is ejected from the Taylor cone when the applied voltage generates an electric field strong enough to break the solution drop. Changing the applied voltage will change initial drop shape, thereby resulting in a change in the fibers' diameters. However, the effect of the applied voltage on the fiber diameter is not well understood. On one hand, many researchers posit that high applied voltages lead to larger fiber diameters, whereas other researchers have reported reductions in fiber diameter with high applied voltages as the electric field force increases on the charged jet. [242] Furthermore, Reneker and Chun observed that applied voltage does not significantly affect the diameter of electrospun polyethylene oxide (PEO) fibers. [243] Applied voltage has an influence on the fiber diameter, but the degree and direction of the effect on the diameter varies with other process parameters such as polymeric solution concentration and on the working distance [244, 245].

Looking at Figures 2.22 and 2.23, the data points from Husain, Lee and Sonntag [121, 130, 139] are outside the principal cluster since they implemented working distances around 10^{-1}m, which is considered to be the threshold between NFES and far-field electrospinning (FFES). One can observe that: a) in NFES fiber diameter increase with increasing applied

voltage; and b) in FFES fiber diameter decrease with increasing applied voltage. On the other hand, data related to Liu's and Beachey's work [117, 126] do not fit the main trend as they performed the electrospinning process with a rotating drum as the collector, instead of the typical xy stage.

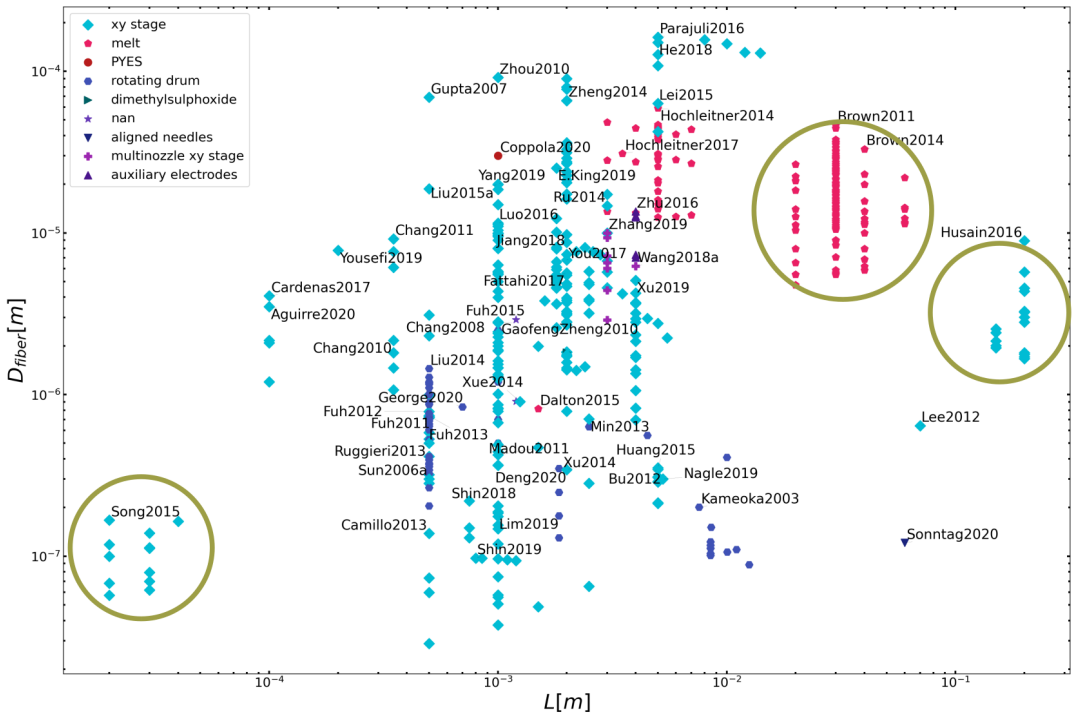

FIGURE 2.22: Scatter Plot of NFES Working Distances and Fiber Diameters from Literature Experimental Results. [11–13, 82–159]

The effect of parameters such as ink concentration, working distance, applied voltage, and stage speed on the diameter of the printed nano-fibers was investigated, a summary is presented in Table 2.2.

2.5 Diameter Prediction of Electrospun Fibers

Electrospinning is a simple process to fabricate fibers of different diameters. However, the final diameter of a fiber depends on various solution, process, and ambient parameters (Table 2.2) with interaction with rheology and fluid dynamics. Given the connection of various parameters, it is not trivial to derive a mathematical model to describe the complete electrospinning process. Current attempts involve limited models that can only describe the steady jet region for specific polymer solutions. [68, 248, 249] From literature [126, 250–252] and as described in Figure 2.19, zero-shear viscosity, flow rate and applied voltage are the main drivers that determine the final fiber morphology and dimensions. Other parameters such as solution

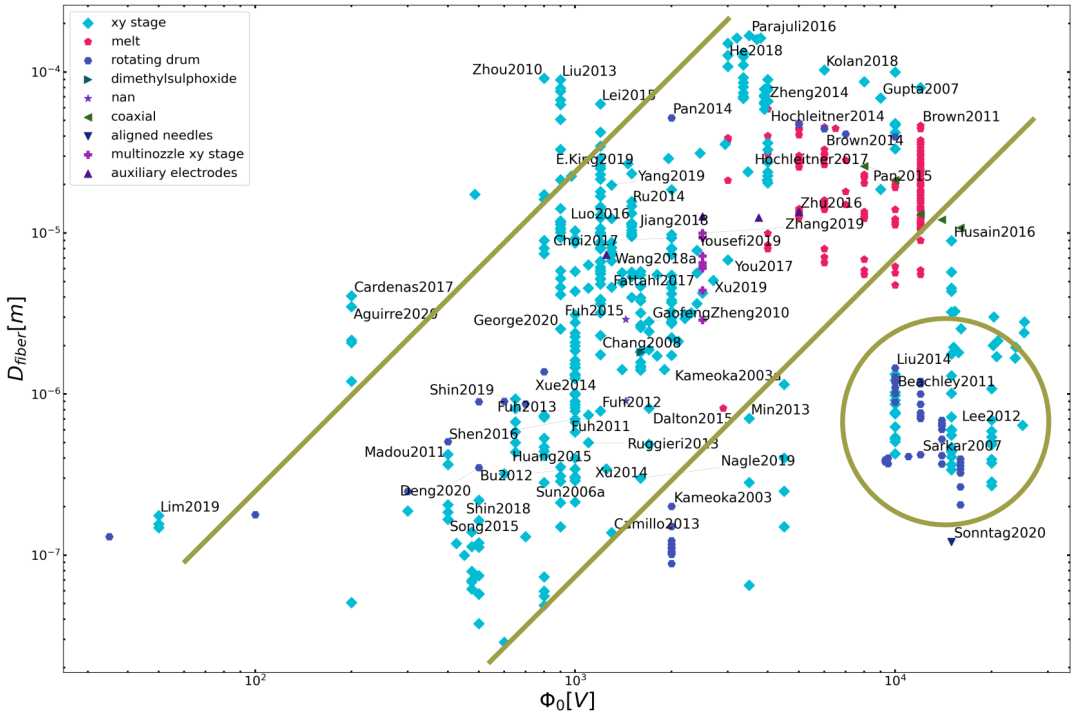

FIGURE 2.23: Scatter Plot of NFES Applied Voltages and Fiber Diameters from Literature Experimental Results. [11–13, 82–159]

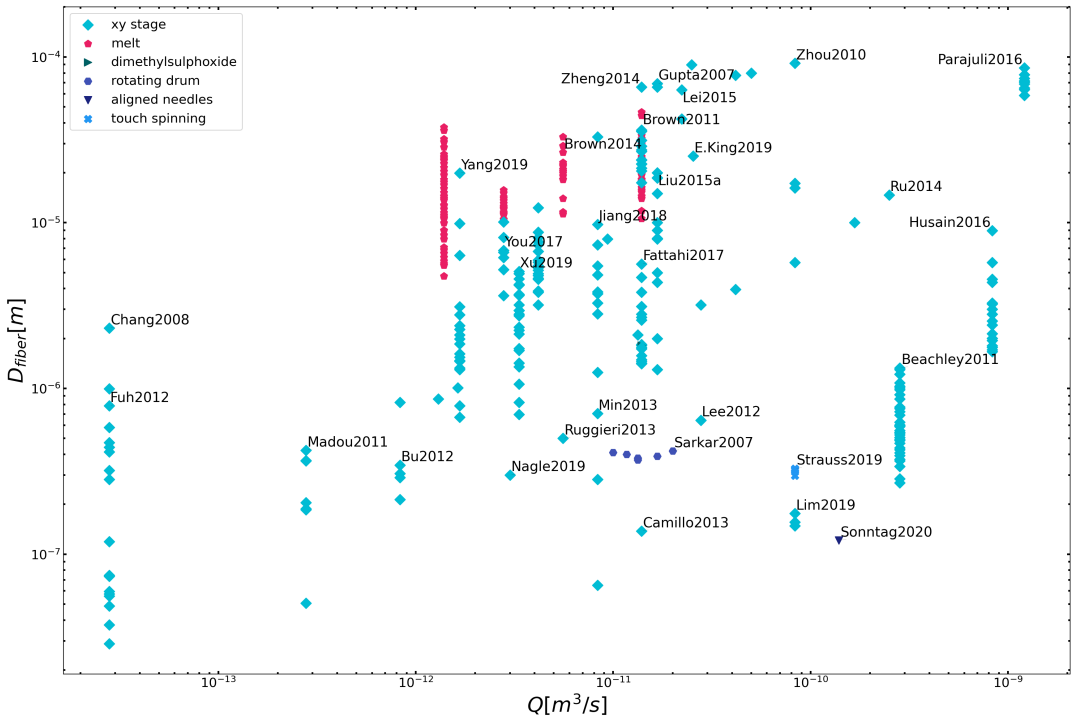

FIGURE 2.24: Scatter Plot of Polymer Solution Flow Rates and Fiber Diameters from Literature Experimental Results. [11–13, 82–159]

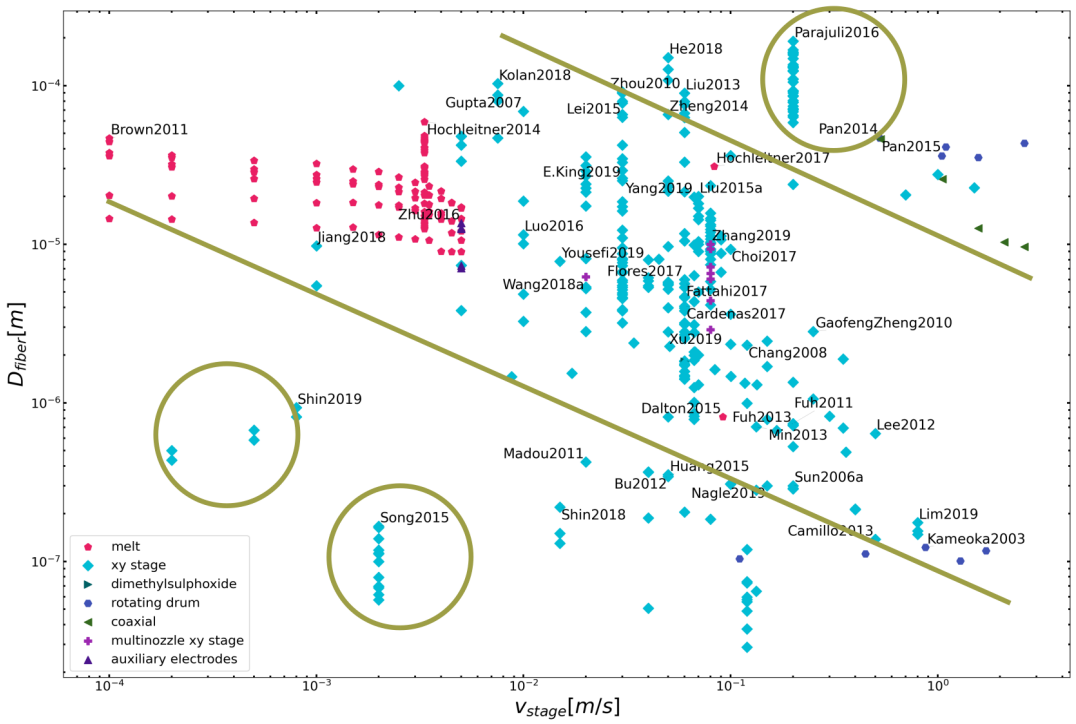

FIGURE 2.25: Scatter Plot of Collector xy Stage Velocities and Fiber Diameters from Literature Experimental Results. [11–13, 82–159]

surface tension, conductivity and working distance have less impact on the electrospun fibers. [67] As shown in Figures 2.24 and 2.20, literature states that flow rate Q and solution concentration $C_{polymer}$ are directly proportional to the fiber diameter D_{fiber}. [253–255]

As mentioned in the previous section, the correlation between the final fiber diameter D_{fiber} and the applied voltage Φ_0 is not well understood. Most authors posit that the fiber diameter decreases with increasing voltage. [242, 256–263] Nevertheless, other publications state the inverse correlation. [264, 265] This discrepancy between the final fiber diameter D_{fiber} and the applied voltage Φ_0 may be attributed to the fact that Φ_0 is also related to the electric field Φ_0/L, which in turn is related to the working distance L. As the electric field Φ_0/L increases, the electric field forces loose influence under the polymer jet as the increased force results into faster evaporation of the solvent promoting faster solidification. On the other hand, polymer concentration $C_{polymer}$, and conductivity K also have an effect on the electric field. [258, 266]

On the other hand, Zhang et al., Kim et al., and Mituppatham et al. studied the relationship between the solution surface tension γ and its conductivity

TABLE 2.2: Summary of the main parameters that drive the electrospinning process, ordered by: polymer solution parameters, process parameters, and ambient parameters. Adapted from [246, 247]

NFES Process Parameters	**Effect**
Solution Parameters:	
Concentration	Concentration shall be high enough to produce uniform nano-fibers, but low enough to prevent nozzle clogging
Molecular weight	High-molecular-weight polymers yield smoother fibers
Viscosity	Zero-shear viscosity shall be optimal to generate a constant jet from the needle
Conductivity	Solution shall be conductive enough for the electric field to have influence on the jet
Process Parameters:	
Applied voltage	Higher voltages eject more material from the nozzle
Flow rate	Slow flow rates yield thinner fibers, but it shall be fast enough to prevent clogging and keep the Taylor cone in a constant size and shape
Working distance	Long distances result in thinner fibers, however the spatial control is hampered
Ambient Parameters:	
Humidity	Increasing humidity produces thicker diameters
Temperature	Increasing temperature yields thinner fibers, however high temperatures make the nozzle prone to clog as the solvent evaporates at a faster rate

K. [242, 267, 268] Kim's and Mituppatham report a increase in fiber diameter with increasing conductivity in the polymer solution, while Zhang reports the inverse relationship. The existing interdependence between the process and solution parameters adds complexity and ambiguity to the effect of each parameter. The fiber morphology not only depends on the process parameters, but also on the type of electrospinning process and on polymer-solvent system. [238]

Helgeson and Wagner [81] have presented a dimension-less analysis to predict the fiber diameter with conservation equations of momentum, mass, electric charge and four dimensionless numbers: Peclet number $Pe = \frac{2\bar{\varepsilon}v_0}{KR_0}$,

Reynold number $Re = \frac{\rho v_0 R_0}{\eta_0}$, Weber number $We = \frac{\rho {v_0}^2 R_0}{\gamma}$, and the dimensionless electric field strength $\Psi = \frac{\bar{\varepsilon} {E_0}^2}{\rho {v_0}^2}$. Where $\bar{\varepsilon}$ is the dielectric permitivity of the atmosphere, K the solution conductivity, ρ the density, η_0 the zero-shear viscosity, γ the surface tension, E_0 the applied electric field, R_0 the initial jet radius, and v_0 the initial jet velocity. Since R_0 and v_0 can neither be controlled nor measured, Helgeson arrived to a correlation between the electrostatic and viscous forces Π_1 describing the stress directing the polymer jet elongation from the source to the collector plate. [81]

$$\Pi_1 = RePe\Psi = \frac{2\bar{\varepsilon}^2 {\Phi_0}^2}{K\eta_0 L^2} \tag{2.1}$$

the Ohnesorge number, resulting from the manipulation of the Reynolds number Re and the Weber number We, is used to explain the behavior of the polymeric solution jet under small disturbances, due the presence of a voltage, leading to the capillary rupture of the fluid jet. [81]

$$Oh = \frac{Re^2}{We} = \frac{\eta_0}{\sqrt{\rho\gamma R_{jet}}} \tag{2.2}$$

Where $R_{jet} = R_f \sqrt{\frac{1}{w_s}}$ is the wet radius of the jet solution, which is calculated from the radius of the dry fiber R_f and the mass fraction of the polymer in solution w_s. [81]

Figure 2.26 plots the Π_1 and Oh values reported by [81] along with new data points from the data collection of NFES fiber diameters and process parameters. It is possible to observe the predominance of the viscous and the electrostatic forces within the solution by the magnitude Π_1 (Equation 2.1). On the other hand Oh (Equation 2.2) reflects the capacity of the viscous forces over the polymeric jet, which allows stability in the electrospinning process. The data points gathered by Helgeson et al. are from far-field electrospinning studies, whereas the new data points belong to near-field electrospinning studies.

The analysis suggests that both types of electrospinning behave in a similar

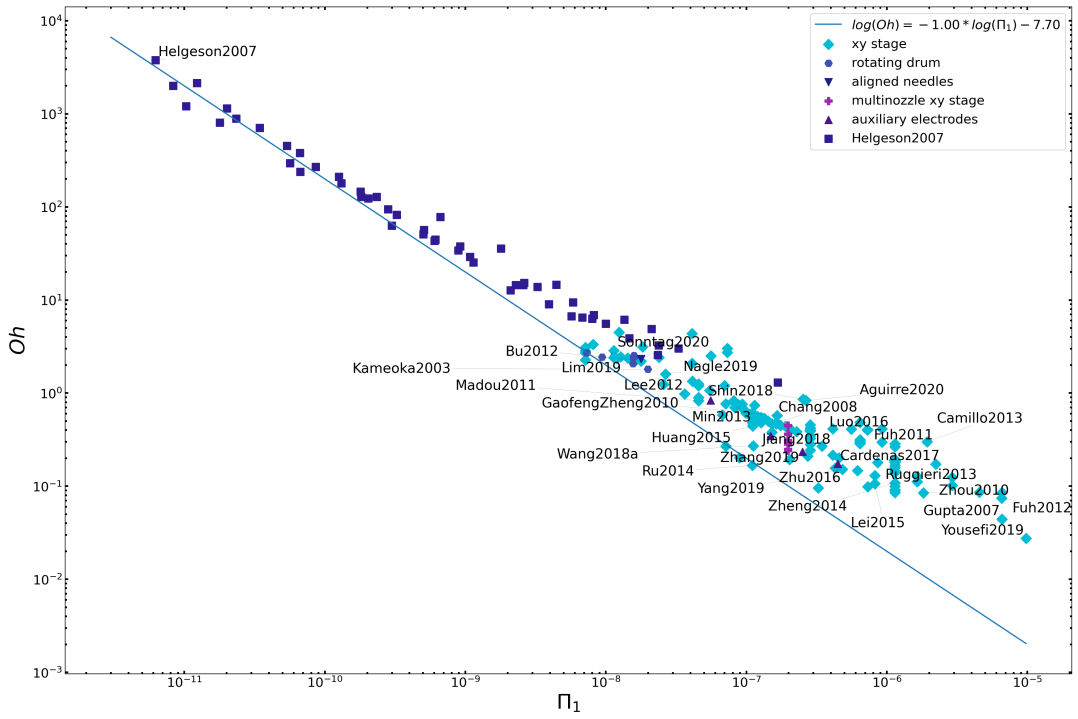

FIGURE 2.26: Image Analysis Algorithm to Measure Fiber Diameters from SEM images. Ilustration uses Yousefi et al.'s work as an example. [11–13, 81–159]

manner, where the FFES data fits better a linear behavior of slope -1. As the working distance closes in NFES, the data points fit a shallower slope with higher Π_1 values and lower Oh values. This suggests that in NFES less viscous solutions have been used, since in long working distances a higher viscosity is needed to keep the integrity of the fiber in the whole traveling distance until it reaches the collector. For high Oh values and elevated viscosity, the entanglement of the polymeric chains is higher, resulting in the formation of individual fibers; also, the jet is prone to faster solidification, due to an early evaporation of solvent, due to the resistance to the change of momentum, caused by the high viscosity in the polymeric solution, hence the need of higher voltages in FFES. Helgeson et al. suggest that the following relationship in Equation 2.3 can be used to predict the fiber diameter, as in the trend in Figure 2.26 Oh has an inverse linear relationship with Π_1. [81]

$$\Pi_1 Oh = \frac{2\bar{\varepsilon}^2 {\Phi_0}^2}{KL^2\sqrt{\rho\gamma R_{jet}}} = 2.5 \pm 0.2 \times 10^{-8} \tag{2.3}$$

The absence of the solution zero-shear viscosity in Equation 2.3 suggests

that η_0 by its own is insufficient to predict the fiber diameter. The solution conductivity, process parameters and surface tension are also needed to describe the diameter of electrospun fibers [81], as stated in section 2.4. Moreover, the viscosity term is embedded within the mass fraction of the polymer in solution w_s in the R_{jet} term. Finally, Equation 2.3 can be validated by the observations from the correlation matrix and scatter plots as the same parameters are present in both analyses with the same proportional relationship.

Chapter 3

Selection of Compatible Polymer-Solvent Combinations for Near-Field Electrospinning and Pyrolysis

Zhenan Bao et al. [155] investigated the effect of the polymer chemical structure (the effect of benzene rings) on the morphology, dimensions, composition, graphitization degree, crystallinity, and electrical conductivity of graphene nano-ribbons derived from four different types of electrospun polymers as templating agents. The authors studied four polymers polystyrene (PS), poly(vinyl alcohol) (PVA), polyvinylphenol (PVP), and a phenolic resin known as Novolac. See Figure 3.1. The authors created electrospun polymer fibers out of the four selected polymers. PVP, Novolac and PVA have hydroxyl groups that can be functionalized with metal cations, while PS does not have such binding capability. On the other hand, PVP and Novolac have one benzene ring in each repeating unit, wheras PVA is mainly made out of sp3-hybridized carbon.

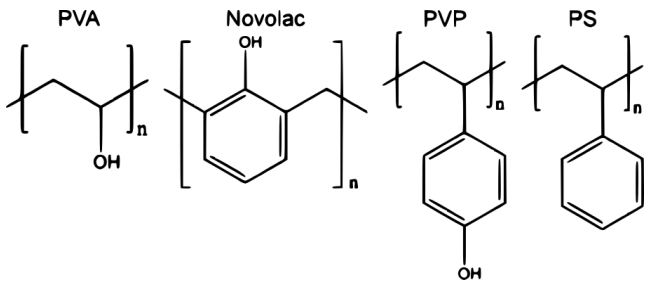

FIGURE 3.1: Studied Polymers by Zhenan Bao et al. [155]

Zhenan Bao et al. [155] found that higher sp2 carbon content (or more benzene rings) in the polymer chemical structure translates into higher graphitization degree and higher electrical conductivity in the final carbon

structures. This finding can be use as a guide when choosing polymer precursors for the fabrication of carbon structures. Furthermore, the authors posit that polymers with functional OH groups are required for the creation of smooth and continuous fibers throw electrospinning. [155]

3.1 Selection of Candidate Spunable Polymer Solutions

Given the conclusions from Zhenan Bao et al. [155] along with the extensive literature review and data analysis of Chapter 2, the following polymer-solvent combinations were selected to be studied in this work. Polymer selection was based on the their high carbon content and presence of benzene rings. The purpose of the polymer selection is to focus the efforts to maximize the likelihood of polymers to yield carbon structures with high electrical conductivity and a higher degree of graphitization as compared to the previously used SU-8/PEO combination in cyclopentanone; as testing every possible polymer-solvent system is not a practical way to carry on this research. Figure 3.2 lists the polymers that are going to be investigated along with their proposed solvents. The selected polymers have been electrospun via far-field electrospinning for the fabrication of fibrous mats [156, 158, 269], but no records of being spunable by NFES.

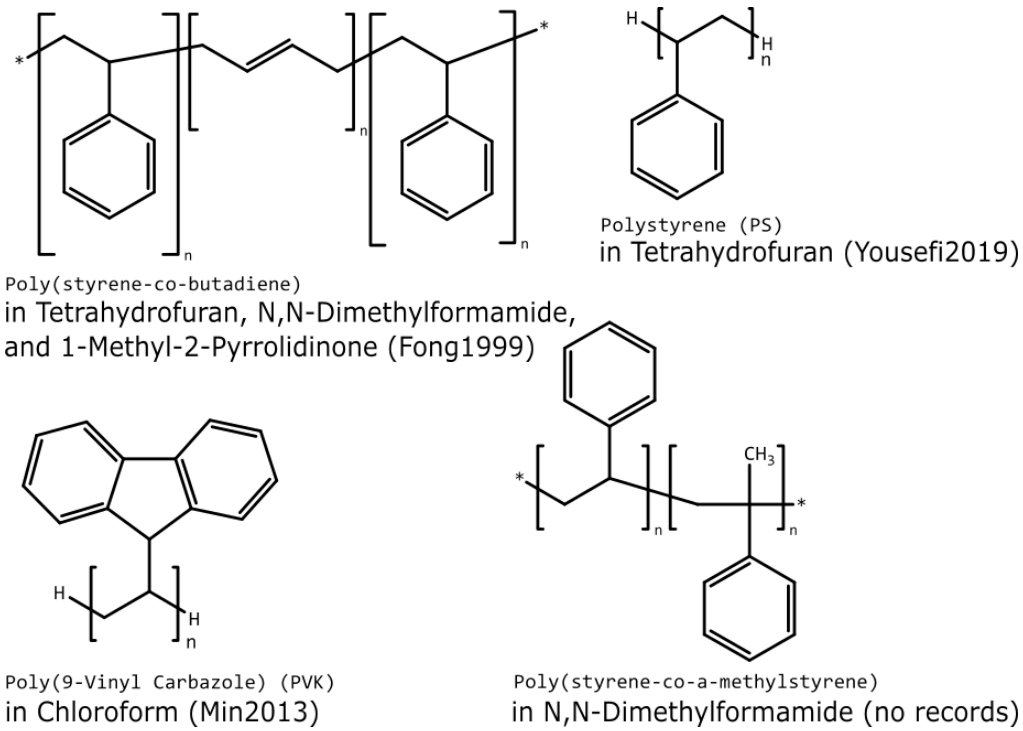

FIGURE 3.2: Selection of Polymer-Solvent Systems to Investigate in this Work. [156, 158, 269]

3.2 Rheology of candidate polymer solutions

As stated in previous sections, near-field electrospinning requires the control of several parameters to obtain fibers with the desired properties. One of the main parameters are related to the polymer precursor such as molecular weight and its concentration in solution. The evaluation of polymer chain entanglements is an effective way to address the spunability of a polymer-solvent system. [270] Polymer concentration and molecular weight are the main factors in determining the entanglement degree between polymer chains.

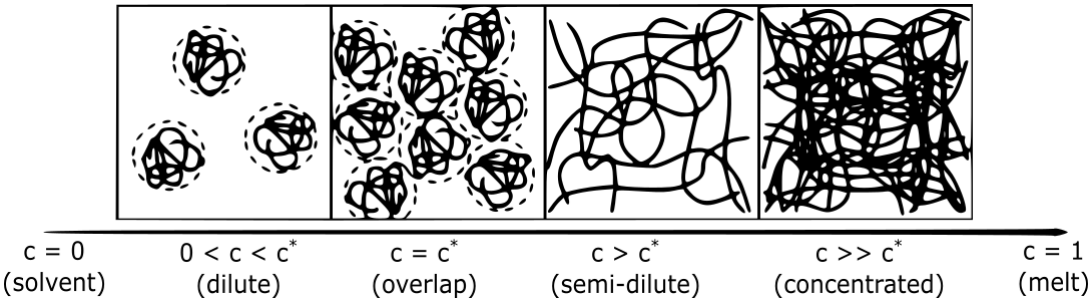

FIGURE 3.3: Effect of the polymer concentration on the structure of polymer chains in solution. Adapted from [271]

Solutions at low concentrations do not allow polymer chains to entangle, leading the viscoeslasticity of the solution dependent only on the interaction of individual polymer chains. As the polymer concentration increases, the chains overlap and becomes entangled. The concentration at which the entanglement initially takes place is the critical concentration c^*. Concentrations above the critical concentration c^* generate a fast increase in chain entanglement (Figure 3.3). This rapid change in chain entanglement is translated into a fast increase in the viscosity of the solution. Figure 3.4 illustrates the relationship between polymer concentration and viscoelasticity. [255, 271]

Electrospinning of smooth, continuous fibers require a polymer concentration equal or higher than the critical concentration. As shown in Figure 3.4, the critical concentration can be estimated from the change in slope of the log-viscosity to log-concentration curve. [142, 255, 271] Therefore, in order to find the critical/spinnable concentrations of the candidate polymer-solvent solutions (poly(styrene-co-butadiene) in tetrahydrofuran, poly(9-vinyl carbazole) in chloroform, polyestyrene in tetrahydrofuran, and poly(styrene-co-a-methylstyrene) - See Figure 3.2), it

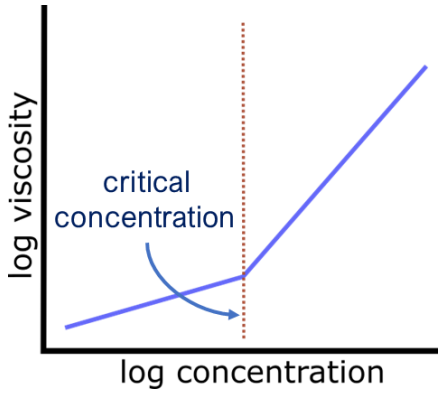

FIGURE 3.4: Effect on solution viscosity, polymer concentration and spinnability. Adapted from [142, 255, 271]

is necessary to build the appropriate viscosity vs. concentration plots as described in the following sections.

3.2.1 Materials and Sample Preparation

Seven polymer-solvent combinations are to be tested. The Poly(Ethylene Oxide) and SU-8 2002 combination is what has been used in previous work [11, 13], and will be used as the control sample set. The selected polymer-solvent combinations were selected to investigate the ability of oxygenless polymers to be electrospun and then carbonized into vitreous carbon. Tables D.1, 3.3, 3.4, 3.5, 3.2, 3.6, and 3.7 list the prepared polymer systems. Tetrabutylammonium tetrafluoroborate (TBF) was added to all solutions to increase the conductivity of the solution. SU-8 contains 71% of cyclopentanone (CPO), which acts as the solvent (Figure 1.7) [76].

TABLE 3.1: Poly(Ethylene Oxide) and SU-8 2002 : Sample Preparation

Sample	**Weight Percent** *wt%*		
	SU-8	**PEO**	**TBF**
1	99.50	0.00	0.50
2	99.25	0.25	0.50
3	99.00	0.50	0.50
4	98.75	0.75	0.50
5	98.50	1.00	0.50
density [g/ml]	1.123		

TABLE 3.2: Polystyrene in Tetrahydrofuran : Sample Preparation

Sample	**Weight Percent** *wt*%		
	THF	**PS**	**TBF**
6	99.25	0.25	0.50
7	94.50	5.00	0.50
8	89.50	10.00	0.50
9	84.50	15.00	0.50
10	79.50	20.00	0.50
11	69.50	30.00	0.50
12	64.50	35.00	0.50
13	59.50	40.00	0.50
density [g/ml]	0.888		

TABLE 3.3: Poly(Styrene-co-Butadiene) in 1-Methyl-2-Pyrrolidinone : Sample Preparation

Sample	**Weight Percent** *wt*%		
	NMP	**PSB**	**TBF**
14	98.50	1.00	0.50
15	95.50	4.00	0.50
16	91.50	8.00	0.50
17	87.50	12.00	0.50
density [g/ml]	1.027		

TABLE 3.4: Poly(Styrene-co-Butadiene) in Tetrahydrofuran and N,N-Dimethylformamide : Sample Preparation

Sample	**Weight Percent** *wt*%			
	THF	**DMF**	**PSB**	**TBF**
18	70.87	23.63	5.00	0.50
19	69.00	23.00	7.50	0.50
20	67.12	22.38	10.00	0.50
21	65.25	21.75	12.50	0.50
22	63.37	21.13	15.00	0.50
23	59.62	19.88	20.00	0.50
24	55.87	18.63	25.00	0.50
density [g/ml]	0.888	0.950		

TABLE 3.5: Poly(Styrene-co-alpha-Methylstyrene) in N,N-Dimethylformamide : Sample Preparation

Sample	**Weight Percent** *wt%*		
	DMF	**PSMS**	**TBF**
25	99.00	0.50	0.50
26	94.50	5.00	0.50
27	89.50	10.00	0.50
28	84.50	15.00	0.50
density [g/ml]	0.950		

TABLE 3.6: Poly(9-Vinylcarbazole) in Chloroform : Sample Preparation

Sample	**Weight Percent** *wt%*		
	CHL	**PVK**	**TBF**
29	99.50	0.00	0.50
30	99.49	0.01	0.50
31	84.50	15.00	0.50
32	79.50	20.00	0.50
33	69.50	30.00	0.50
density [g/ml]	1.492		

TABLE 3.7: Poly(9-Vinylcarbazole) and SU-8 2002 : Sample Preparation

Sample	**Weight Percent** *wt%*		
	SU-8	**PVK**	**TBF**
34	99.50	0.00	0.50
35	99.495	0.005	0.50
36	98.75	0.75	0.50
37	94.50	5.00	0.50
38	79.50	20.00	0.50
density [g/ml]	1.123		

SU-8 2002 was obtained from MicroChem (Newton, MA, USA), while Tetrabutylammonium Tetrafluoroborate (TBF) of 99% purity were, Poly(Ethylene Oxide) (PEO), Polystyrene (PS), Poly(Styrene-co-Butadiene) (PSB), Poly(Styrene-co-alpha-Methylstyrene) (PSMS), Poly(9-Vinylcarbazole) (PVK), Tetrahydrofuran (THF), 1-Methyl-2-Pyrrolidinone (NMP), N,N-Dimethylformamide (DMF), and Chloroform (CHL) were obtained from Sigma-Aldrich (Saint Louis, MI, USA). PEO has a viscosity-average molecular weight Mw of 4,000,000, with less than 1000 ppm of Butylated Hydroxytoluene (BHT) as an inhibitor. PS has an average molecular weight Mw of 192,000. PSB has a melt index of $6\text{g}/10\text{min}(200^{\circ}C/5\text{kg})$, where the butadiene comprises 4 $wt\%$ PSMS has a melt viscosity of $10\text{Pa}\cdot\text{s}$ at $161^{\circ}C$. PVK has an average molecular weight Mw of 1,100,000 in powder form. THF is anhydrous and contained no inhibitor with 99.9% purity. NMP is anhydrous with 99.5% purity. DMF is anhydrous with 99.8% purity. CHL has 99.5% purity, a melting point of $-63^{\circ}C$, boiling point of $60.5^{\circ}C$, and a density of $1.492\text{g}/\text{ml}$ at $25^{\circ}C$. CHL contains between 100 to 200 ppm amylenes as stabilizer. SU-8 is a high contrast, epoxy-based negative photoresist. All of the reactants were used as received.

Samples of 3 milliliters were prepared with the adecuate amounts of polymer, salt and solvent. Solutions were stired at 160 rpm for 2 hours at $60^{\circ}C$. Samples with higher polymer concentrations often required more stirring time to eliminate all polymer aggregates. All solutions were left undisturbed for 3 hours in 4 ml vials to eliminate bubbles from the solution.

3.2.2 Rheological Characterization of polymer Solutions

All of the rheological tests were performed in a rotational rheometer (Discovery Hybrid Rheometer DHR, TA Instruments) equipped with a cone-and-plate (CP) geometry (diameter of 60 mm, angle of 0.9969°, and truncation of 23 μm) in a steel Peltier plate (Figure 3.5a). The experiments were conducted at $20^{\circ}C$ and 3 hours after polymer solution preparation. Flow curve (FC) tests were conducted to obtain viscosity curves as a function of the shear rate. Analysis were performed at shear rate range from $10^{-3}\,1/\text{s}$ to $10^{4}\,1/\text{s}$. A solvent trap cover (Figure 3.5f) and solvent trap geometry (Figure 3.5a) were used to create a thermally stable vapor barrier, virtually eliminating any solvent loss during the rheological experiments and improving temperature uniformity. Distilled water was used to create a seal between the CP geometry and the solvent trap cover (Figure 3.5e).

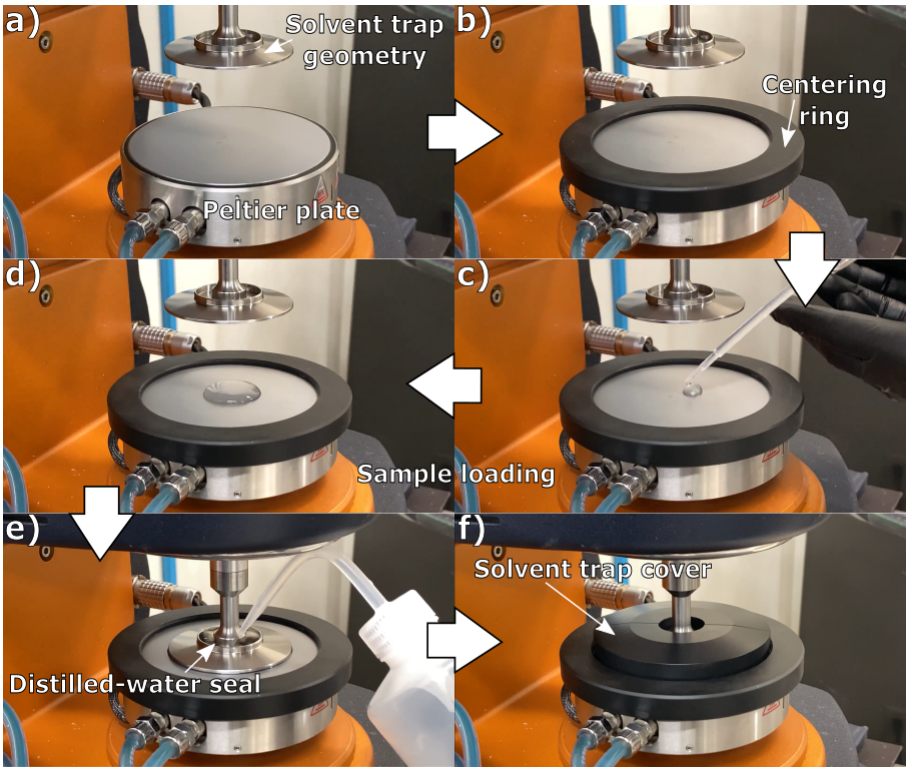

FIGURE 3.5: Rheometer - Solvent Trap Setup

Flow curves determine the flow behaviour of a sample by measuring the viscosity as a function of shear rate. For shear rates under $10^{-2.25}$ 1/s the rheometer was unable to take viscosity measurements, on the other hand for shar rates over $10^{-3.5}$ 1/s the measurements are discarded. At high shear rates, several factors such as inertial effects, and viscous heating can alter the rheometric measurements [272, 273]. As the shear rate increases, the centrifugal stresses become large enough to overcome the surface tension stresses that keep the sample within the gap between the geometry and the plate. High centrifugal stresses result in the sample being thrown out of the measuring area; a phenomenon known as 'radial migration effect' [274]. Once the 'radial migration effect' partially ejects the sample, the viscosity measurements are lower than expected due to a drop in torque. [275]

As depicted in the rheological results in Figures A.1, A.2, A.3, A.4, A.5, A.6 and A.7, the constant-viscosity (Newtonian-like) behavior before the shear thinning onset was captured. In all samples, a noticeable shear-thinning behavior is observed with an increase in viscosity with concentration increments. The shear-thinning behavior can be interpreted as the alignment of polymer chains to the flow in the direction of the applied shear stress.

[276] The Carreau–Yasuda model (Equation 3.1) [272] was fitted to the cone-and-plate measurements to compute the zero-shear viscosity of each sample.

$$\eta = \frac{\eta_0 - \eta_\infty}{\left[1 + (\kappa\dot{\gamma})^a\right]^{\frac{(1-n)}{a}}} + \eta_\infty \tag{3.1}$$

Where: η is the viscosity, $\dot{\gamma}$ the shear rate, η_∞ the infinite shear rate viscosity, η_0 the zero shear rate viscosity, κ is the time constant, n the Power Law index, a the width of the transition region between the zero shear viscosity and the Power Law region. The features of the flow curves shown in Appendix A can be modeled using the Carreau-Yasuda model, with the benefits that it is possible to describe the shape and curvature of a flow curve through six fitting parameters and to predict behavior at unmeasured shear rates. The Carreau-Yasuda model is most applicable model due to the range of the measured data. Unlike the Sisko and Williamson models, the Carreau-Yassuda model considers both the infinite- and zero-shear rate viscosities.

The Carreau-Yasuda model was fitted to the rheologial data to estimate η_0. Then, η_0 values are used to create diagrams that describe the effect of polymer concentration on the solution viscosity, as described in Figure 3.4. The critical concentrations are calculated from the change in slope in the zero-shear viscosity to concentration relationship as depicted in Figure 3.6 for the PEO in SU-8 solutions. Appendix B contains the diagrams of the other polymer-solvent systems.

TABLE 3.8: Calculated Critical/Spinnable Concentrations for each Polymer-Solvent System

Polymer	**Molecular Weight** $[\mathbf{g \cdot mol}]$	**Solvent**	$c^*[\mathbf{wt\%}]$	$\eta_0[\mathbf{Pa \cdot s}]$
PEO	4,000,000	CPO (SU-8)	0.25	60.022
PS	192,000	THF	20.00	0.166
PSB	490,000 [277]	NMP	8.00	0.028
PSB	490,000 [277]	THF and DMF	15.00	0.092
PSMS	2,658,076 [278]	DMF	5.00	0.282
PVK	1,100,000	CHL	15.00	41.861
PVK	1,100,000	CPO (SU-8)	0.75	49.657

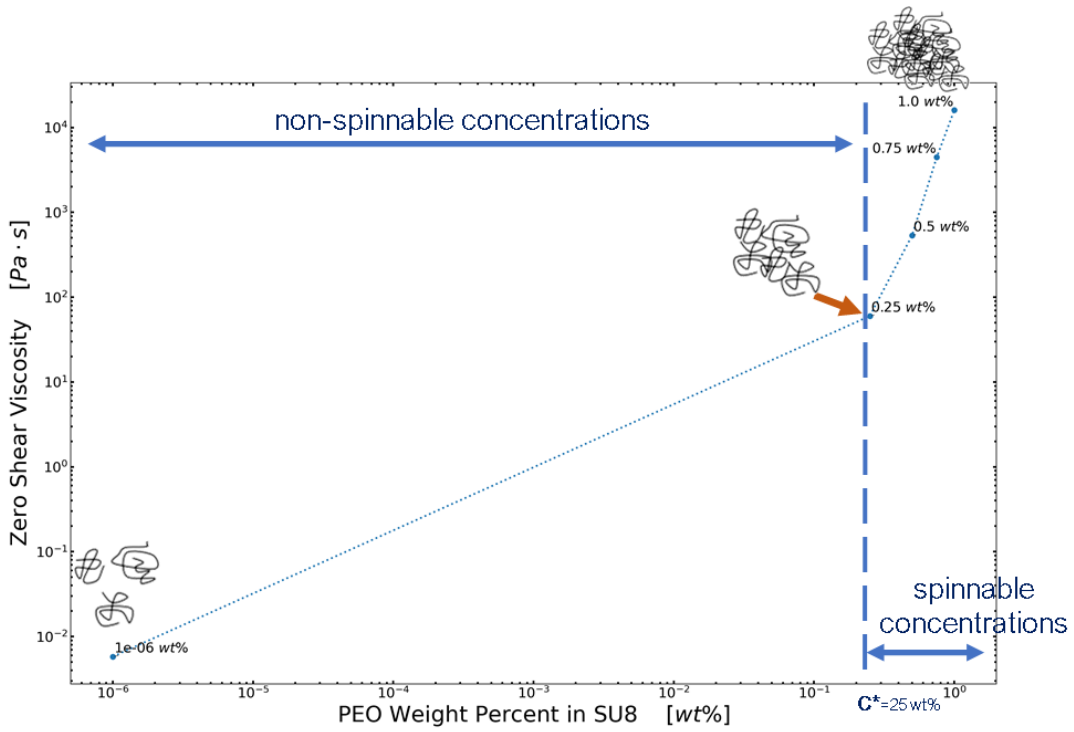

FIGURE 3.6: The change in slope is given at 25 *wt*% PEO, which suggests that at 25 *wt*% the polymer chains are entangled.

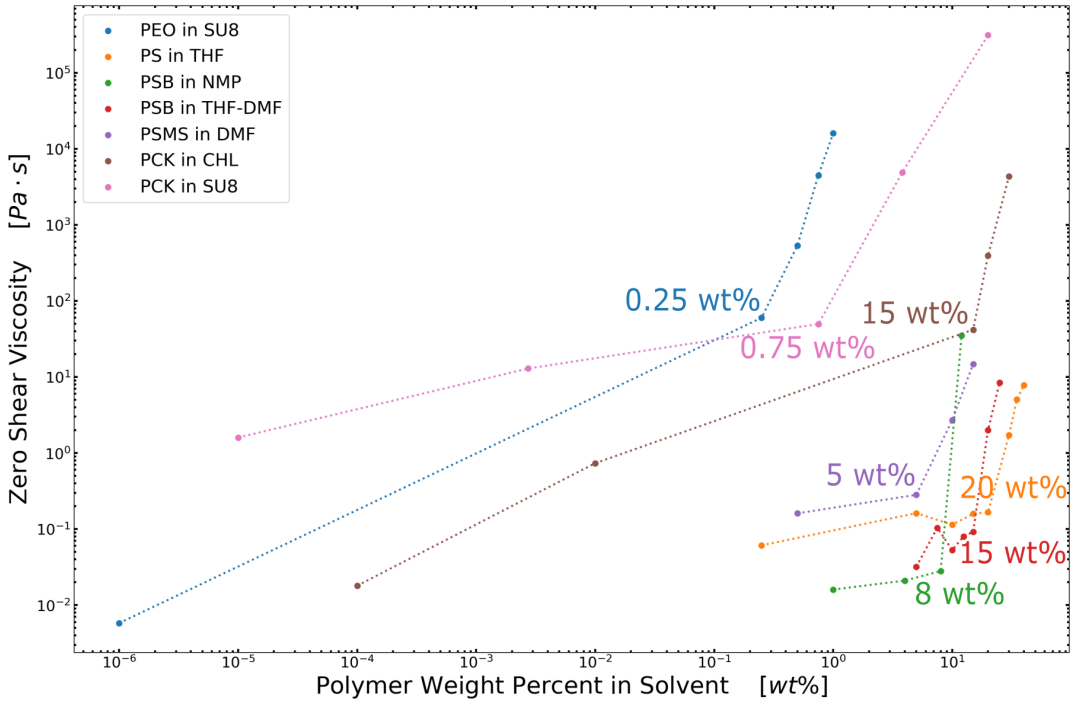

FIGURE 3.7: Estimation of the Critical Concentration of the Candidate Polymer-Solvent Combinations. Individual plots are available in Appendix B

Table 3.8 was built from Figure 3.7, and summarizes the calculated critical concentrations for each system. In general, the critical concentration c^* has a directly proportional relationship with the polymer molecular weight, as a polymer's molecular weight greatly influences the solution viscosity. First, the structure of the polymer chain has an effect on its solubility as the inter-molecular interactions between long molecules are stronger and the solvent molecules take longer to diffuse within the polymer aggregates. [67, 276] Second, the viscosity of a polymer solution will be smaller when a polymer of low molecular weight is dissolved than a solution of the same polymer but of a higher molecular weight. [67] The molecular weight of the polymer describes the length of the polymer chain, which has an effect on the viscosity of the solution. Since the polymer length defines the amount of entanglement of the polymer chains in the solvent, a lower molecular weight shall be compensated by higher concentrations to reach the desired viscosity, see Figure 3.8.

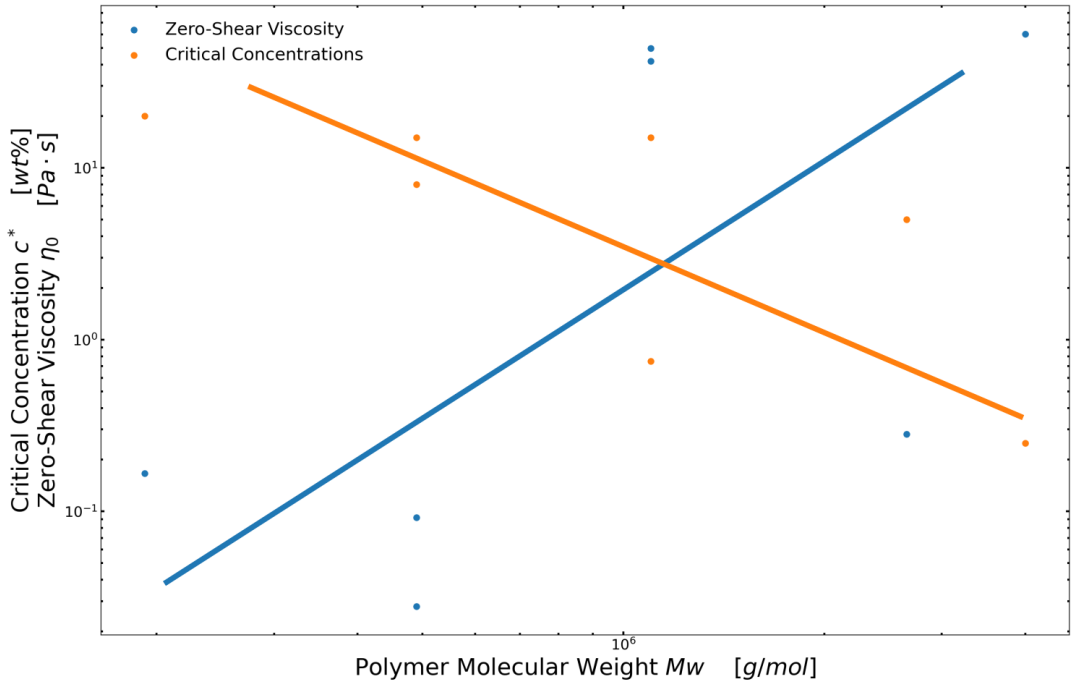

FIGURE 3.8: Relationship between the critical concentrations, molecular weights, and zero-shear viscosities of the selected polymer solutions.

Chapter 4

Fabrication and Characterization of Polymeric Fibers through Near-Field Electrospinning

The fabrication and characterization of polymeric fibers is addressed in this chapter as the last screening procedure to select the PEO/SU-8 replacement. The PEO/SU-8 replacement is to produce microscopic polymer fibers with potential for the fabrication of carbon nano-wires. This chapter reports PEO, PS, PSB, and PVK micro-fibers fabricated by low-voltage near-field electrospinning. The fabrication process is carried on to study the influence of applied voltage on the fiber diameter. The materials and sample preparation for the LV-NFES process are the same as those used in the rheological analyses in Chapter 3.

4.1 Near-Field Electrospinning Setup

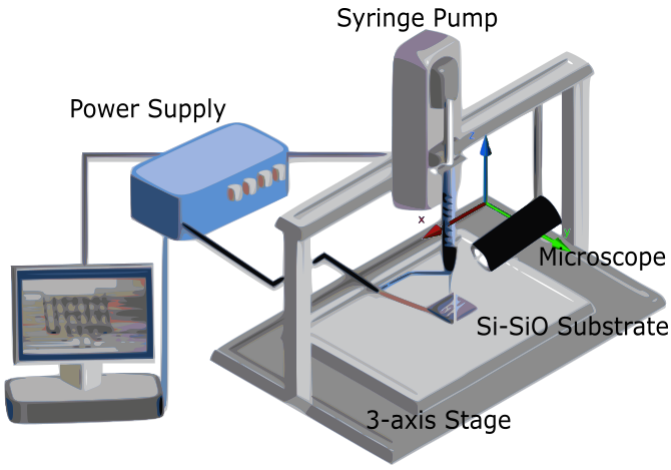

FIGURE 4.1: NFES experimental setup. Adapted from [276]

The near-field apparatus (Figure 4.1) is comprised by a high voltage supply (HVS448 3000 V, LabSmith, Livermore, CA, USA), a three-axis stage, syringe pump (Pump 11 Elite, Harvard Apparatus, Cambridge, MA, USA). Samples were prepared as per the rheology measurements in Chapter 3. Experiments were conducted with 1 milliliter slip-tip insulin syringes with 21 gauge precision tips (Nordson Engineered Fluid Dispensing, Westlake, OH, USA). The power supply and 3-axis stage are controlled through a desktop computer, while the syringe pump is controlled manually. Fiber depositions were placed on a $Si - SiO_2$ wafer. The voltage between the nozzle tip and the collector was varied between 200[V] and 600[V] in increments of 100[V], keeping a constant current of 10 μA. For applied voltages under 400[V], the electric field was not strong enough to overcome the surface tension of the polymer solution and initiate the jet. To enable the fiber deposition at low voltages, the polymer jet was manually initialized by breaking the surface tension with a sharp glass tip. The working distance L and stage velocity was set at a constant values for all the experiments at $0.5mm$ and $10mm/s$ respectively. The syringe pump was set at a steady flow rate of 0.04μL/min.

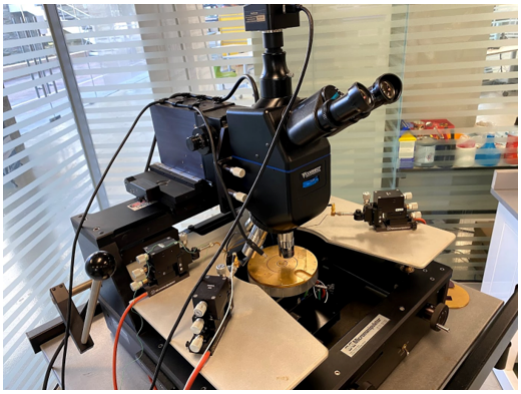

FIGURE 4.2: Correct, Seiwa Optical - Optical Microscope

The applied voltage range was set in a range between 200[V] and 600[V], since within that range fibers were able to electrospun into continuous and straight fibers. As shown in Figure 4.3, PEO/SU-8 fibers are produced with a meander morphology when the applied voltage is around 900[V]. Under 600[V], straight and aligned fibers were fabricated and characterized.

The calculated critical concentrations in Chapter 3 (Table 3.8) are used for the fabrication of polymeric fibers. One set of experiments was conducted for each polymer-solvent system to study the effect of applied voltage on fiber diameter. The morphology of the fibers was characterized with an

optical microscope (Correct, Seiwa Optical, Dallas, TX, USA, Figure 4.2). Each sample was measured at 30+ points within the microscope field of view (Appendix C).

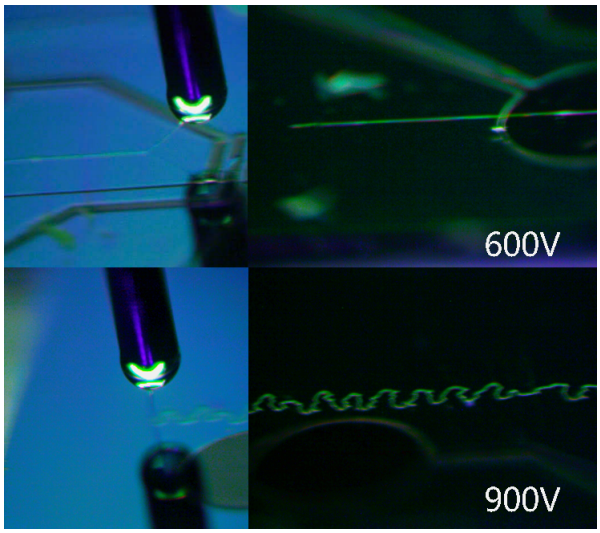

FIGURE 4.3: Effect of applied voltage in fiber morphology

4.2 Results

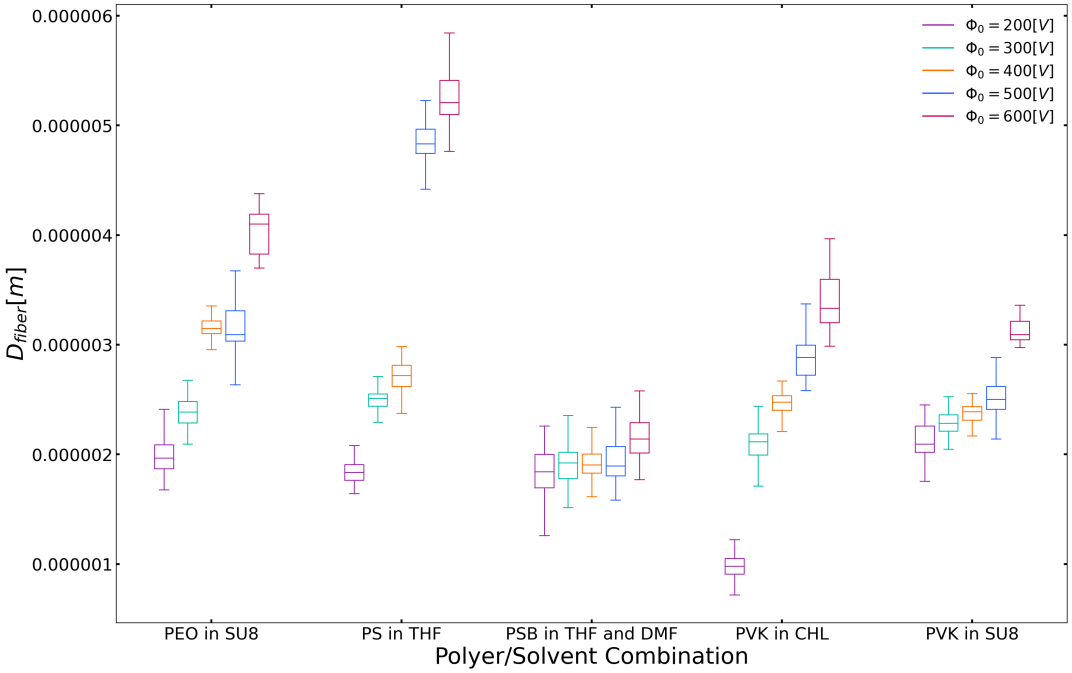

FIGURE 4.4: Diameter of fibres for all the experiments with varing applied voltage Φ_0. Appendix D

Figure 4.4 shows a dependence of fiber diameter as a function of the applied voltage and confirms what was already noticed in the correlation

matrix and the adimensional analysis in Chapter 2, as lower voltages yield fibers with thinner diameters. This results verify the electro-spinnability of oxygen-less polymers by NFES into fibers of $1\mu m$ to $5\mu m$ in diameter. PS presented complications during the NFES process as fibers of this polymer do not adhere onto the substrate making them prone to fracture or substrate abandonment, specially when printing fibers of thin diameters. To ease this complication the working distance L can be reduced to let the fibers dry on the surface and prevent complete solidification while traveling the distance L. The increase in applied voltage can also help with this problem as more material is pulled out of the dispensing needle, however this two fixes will translate into thicker fibers.

The effect of applied voltage on fiber diameter can be contributed to the effect of the electric field on the surface tension of the polymer solution drop. Bateni and coworkers [279] have shown that surface tension increases with increasing applied voltage. Bateni also states that the effect of an electric field is stronger on alcohols with higher molecular weights [279]. Bateni's findings agree with Zhenan Bao's statements regarding polymers with OH functional groups are more easily electrospun than those without functional groups [155, 279]. Since the tested polymers are of different molecular weights, the effect of applied voltage is more significant in the PEO/SU-8 formulation as PEO has the highest molecular weight. On the other hand, the PSB in THF and DMF solution was the least affected by changes in applied voltage as PSB has the smallest molecular weight. Disregarding the molecular weight, the PS formulation has higher variation in fiber diameter. This outcome can be explained by the poor adhesion of the fibers to the substrate, as explained above. The effect of the applied voltage between the two PVK samples present some differences. The PVK in CHL solution has a stronger reaction to the electric field than the PVK in SU-8 formulation. This difference can be attributed to the fact that SU-8 is comprised by a series of monomers of low molecular weight.

The PVK and CHL system was the one that behaved with more similarity as the control sample of SU-8 and PEO. Uniform, 700 nm diameter fibers were achieved with PVK and CHL at the lowest voltage setting (200 V). Given the similarities with the control sample, PVK was choosen to replace the PEO to increase the spinnability of SU8. Therefore, the PVK in SU-8 system was tested in the same conditions as the previous experiments. Both polymers

(PEO and PVK) in SU-8 yield parallel results in fiber morphology and in electrospinning preformanc. However, at high voltages, the PVK solution produced thinner fibers than those produced by the PEO solution. Moreover, as PVK does not contain any additional oxygen content in its structure, adding PVK can be a better alternative to electrospun SU-8 based fibers intended for carbonization as thinner fibers will have better opportunities to survive the pyrolysis process without breaking.

On the other hand, the polymer-solvent systems comprised by Poly(Styrene-co-Butadiene) (PSB) in 1-Methyl-2-Pyrrolidinone (NMP) and Poly(Styrene-co-alpha-Methylstyrene) (PSMS) in N,N-Dimethylformamide (DMF) were unable to yield fibers. In the case of the PSB/NMP solutions, a hard shell was formed around the polymer drop at the tip of the nozzle preventing the jet to initiate, which causes clogging. Seems that rapid volatilization of NMP is not the case as PSB was successfully electrospun with more volatile solvents (THF and DMF). Notice that vapor pressure of NMP is around 39Pa at $25^{\circ}C$, THF and DMF have vapor pressures of about 19.3kPa at $20^{\circ}C$ and 0.49kPa at $25^{\circ}C$ respectively. [280] On the other hand, PSMS in DMF was not able to produce fibers as the jet was not initiated. After noticing that que calculated critical concentration c^* is not spinnable the solutions of 10 and 15 $wt\%$ were also tested in the NFES apparatus with no success. The cause of the non-spinnable nature of PSMS can be laid on the fact that PSMS pellets were brittle and capable of making fine PSMS dust with ease, unlike PS and PSB pellets which have an elastic behavior.

Chapter 5

Concluding Remarks

5.1 Conclusions

As stated within the introductory chapter 1, this thesis is to verify the near-field electrospinnability of high-carbon oxygen-less polymers in solution. The spinnability of the tested solutions is used as a screening to choose candidate formulations that can replace the PEO in SU-8 solution. A near-field electrospinning literature review was used to learn about the effect of the process parameters and solution properties in the control of the fiber diameter. The review analyses (data analysis, parameter correlation, and adimensional analysis) declare that the polymer concentration is the parameter with the biggest impact on the fiber diameter, followed by the applied voltage, the working distance, and the zero-shear viscosity.

Rheological analyses were performed to determine the viscoelastic properties of the candidate polymer solutions. Zero-shear viscosities of the solutions in interest are measured to find solutions with spunable polymer concentrations. As explained in the following, viscosity and polymer concentration have a significant impact on the spinnablity of polymer solutions, but they are not sufficient by themselves. As demonstrated by the experiments to fabricate fibers through NFES, PSMS in DMF and PSB in NMP formulations were not spinnable at their critical concentrations.

A series of experiments were carried out in order to find a correlation between the rheological properties of different polymer solutions in near-field electro-mechanical spinning for carbon structures. Flow curve measurement tests where carried out in an oscillatory rheometer to estimate the critical concentrations of various polymer-solvent systems at which they

are spinnable by NFES. Since the formulation is 0.25 $wt\%$ PEO in SU-8 2002 has been studied in the past and is known to yield good polymer solutions but fails at the pyrolysis, this work intends to find spinnable and pyrolyzable systems as well as a method to discover new spinnable polymer solutions.

From the flow curve measurements, the zero-shear viscosity was estimated using the Carreau-Yassuda model. For all solutions, a shear thinning behavious was noticed. It was found that the viscosity-concentration plot is a good method to find the critical concentration at which the solution is able to produce fibers through NFES. However the method failed at calculating the spinnable concentration of PSMS. An significant takeaway is that a polymer does not have elastic properties in the pellet form, it will probably not work as a NFES polymer precursor.

Fibers were fabricated at different applied voltages for each set of solutions in order to very that in NFES fiber diameter increases with increasing applied voltage, whereas the inverse relationship is true for FFES. Other parameters such as working distance, stage velocity, nozzle diameter, flow rate were kept constant for all experiments; however, for low applied voltages the jet shall be initialed by manually breaking the polymer drop. the thickest average fiber diameter was achieved with the PS in THF system ($\Phi_0 = 600V$, $D_{fiber} = 5.304\mu m$) and the thinnest was $0.976\mu m$ using the PVK in CHL system and an applied voltage of $200V$. It was proved that attainable rehological information can be used to modify the NFES process parameters to yield the desired fiber morphology.

Moreover a data analysis was done on the NFES publications of the last 13 years to identify relationships between fiber diameter and the process parameters. For instance, it was confirmed that thin fibers are achived with los polymer concentrations, small nozzle diameters, low applied voltage, slow flow rates and high stage velocities. Also, using the collected data and the input of Helgeson's work [81], an dimensionless analysis was done to predict fiber diameters with easy to get parameters.

Finally, the fabricated fibers can be classified into three groups: a) the control sample (PEO in SU-8); b) poor quality fibers (PS in THF, and PSB in THF and DMF); and c) good quality fibers (PVK in CHL and PVK in SU-8). PS and PSB fibers have rough textures and low adhesion to the collector substrate. The rough surface and low adhesion is due to the rapid solvent volatilization,

which results in fibers to solidify before landing on the substrate. The fast solidification minimize the fiber adhesion to the collector, causing the fibers to slip, and therefore the mechanical drag force in the fibers is reduced. Due to the low influence of the mechanical force, fibers are not stretched by the moving stage, which may explain the rough surface.

On the other hand, the formulation regarding PVK deposited smooth fibers with good adhesion to the substrate, similar to the PEO/SU-8 solution. The thinnest fibers (700 nm in diameter) were achieved PVK in CHL formulation. Moreover, the PVK in SU-8 solution seems to be the formulation to replace the PEO in SU-8 solution. Assuming that the additional oxygen content in PEO negatively affects the fiber yield rate and electrical resistivity variance due to degassing during pyrolysis, the PCK does not contain additional oxygen content and has sp2-hybridized carbon which can promote the formation of graphitic carbon during pyrolysis. The already oxygen in SU-8 is necesary to create closed pores during annealing, characteristic of glass-like carbon.

5.2 Future work

Apart from the work done, this dissertation opens pending research to enable NFES for the fabrication of carbon structures. The following lists future work that could be done as a continuation of this thesis.

- Helgeson's model [81] was thought to work with far-field electrospinning, hence the deviation of the NFES data from the model trend. For an accurate NFES fiber diameter prediction, the mechanical stresses introduced by the moving stage shall be considered in the model (Equation 2.3).

- This work verifies the electro-spinnability of four new formulations, however fibers were not carbonized into carbon structures. Further work shall study the pyrolysis process of the proposed fibers to get carbon structures with good electrical conductivity. A photo-polymerization process could be introduced before pyrolyzation to increase the order of the molecules and achieve carbon with higher conductivity.

- Near-field electrospinning solutions require specific viscosities to

initialte a polymer jet. The viscosity-concentration plot is a helpful tool to estimate the critical spinnable concentration of a polymer-solvent system. However there is room for improvement as this method only considers reological data. Other methods could be adopted to better tune other process parameters such as stage velocity, and applied voltage.

Acronyms and Abbreviations

CEM	**C**ampus **E**stado de **M**éxico
CNWs	**C**arbon **N**ano-**w**ire**s**
DC	**D**irect **C**urrent
EMS	**E**lectro**m**echanical **S**pinning
FFES	**F**ar **F**ield de **E**lectro**s**pinning
ITESM	**I**nstituto **T**ecnonólogico y de **E**studios **S**uperiores de **M**onterrey
MA	**Ma**ssachusetts
MEMS	**M**icro**e**lectro**m**echanical **S**ystems
MNT	**M**aestría en **N**ano**t**ecnología *(Master of Science in Nanotechnology)*
MTY	**M**on**t**erre**y** *or* Campus **M**on**t**erre**y**
NFEMS	**N**ear-**F**ield **E**lectro**m**echanical **S**pinning
NFES	**N**ear **F**ield de **E**lectro**s**pinning
USA	**U**nited **S**tates of **A**merica
UV	**U**ltra**v**iolet

Variables and Symbols

Symbol	Name	Unit
Mw	Molecular Weight	g/mole
η_0	Zero-shear Viscosity	Pa · s
K	Electrical Conductivity	S/m
γ	Surface Tension	N/m
$\dot{\gamma}$	Shear Rate	1/s
ρ	Density	Kg/m^3
$C_{polymer}$	Polymer concentration	wt%
D_{nozzle}	Nozzle Inner Diameter	m
Q	Flow Rate	m^3/s
L	NFES Working Distance	m
Φ_0	NFES Applied Voltage	V
v_{stage}	Collector/Stage velocity	m/s
D_{fiber}	Fiber Diameter	m
$FiberGap$	Distance between fibers	m
R_{jet}	NFES Jet Radius	m
Oh	Ohnesorge number	NA.
Pe	Peclet number	NA.
Re	Reynolds number	NA.
We	Weber number	NA.
Ψ	Dimensionless Field Strength	NA.

Appendix A

Flow Curves

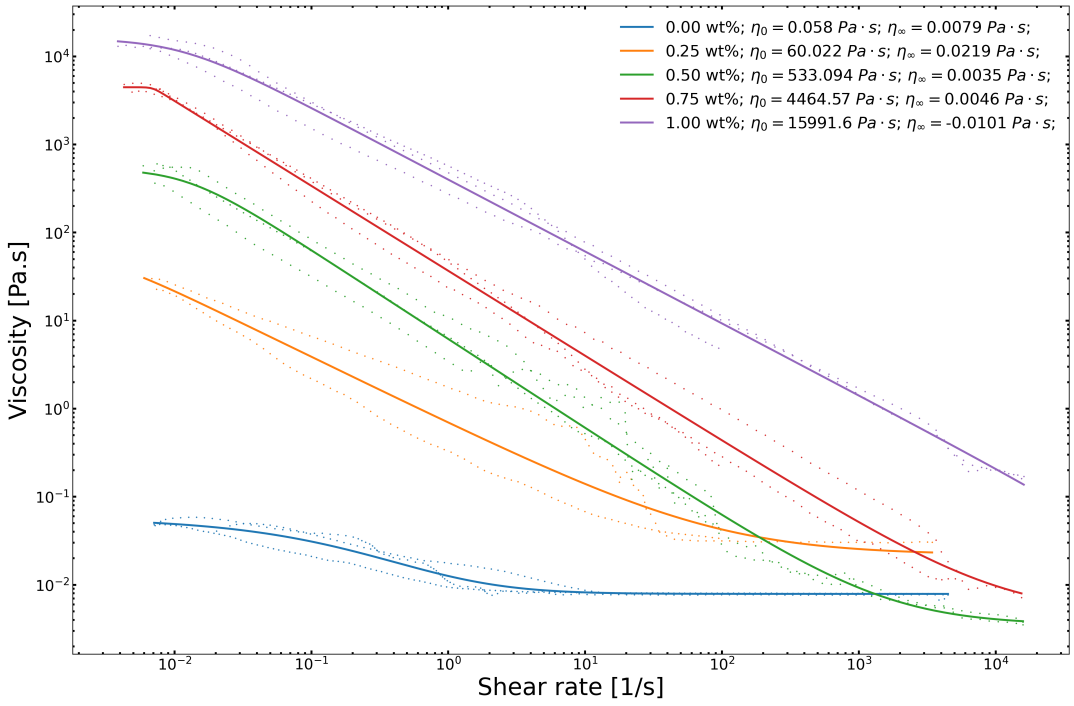

FIGURE A.1: Viscosity as a function of shear rate for Poly(Ethylene Oxide) (PEO) and SU-8 2002 solutions

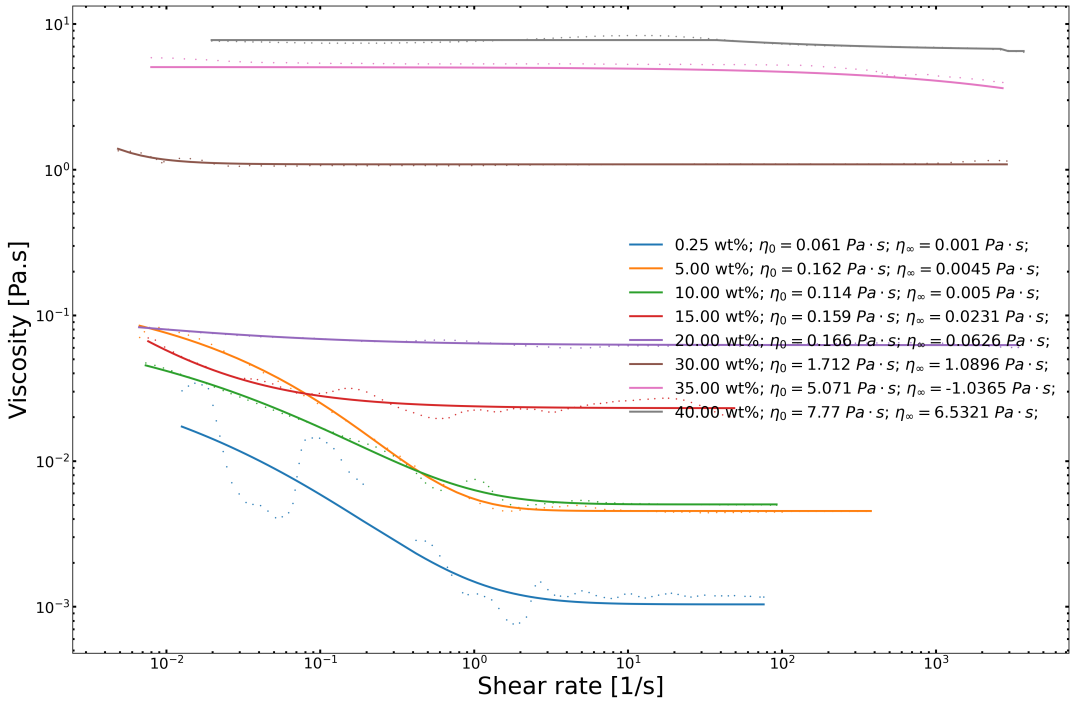

FIGURE A.2: Viscosity as a function of shear rate for Polystyrene (PS) and Tetrahydrofuran (THF) solutions

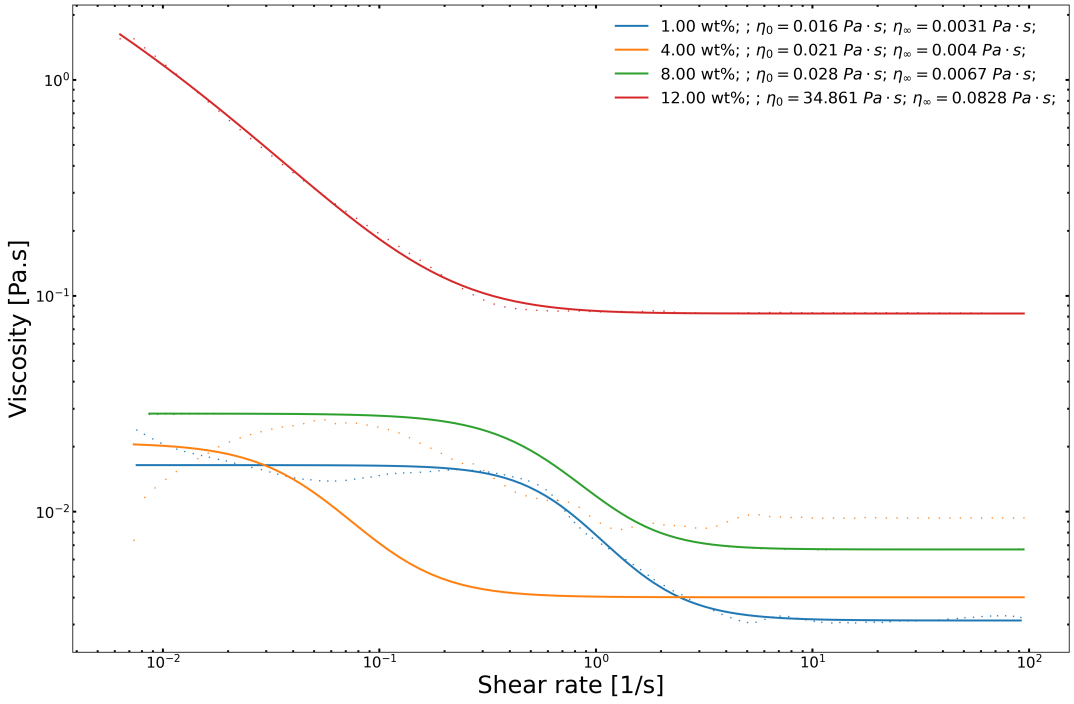

FIGURE A.3: Viscosity as a function of shear rate for Poly(Styrene-co-Butadiene) (PSB) and 1-Methyl-2-Pyrrolidinone (NMP)

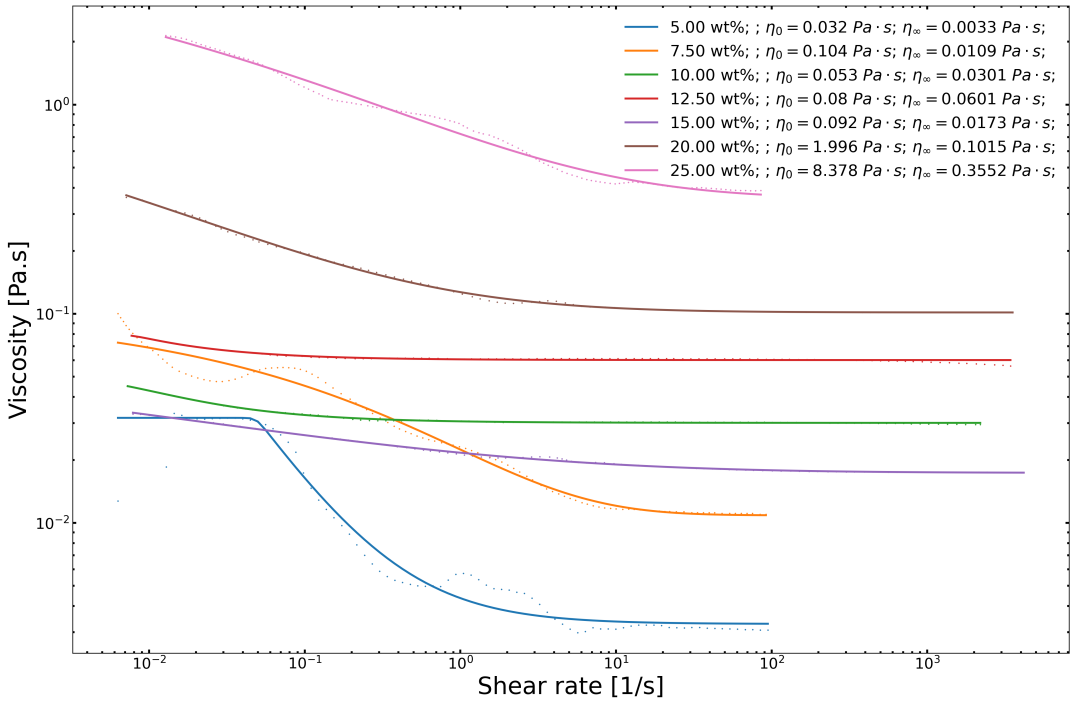

FIGURE A.4: Viscosity as a function of shear rate for Poly(Styrene-co-Butadiene) (PSB), Tetrahydrofuran (THF) and N,N-Dimethylformamide (DMF) solutions

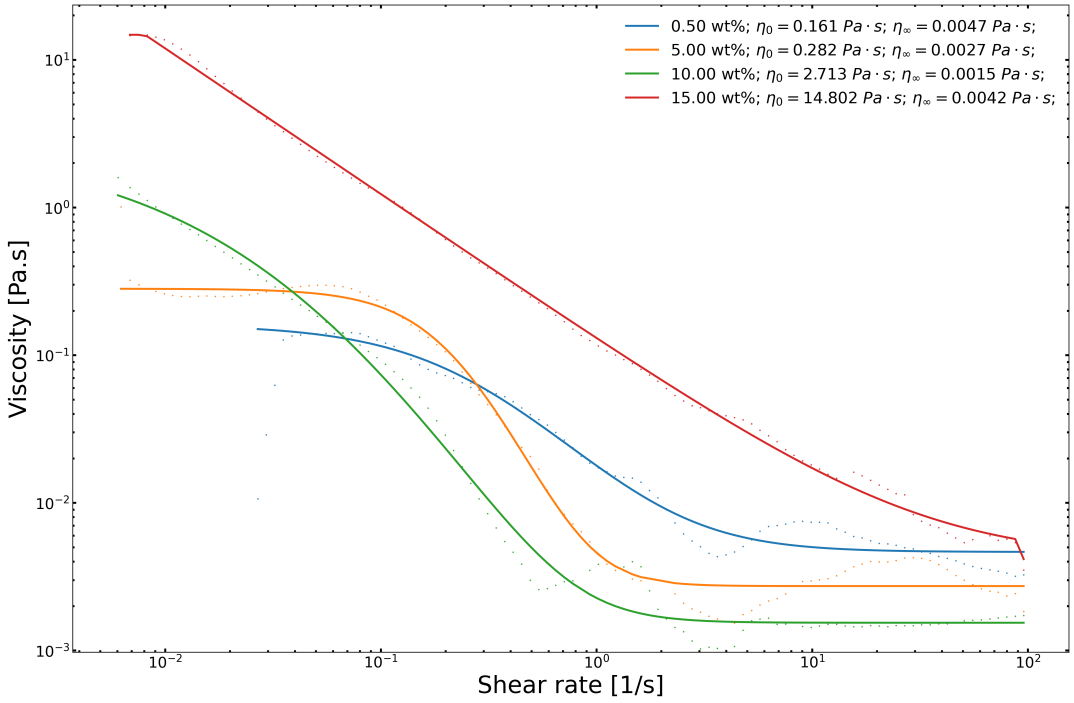

FIGURE A.5: Viscosity as a function of shear rate for Poly(Styrene-co-alpha-Methylstyrene) (PSMS) and N,N-Dimethylformamide (DMF) solutions

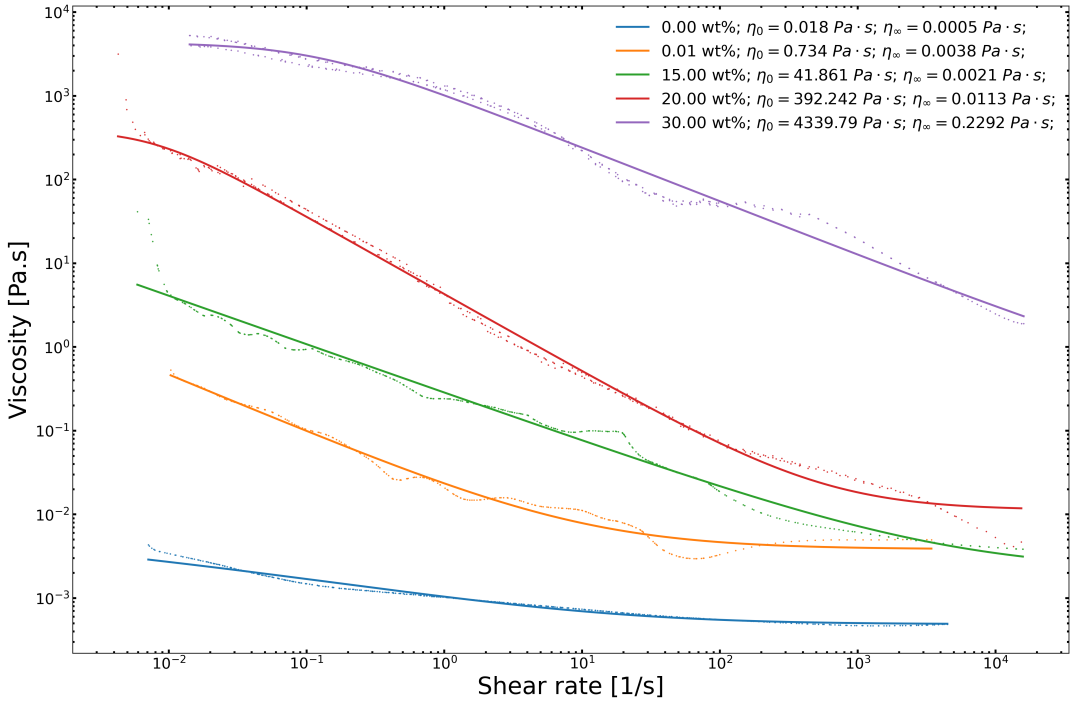

FIGURE A.6: Viscosity as a function of shear rate for Poly(9-Vinylcarbazole) (PVK) and Chloroform (CHL) solutions

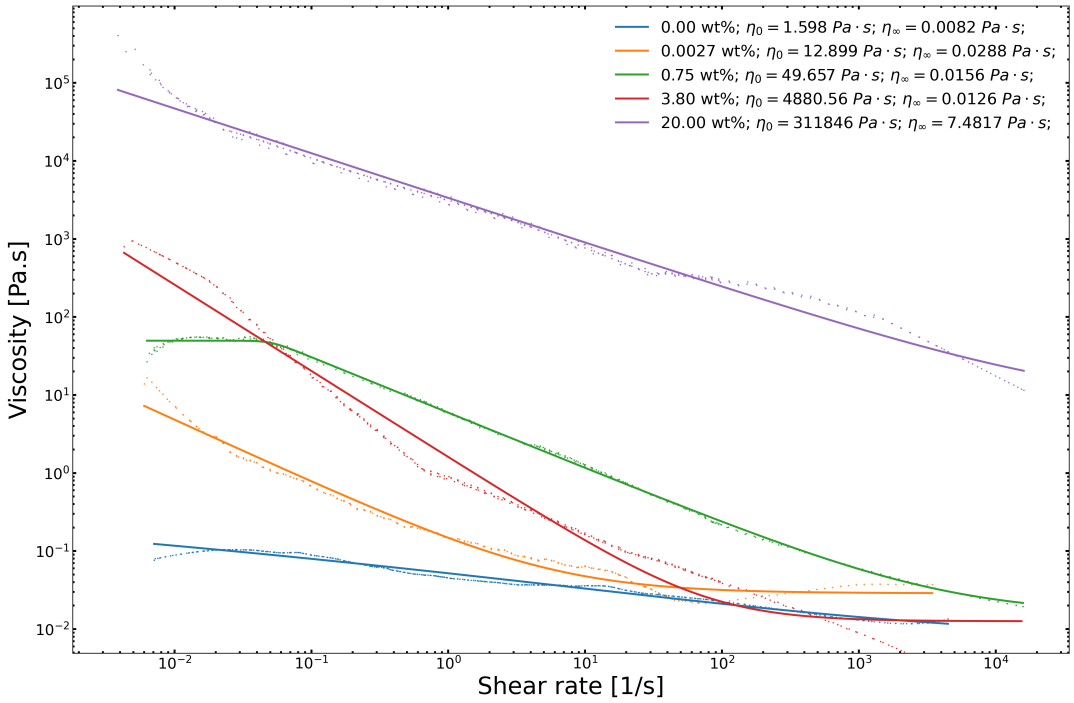

FIGURE A.7: Viscosity as a function of shear rate for Poly(9-Vinylcarbazole) (PVK) and SU-8 2002 solutions

Appendix B

Critical Concentrations

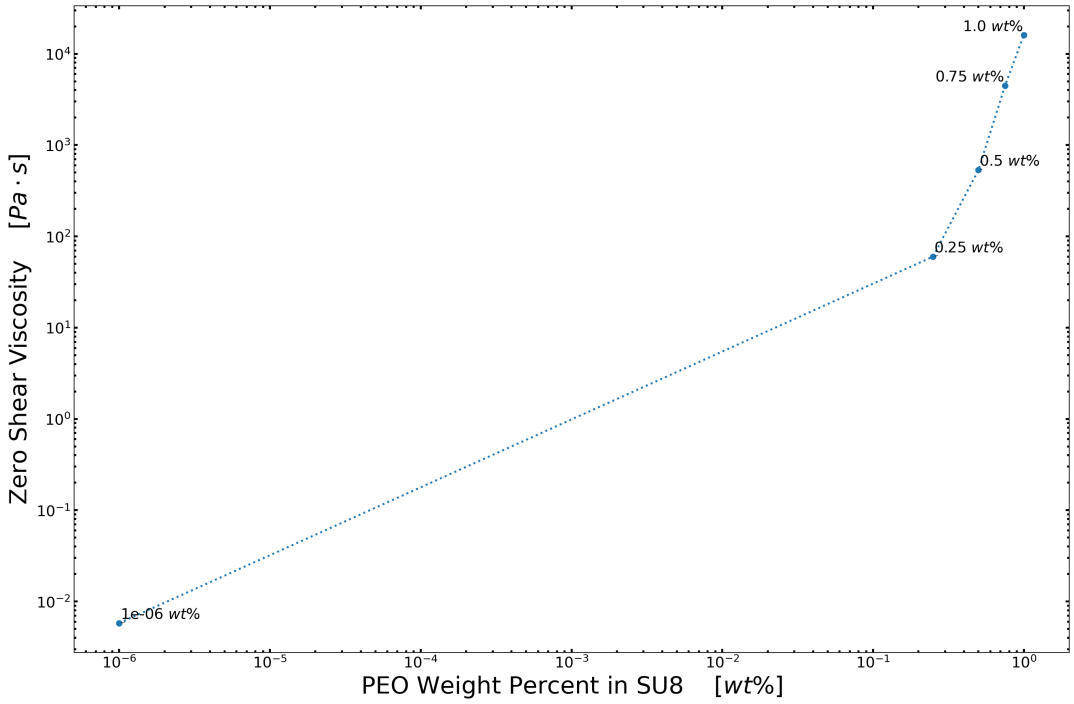

FIGURE B.1: Viscosity as a function of shear rate for Poly(Ethylene Oxide) (PEO) and SU-8 2002 solutions

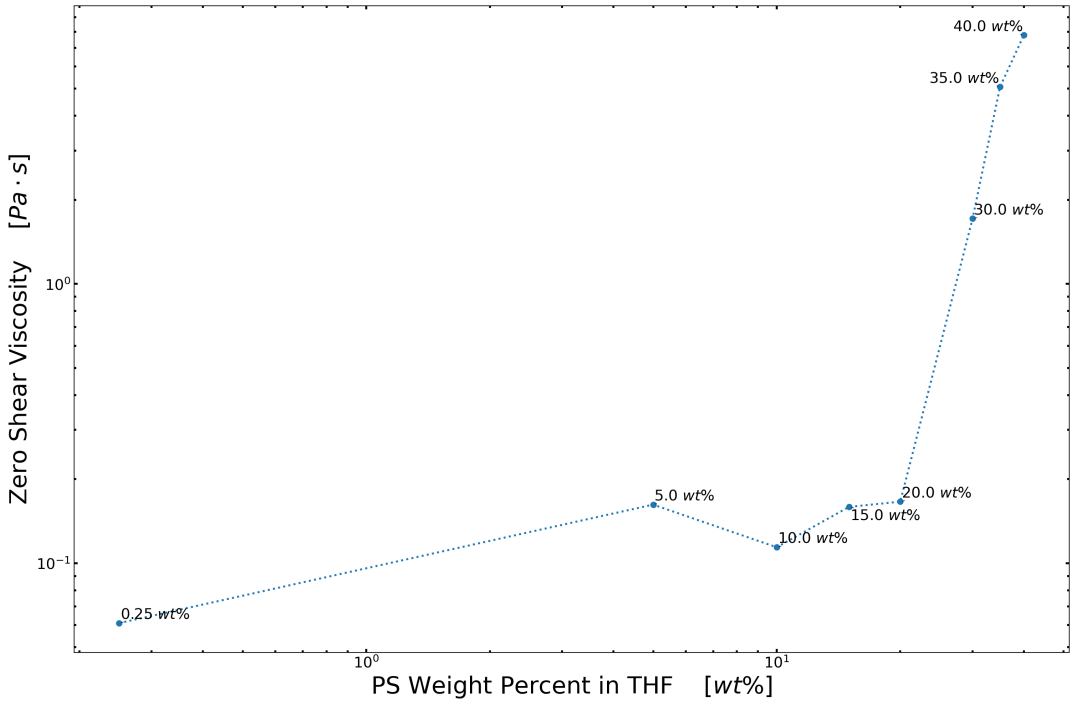

FIGURE B.2: Viscosity as a function of shear rate for Polystyrene (PS) and Tetrahydrofuran (THF) solutions

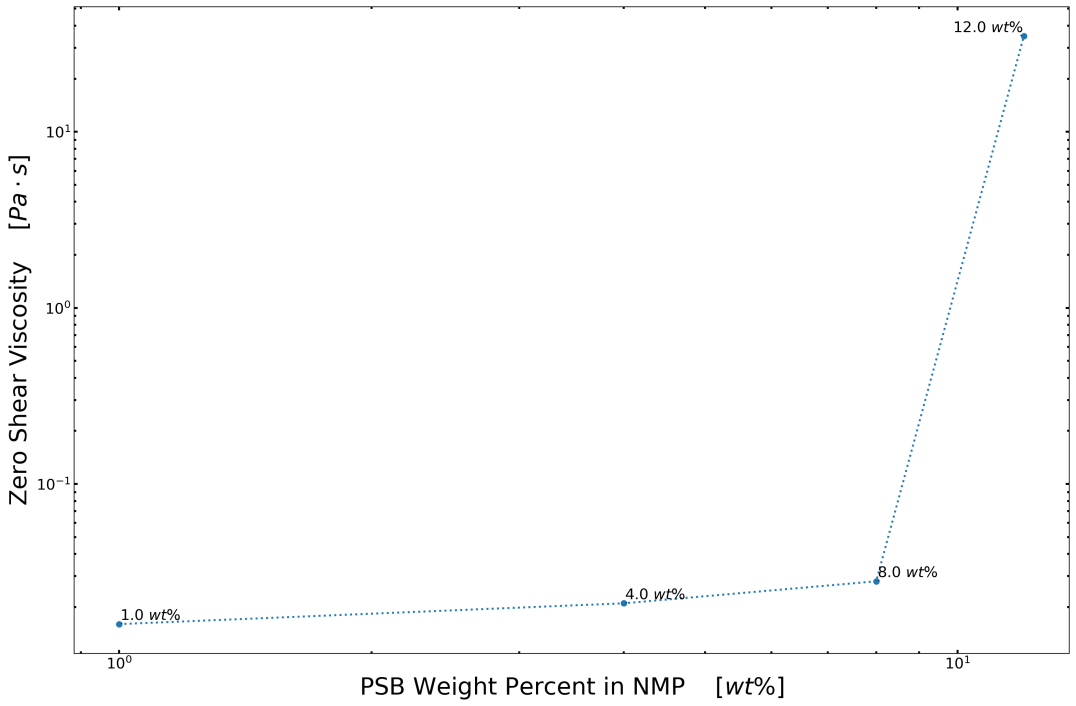

FIGURE B.3: Viscosity as a function of shear rate for Poly(Styrene-co-Butadiene) (PSB) and 1-Methyl-2-Pyrrolidinone (NMP)

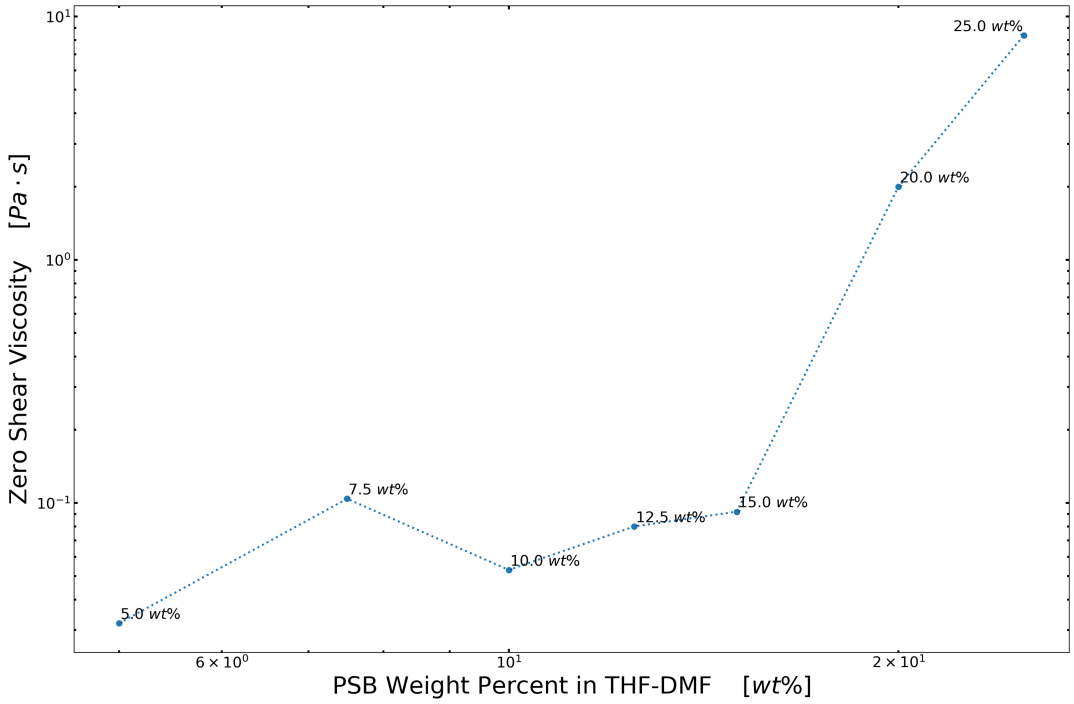

FIGURE B.4: Viscosity as a function of shear rate for Poly(Styrene-co-Butadiene) (PSB), Tetrahydrofuran (THF) and N,N-Dimethylformamide (DMF) solutions

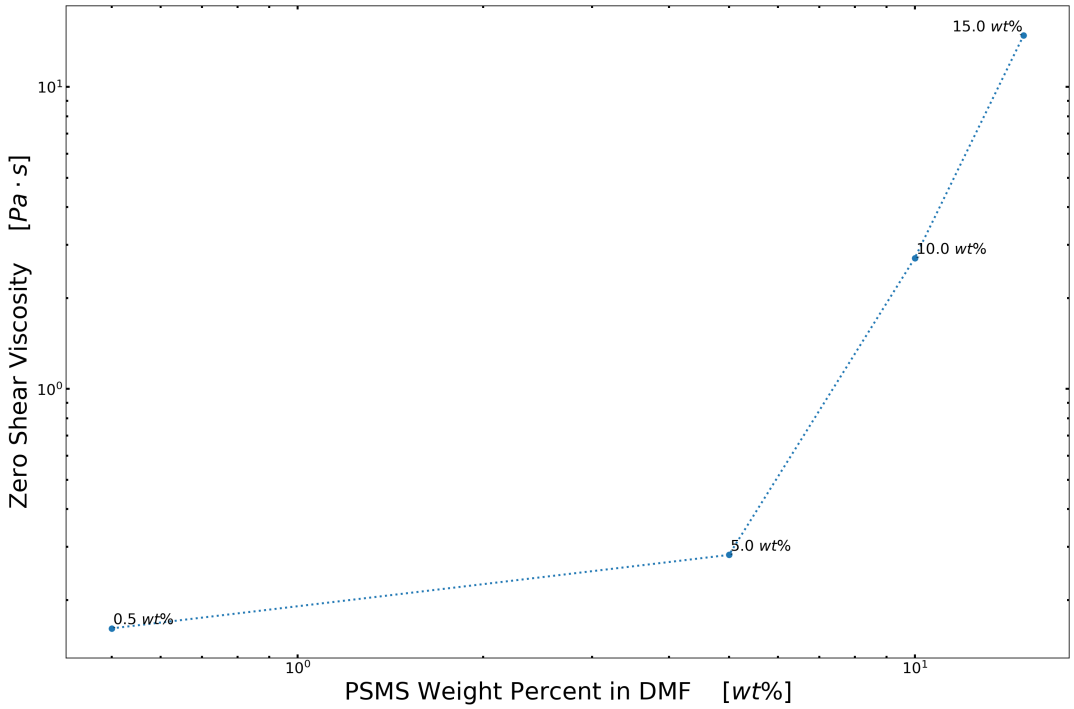

FIGURE B.5: Viscosity as a function of shear rate for Poly(Styrene-co-alpha-Methylstyrene) (PSMS) and N,N-Dimethylformamide (DMF) solutions

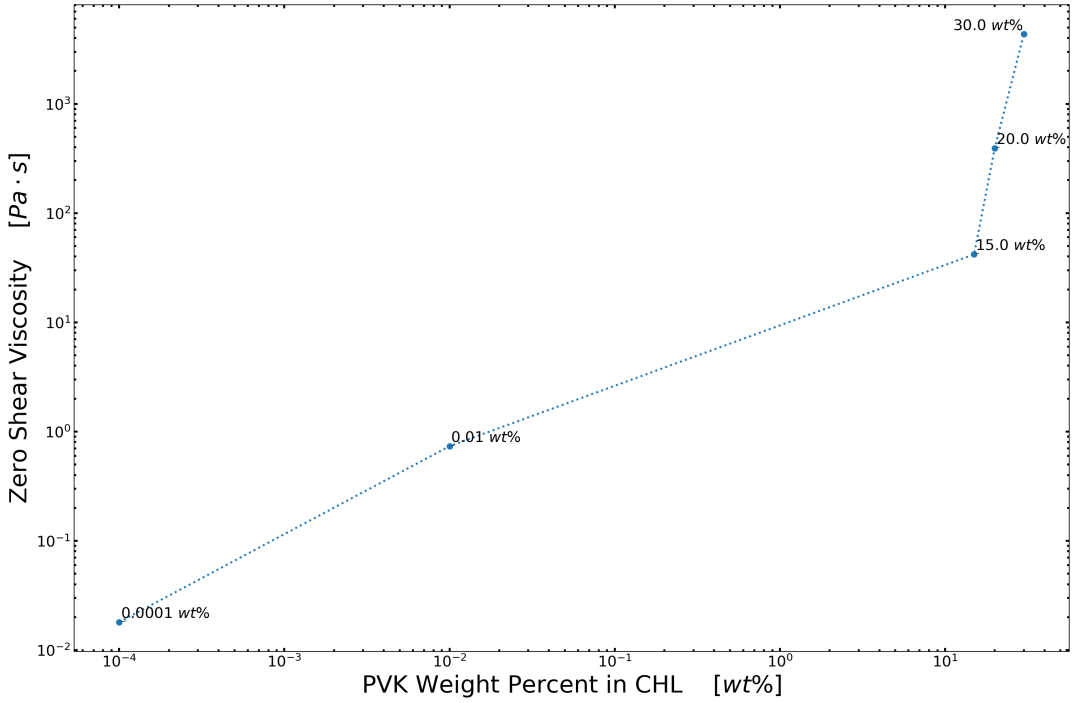

FIGURE B.6: Viscosity as a function of shear rate for Poly(9-Vinylcarbazole) (PVK) and Chloroform (CHL) solutions

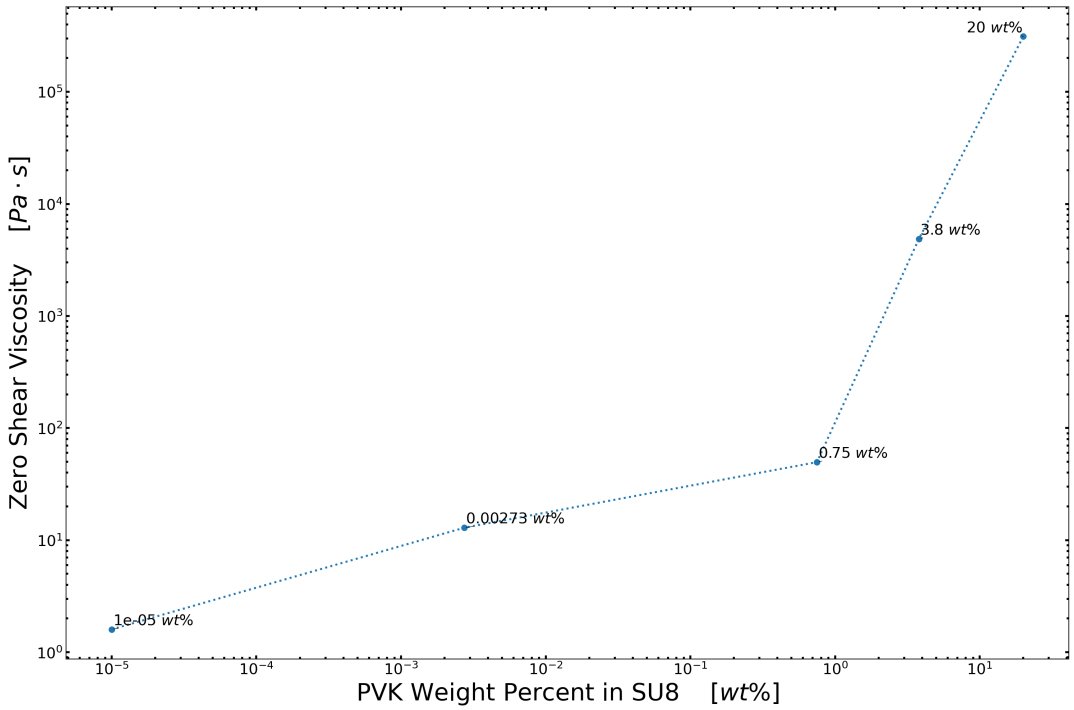

FIGURE B.7: Viscosity as a function of shear rate for Poly(9-Vinylcarbazole) (PVK) and SU-8 2002 solutions

Appendix C

Optical Microscopy Characterization of Electrospun Fibers

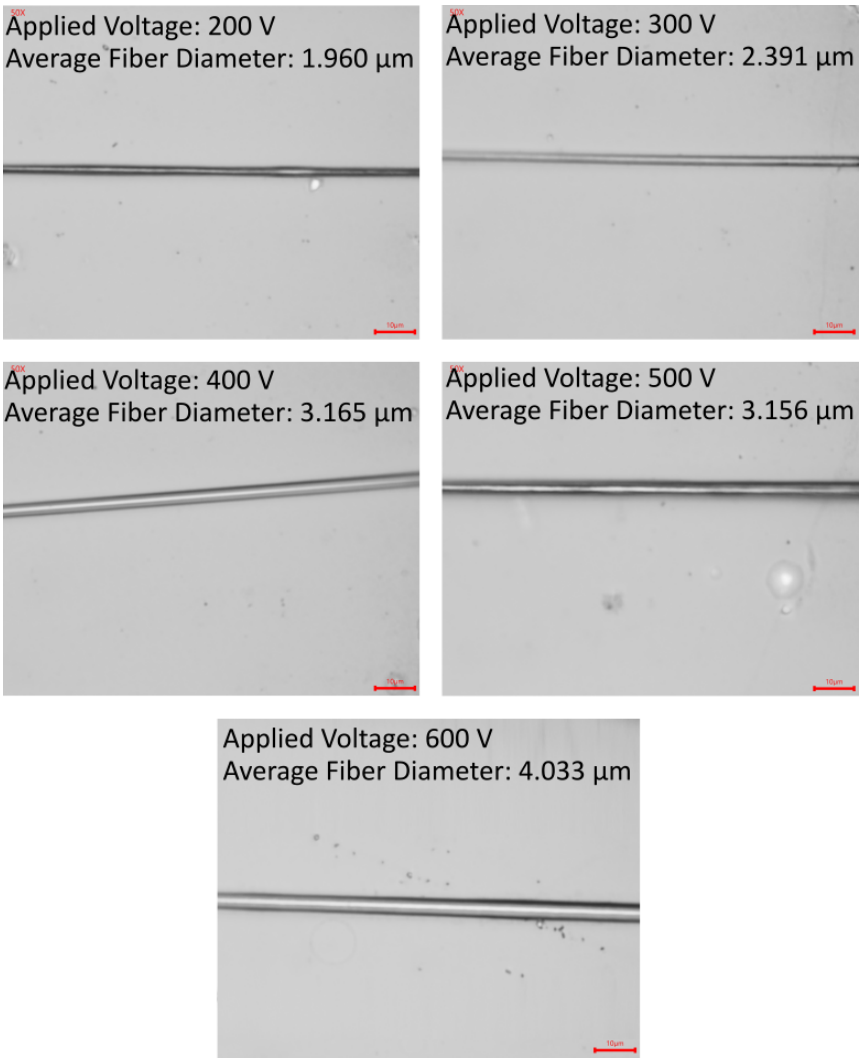

FIGURE C.1: Morphology and Characterization of Electrospun Fibers at Different Voltages : Poly(Ethylene Oxide) (PEO) and SU-8 2002

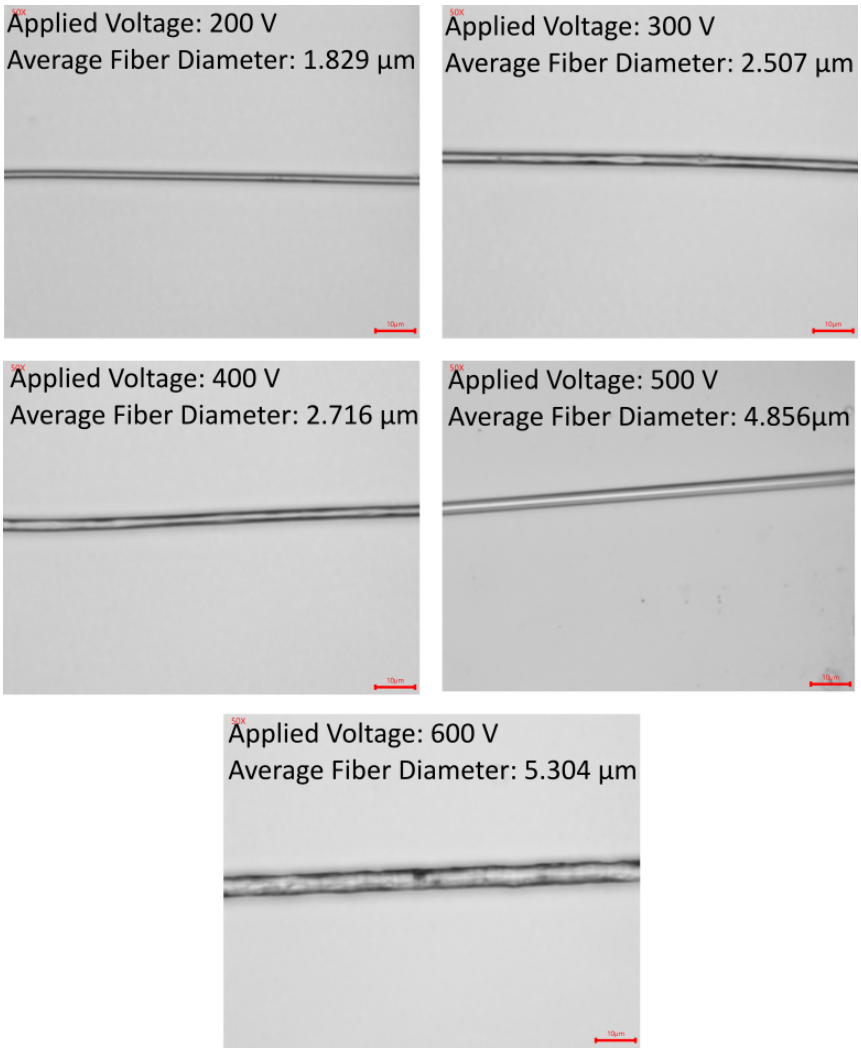

FIGURE C.2: Morphology and Characterization of Electrospun Fibers at Different Voltages : Polystyrene (PS) in Tetrahydrofuran (THF)

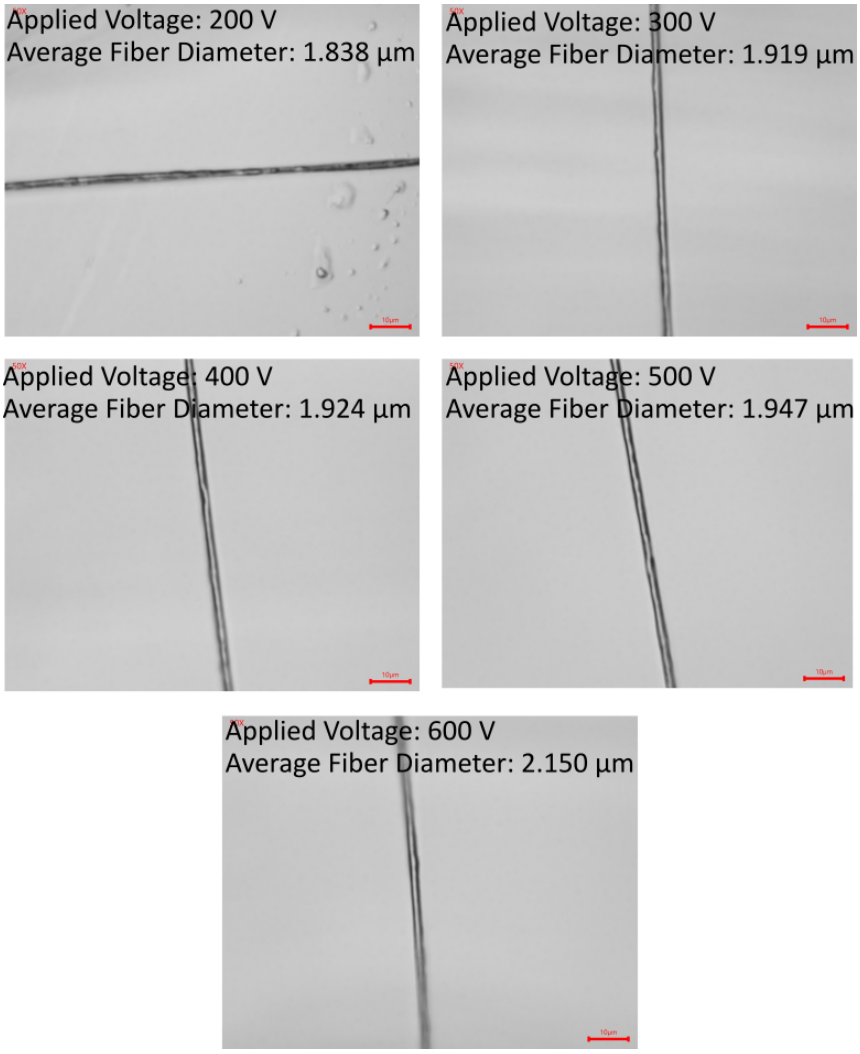

FIGURE C.3: Morphology and Characterization of Electrospun Fibers at Different Voltages : Poly(Styrene-co-Butadiene) (PSB) in Tetrahydrofuran (THF) and N,N-Dimethylformamide (DMF)

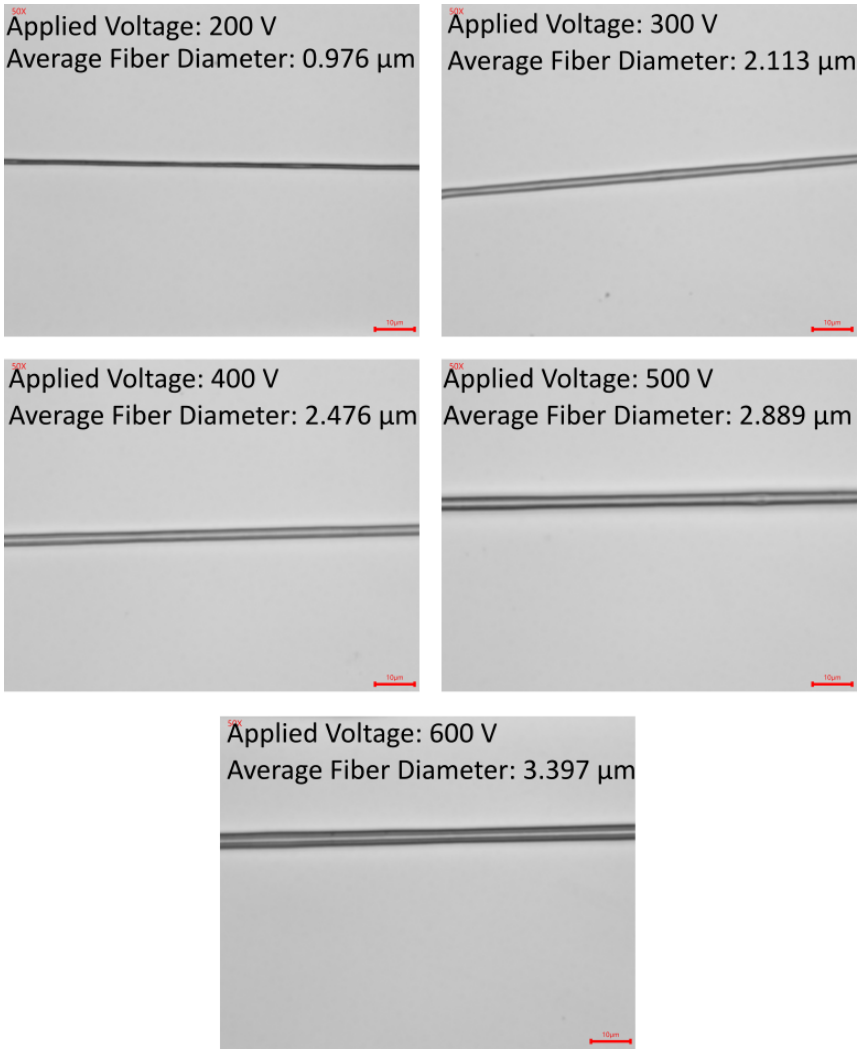

FIGURE C.4: Morphology and Characterization of Electrospun Fibers at Different Voltages : Poly(9-Vinylcarbazole) (PVK) in Chloroform (CHL)

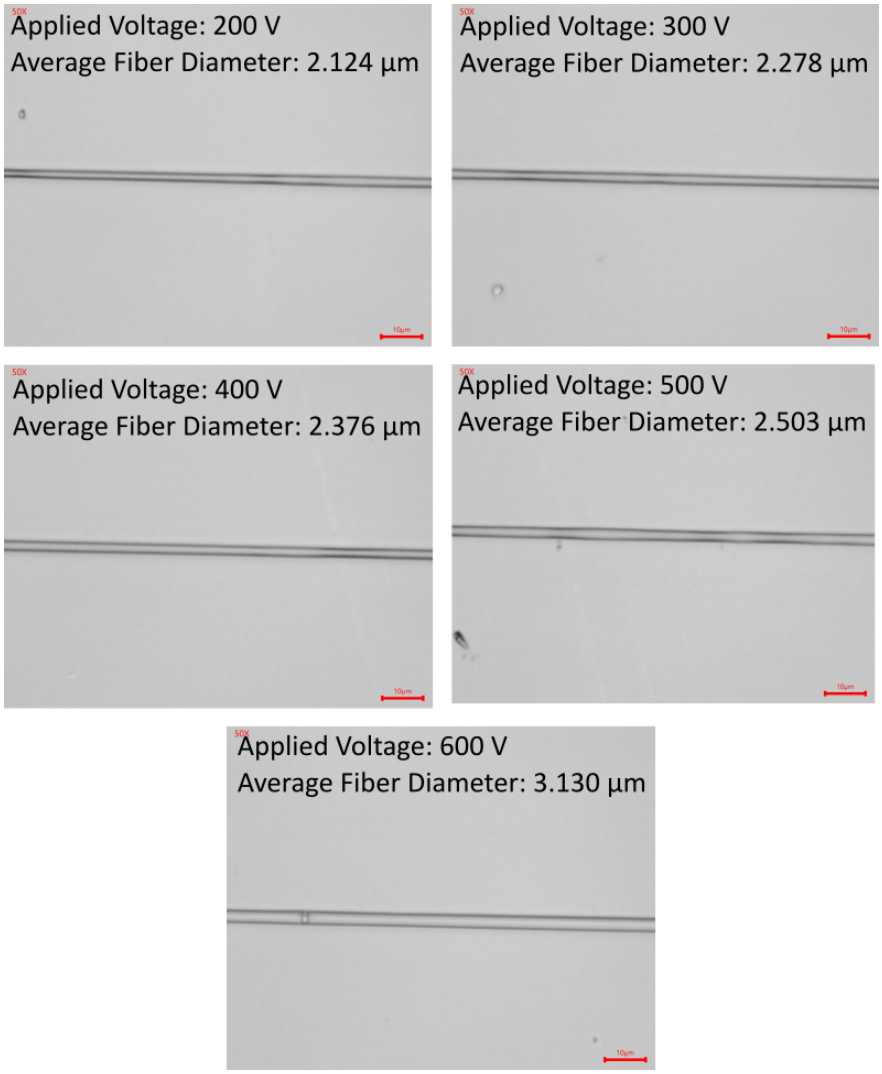

FIGURE C.5: Morphology and Characterization of Electrospun Fibers at Different Voltages : Poly(9-Vinylcarbazole) (PVK) and SU-8 2002

Appendix D

Average Fiber Diameters, Minimums and Maximums

			$D_{fiber}[\mu m]$		
Sample	$C_{polymer}[wt\%]$	$\Phi_0[V]$	**average**	**minimum**	**maximum**
PEO in SU8	0.25	200	1.96 ± 0.185	1.48	2.41
		300	2.39 ± 0.156	2.09	2.67
		400	3.16 ± 0.129	2.81	3.41
		500	3.15 ± 0.247	2.63	3.86
		600	4.03 ± 0.201	3.69	4.37
PS in THF	20.00	200	1.82 ± 0.101	1.64	2.08
		300	2.50 ± 0.105	2.29	2.73
		400	2.71 ± 0.140	2.37	2.98
		500	4.85 ± 0.172	4.41	5.22
		600	5.30 ± 0.388	4.76	6.57
PSB in THF and DMF	15.00	200	1.83 ± 0.251	1.25	2.25
		300	1.91 ± 0.221	1.51	2.54
		400	1.92 ± 0.138	1.61	2.27
		500	1.94 ± 0.201	1.58	2.53
		600	2.15 ± 0.208	1.77	2.76
PVK in CHL	15.00	200	0.97 ± 0.106	0.71	1.26
		300	2.11 ± 0.179	1.71	2.54
		400	2.47 ± 0.134	2.16	2.86
		500	2.88 ± 0.199	2.58	3.37

		600	3.39 ± 0.236	2.98	3.96
PVK in SU8	0.75	200	2.12 ± 0.169	1.75	2.45
		300	2.27 ± 0.117	2.04	2.52
		400	2.37 ± 0.117	2.12	2.65
		500	2.50 ± 0.169	2.06	2.88
		600	3.13 ± 0.109	2.97	3.35

TABLE D.1: Average Fiber Diameter for All the Experiments

Appendix E

Appendix NFES Review Table

TABLE E.1: Electrospun Polymer Solutions - Solution and Process Parameters

Polymer	*Mw*	Solvent	η_0 [Pa s]	*K* [S / m]	γ [N / m]	ρ [Kg / m^3]	NFES Type	$C_{polymer}$ [wt%]	D_{nozzle} [m]	*Q* [m^3 / s]	Substrate	*L* [m]	Φ_0 [V]	v_{stage} [m / s]	D_{fiber} [m]	*FiberGap* [m]	Fiber Morphology	Fiber Structure	Reference
PEO / SU8	4e6	Cyclopentanote	0.2 - 32e-3	8e-3 - 11e-3	25	1149 - 1318	xy stage	0.25 - 1	108e-6		Si	0.1e-3	200		1.2e-6 - 3.49e-6		straight	single	Aguirre2020
PCL	80e3	DCM / Methanol	7e-3			1218.538	xy stage	8 - 20	337e-6	2.83e-10	Al		10000 - 20000		374e-9 - 1.33e-6		straight	cross aligned	Beachley2011
PCL	50e6	CF / DMF	0.747			1142.62	melt		514e-6	1.39e-11		0.03	12000	4.5e-3 - 0.1e-3	10.6e-6 - 46.5e-6		coil and straight	single	Brown2011
PCL	80e3	CF / DMF	747e-3			1142.62	melt		743e-6	1.39e-12 - 5.56e-12	Al	0.02 - 0.04	6000 - 12000		4.76e-6 - 33e-6		coil	randomly distributed	Brown2014
PEO	300e3	Water	0.95	400e-6	1825.5	1000.6	xy stage	3	0.16e-3	8.33e-13	Si	0.005	1000	0.05 - 0.5	214e-9 - 344e-9	4.21e-5	meander and straight	single	Bu2012
MEH - PPV / PEO	380e3	Toluene	573e-6	956.e-3	17e-3	865	xy stage	0.08	0.26e-3	1.39e-11	SiO2 / Si	0.5e-3	1300	0.5	1.38e-7	8.84e-5	straight	aligned	Camillo2013
PEO / SU8	4e6	Cyclopentanote	0.056	9e-3	25	1215.5	xy stage	0.25	108e-6		Si	0.1e-3	200	0.06	4.08e-6		straight	single	Cardenas2017
PEO	300e6	Water	0.95	5.7e-3	8886.7	1000.6	xy stage	3 - 9	0.0001	2.80E - 14		0.0005 - 0.001	500 - 1200	0.12	119e-9 - 2.31e-6		straight	mesh	Chang2008
PVDF	534e6	CF / DMF	0.74			1142.62	xy stage	18				0.35e-3			1.07e-6 - 2.16e-6		straight	single	Chang2010
PVDF	534e3	CF / DMF	0.74			1142.62	xy stage	18				0.35e-3			6.13e-6 - 9.19e-6		straight	aligned	Chang2011
PU		CF / DMF	0.74			1142.62	xy stage	10			acrylic		2000	0.1	9.32E - 06	5.22e-5	straight	aligned	Choi2017
PLGA		CF / DMF	0.74			1142.62	PYES				PTFE				3.5e-7		straight	aligned	Coppola2014
PLGA	54e3	CF / DMF	0.74			1142.62	PYES	25			Si	0.001			0.01e-3 - 0.03e-3		straight	aligned	Coppola2020
PCL	83e3						melt		0.18e-3		Al	1.5e-3	2900	91.67e-3	8.17e-7	100.6e-6	straight	mesh	Dalton2015

Continued on next page

Table E.1 continued

PAN		CF / DMF	0.74			1142.62	rotating drum	9			Si	1.85e-3	35 - 500		0.13e-6 - 0.349e-6		straight	aligned	Deng2020
PDO		CF / DMF	0.0162 - 0.74			1142.62 - 1484	xy stage	14 - 20	340e-6 - 840e-6	2.78e-12 - 25.4e-12	Al	1.8e-3 - 0.003	1200 - 1600	0.01 - 0.1	3.19e-6 - 25.2e-6		straight	mesh	E.King2019
PMMA		CF / DMF	0.74			1142.62	xy stage	16 - 24		13.9e-12 - 41.7e-12		0.0016 - 2.4e-3	1200 - 2400	0.06	1.41e-6 - 5.64e-6		straight	mesh	Fattahi2017
PEO / SU8	4e-6	CF / DMF	0.74			1142.62	xy stage	0.5						0.02 - 0.06	5.98E - 06		straight	aligned	Flores2017
PEO	300e3	Water	0.95	859e-6	79e3	1e3	xy stage	8	0.4e-3		Si	0.5e-3	1100	0.2	7.4e-7	2e-5	straight	single	Fuh2011
PEO / Chitosan	900e3	DMSO	2.1e-3	62e-3	4.48	1095.6	xy stage	5	0.4e-3	2.8e-14		0.5e-3 - 1e-3	800 - 1200		282e-12 - 785e-12	0.1e-3	curved	aligned	Fuh2012
PEO / Chitosan	900e3	CF / DMF	0.74			1142.62	xy stage	5			PPy	0.5e-3	800	0.2	7.3e-7	0.02e-3 - 0.1e-3	straight	mesh, randomly distributed and aligned	Fuh2013
PVDF	534e-3	CF / DMF	0.74			1142.62		16				1.2e-3	1440		907e-9 - 2.91e-6		straight	aligned	Fuh2015
PEO	300e-3	Water / Ethanol	1.048316	2.6e-3 - 7.8e-3	11886.69	894.31	xy stage	20	4e-5		Si	1e-3	1700	0.05 - 0.35	816e-9 - 2.82e-6		meander, coil and straight	single	GaofengZheng2010
PAN	150e3	DMF	0.94			802	rotating drum	11	159e-6		Si	0.7e-3 - 0.01	400 - 900		2.53e-6		straight	aligned	George2020
POSS - PCL - PCU	2000	CF / DMF	0.74	10.2e-3	32235.64	1142.62	xy stage	20	750e-6	1.67e-11		0.5e-3	9000	0.01	18.7e-6 - 690e-6	352e-6 - 0.48e-3	meander	mesh	Gupta2007
PCL	80e3	CF / DMF	0.74			1142.62	xy stage		912e-6			0.005	3000	0.05	108.3e6 - 150.5e-6	0.001	straight	mesh	He2018

Continued on next page

Table E.1 continued

PEtOx	50e3						melt		160e-6 - 337e-6		Al	0.003 - 0.007	3000 - 7000	3.33e-3	12.5e-6 - 59.1e-6		straight	cross aligned	Hochleitner2014
PLA / PEG	72000						melt		337e-6		Si	3.5e-3	4000	83.3e-3	3.1e-5		straight	mesh	Hochleitner2017
PEO	300e3	CF / DMF	0.744	6.12e-5	34838.96	1142.62	xy stage	6		2e-11		0.005 - 7.5e-3	900	0.05 - 0.4	212e-9 - 352e-9	5e-6	straight, coil, and meander	single and aligned	Huang2015
PEO	30000	Water / Ethanol	1.04	524.3e-6	11906.09	894.31	xy stage	8	210e-6	8.33e-12	Si	2e-3	2000	0.001 - 0.02	3.27e-6 - 9.77e-6		meander	aligned	Jiang2018
PEO	100e3	CF / DMF	0.74	736.4e-6	4729.5	1142.62	rotating drum	10			Si	7.56e-3 - 12.5e-3	2000	0.11 - 1.70	101e-9 - 201e-9		straight	aligned	Kameoka2003
PEO	900e3	CF / DMF	0.77			1142.62	xy stage	5 - 30					4500		150e-9		coil	randomly distributed	Kameoka2003a
PVDF	534e3	Acetone / DMSO	0.16			943.42	auxiliary electrodes	17	0.1e-3	3.89e-12	Paper	750e-6	1900	0.01			meander	single	Kim2018
PCL	50e3	CF	0.55			1483.24	xy stage	18.3	250e-6				6000 - 12000	5e-3 - 7.5e-3	33.4e-6 - 103e-6		coil	single	Kolan2018
PCL	80e3	CF	0.55	997e-6	1978.8	1483.24	xy stage	8.8	0.2e-3	2.78e-11	Si	0.07	25e3	2e-3 - 0.5			coil and meander	single	Lee2012
PVDF	534e3	CF / DMF	0.74	1.47e-5	4733.12	1142.62	xy stage	12		2.22E - 11	Si	5e-3	1200	0.03	4.23e-5	263.1e-6	curved	mesh	Lei2015
PVP	1300e3	CF / DMF	0.73	2.94e-5	4737.7	1142.62	xy stage	17.4	510e-6	8.33e-11	Si / SiO2	1e-3	50	0.8	1.7e-7		straight	mesh	Lim2019
PVDF	534e-3	Acetone / DMSO	0.162			943.42	xy stage	18	0.3e-3				900 - 1200	0.03 - 0.09	2.54e-6 - 89.6e-6		straight	aligned	Liu2013
PVDF	534e-3	Acetone / DMSO	0.162			943.42	rotating drum	18	381e-6		Si	0.5e-3	10e3 - 16e3		205e-9 - 1.45e-6		straight	cross aligned	Liu2014
PVDF	534e3	Acetone / DMSO	0.16			943.42	xy stage	16 - 20	260e-6	1.67e-11	Si	1e-3		0.07	0.5e-6 - 20e-6		straight	cross aligned	Liu2015a

Continued on next page

Table E.1 continued

PVDF / PVA / SWCNT	534e3	Acetone / DMSO	0.1	0.003	270	94	xy stage	21	159e-6		paper	0.001	1000 - 1800	0.01 - 0.09	3.99e-6 - 11.5e-6	0.1e-3	straight	aligned	Luo2016
PEO	4e6	Water	0.95	0.57e-3	8892.6	1000.62	xy stage	2	210e-6	2.78e-13	C /Si	0.001	200 - 400	0.02 - 0.08	50.7e-9 - 423e-9		straight	aligned and single	Madou2011
PVK	1100e3	Styrene	696e-6	6.31	3.6e-3	1300	xy stage	3.96	0.1e-3	8.33e-12	Si / SiO2	2.5e-3	3500	133e-3 - 0.15	65e-9 - 707e-9	5e-5	straight	aligned	Min2013
PEO	200e3	Water / Ethanol	1.04	523e-6	11907.5	894.3	xy stage	14	250e-6	3e-12	Si	5.25e-3	1600	0.15	3e-7	0.3e-3	meander	aligned	Nagle2019
PVDF	534e3	CF / DMF	747e-3			1142.62	rotating drum	10 - 18			Cu		2000 - 10000	523.6e-3 - 2.6	35.3e-6 - 51.9e-6		straight	aligned	Pan2014
PVDF	534e3	CF / DMF	747e-3			1142.62	coaxial	15 - 19	630e-6		Cu		8000 - 16000	0.53 - 2.62	10.3e-6 - 45.9e-6		straight	aligned	Pan2015
PCL	45028	CF / DMF	0.74			1142.62	xy stage	25 - 70	0.3e-3 - 0.6e-3	0 - 1.21e-9		5e-3 - 0.01	3500 - 3900	0.2	58.7e-6 - 190e-6		straight	single	Parajuli2016
PEO / NaCl		CF / DMF	0.7474335			1142.62	xy stage	0.1 - 1							92e-9 - 239e-9		straight	aligned	Park2020
PEO	1000e3	Water / Ethanol	1.04	339e-6	11923.7	894.1	xy stage	4	160e-6	83.3e-12 - 25e-9		0.003	1500		5.74e-6 - 14.7e-6		straight	mesh	Ru2014
PEO / TiO2	300e3	CF / DMF	747e-3	618e-6	363503.0357	1142.62	xy stage	5.44		5.56e-12	Si3N4	0.5e-3	1100		5e-7	4e-5	straight	aligned	Ruggieri2013
PIB							rotating drum	15	360e-6	2e-11			12000		4.2e-7		straight	cross aligned	Sarkar2007
PS							rotating drum	20	0.36e-3	1e-11			11000		4.1-7		straight	cross aligned	Sarkar2007
PEO / FeAl NP							rotating drum	6	0.36e-3	1.17e-11			9500		4e-7		straight	cross aligned	Sarkar2007
PEO / Au NP							rotating drum	10	0.36e-3	1.67e-11			9300		3.9e-7		straight	cross aligned	Sarkar2007

Continued on next page

Table E.1 continued

PEO / SWCNT							rotating drum	8	360e-6	1.33e-11			9300		3.8e-7		straight	cross aligned	Sarkar2007
PEO							rotating drum	8	360e-6	1.33e-11			9500		3.7e-7		straight	cross aligned	Sarkar2007
PEO / PPy	5e6	DMF / Acetone	633.4e-3			948.8	xy stage	8	2.5e-5				1000		0.4e-6 - 0.7e-6	265e-6	straight	aligned	Shen2016
PEO	400e3	Water	958.2e-3	286e-6 - 11e-3	2225.7 - 35611.8588	1000.62	xy stage	10	108e-6			750e-6	500 - 700	15e-3	130e-9 - 220e-9		straight, coil and meander	single	Shin2018
PEO	4000e3	Water	958e-3			1000.62	xy stage	1.5	108e-6				650	0.2e-3 - 0.8e-3	94e-9 - 933e-9		meander, coil and meander	single	Shin2019
PS		TCB	2.05e-3			1449.6	xy stage	5	2e-6		Si	20e-6 - 40e-6	400 - 500	2e-3	57.3e-9 - 167e-9		straight	single	Song2015
PCL	80e3	CF / DMF	0.73	735e-6	4729.9	1142.62	aligned needles	10	337e-6	1.39e-10	Si	0.06	15000		1.21e-7		straight	randomly distributed	Sonntag2020
PEU		CF / DMF	747e-3			1142.62	touch spinning	5		8.33e-11					3.28e-7		straight	cross aligned	Strauss2019
PCL		CF / DMF	747e-3			1142.62	touch spinning	8		8.33e-11					3.26e-7		straight	cross aligned	Strauss2019
PEO / NT		CF / DMF	0.7474335			1142.62	touch spinning	0.5		8.33E - 11					3.20E - 07		straight	cross aligned	Strauss2019
PEO		CF / DMF	0.7474335			1142.62	touch spinning	0.5		8.33E - 11					2.98E - 07		straight	cross aligned	Strauss2019
PEO	300000	CF / DMF	0.7474335			1142.62	xy stage	3			Si and SiO2	0.0005 - 0.003	598 - 1255	0.2	3.00E - 07	2.50E - 05	meander	single	Sun2006a
PEO	2000000	CF / DMF	0.7474335			1142.62	multinozzle xy stage	5		3.33E - 11		0.002 - 0.006	1700 - 2700			0.00547	straight	aligned	Wang2015
PEO	2000000	Water	0.958822			1000.62	multinozzle xy stage	5	0.00018	3.33E - 12		0.003 - 0.005	2300 - 2800	0.02		0.003034	straight	aligned	Wang2017

Continued on next page

Table E.1 continued

PEO	2000000	Water	0.958822	0.000574931	8906.09431	1000.62	multinozzle xy stage	5	0.00018		SST	0.004	2500	0.02	6.23E - 06	0.02520032	straight	aligned	Wang2018a
PEO	4000000						xy stage	2	0.00015		Si	0.002	1250			0.000007 - 0.000074	meander	aligned	Xu2014
PEO	2000000	CF / DMF	0.7474335			1142.62	xy stage	5		3.33E - 12		0.0025 - 0.004	1900 - 2700	0.05 - 0.3	0.000000696 - 0.00000508		meander	aligned	Xu2019
Gelatin		CF / DMF	0.7474335			1142.62	xy stage	11			PDMS	0.00125	1000		9.02E - 07	4.00E - 05	straight	aligned	Xue2014
PEO	900000	Water	0.958822	0.00057282	8923.275983	1000.62	xy stage	5	0.00011	0.0000000000833 - 0.00000000000278	ITO	0.0005 - 0.0015	1000 - 1300	0.008774731 - 0.166854679	0.000000671 - 0.0000199		straight	aligned	Yang2019
PCL	80000						xy stage		0.00026	0.0000000000833 - 0.00000000000278	ITO	0.002	3000		6.80E - 06		meander	aligned	You2017
PS	240000	CF / DMF	0.7474335	0.003085799	910845.5556	1142.62	xy stage	30	0.000455	0	Au	0.0002	2400	0.015	7.81E - 06		straight	mesh	Yousefi2019
PEO	2000000	CF / DMF	0.7474335	0.000735049	4749.867762	1142.62	multinozzle xy stage	8				0.003	2500	0.08	0.00000289 - 0.00001	0.002061	straight	aligned	Zhang2019
PEO	300000	Water / Ethanol	1.048316	0.010481536	11917.29913	894.313	xy stage	18	4.00E - 05		Si	0.001	1700	0.36	4.89E - 07		coil	single	Zheng2010
PEO	300000	Water / Ethanol	1.048316	0.0005243	11910.45426	894.313	xy stage	14	0.00021	1.39E - 11	PET	0.002	500 - 4000	0.02 - 1	0.0000174 - 0.0000658	0.0003	meander	aligned	Zheng2014
PCL	90000	CF / DMF	0.7474335	7.37E - 05	4735.564517	1142.62	xy stage	10	0.00041	0.0000000000167 - 0.0000000000833	Al	0.001 - 0.003	800 - 4000	0.03	0.00000799 - 0.0000915		straight	single	Zhou2010
PEO	2000000	Water	0.958822	0.000572353	8896.483826	1000.62	auxiliary electrodes	4	0.00016		Si	0.004	0 - 5000	0.005	0.00000706 - 0.0000136		meander and straight	single	Zhu2016

Appendix F

Image Analysis Python Source Code

```
# import the necessary packages
import numpy as np
import argparse
import imutils
import cv2 # pip install opencv-python
import matplotlib.pyplot as plt
# import torch
# import torchvision.transforms as T

from IPython.display import display, Image
from easydict import EasyDict
from scipy.spatial import distance as dist
from imutils import perspective
from imutils import contours

def midpoint(ptA, ptB):
    return ((ptA[0] + ptB[0]) * 0.5, (ptA[1] + ptB[1]) * 0.5)

def order_points(pts):
    # sort the points based on their x-coordinates
    xSorted = pts[np.argsort(pts[:, 0]), :]

    # grab the left-most and right-most points from the sorted
    # x-roodinate points
    leftMost = xSorted[:2, :]
    rightMost = xSorted[2:, :]

    # now, sort the left-most coordinates according to their
    # y-coordinates so we can grab the top-left and bottom-left
    # points, respectively
    leftMost = leftMost[np.argsort(leftMost[:, 1]), :]
    (tl, bl) = leftMost

    # now that we have the top-left coordinate, use it as an
```

```
35      # anchor to calculate the Euclidean distance between the
36      # top-left and right-most points; by the Pythagorean
37      # theorem, the point with the largest distance will be
38      # our bottom-right point
39      D = dist.cdist(tl[np.newaxis], rightMost, "euclidean")[0]
40      (br, tr) = rightMost[np.argsort(D)[::-1], :]
41
42      # return the coordinates in top-left, top-right,
43      # bottom-right, and bottom-left order
44      return np.array([tl, tr, br, bl], dtype="float32")
45
46  def measureImg(
47      orimgname_, imgname_, refIsXval, refImg, refVal, edgeType,
48      minObjArea, invertPimg, Threshold=128, denoise=0):
49
50      #TUNE fineTuning TO MATCH THE REFERENCE OBJECT
51
52      ### IMAGE PRE-PROCESSING
53      # load the image
54      orimg = cv2.imread(orimgname_)
55      img = cv2.imread(imgname_)
56
57      # Image Denoising
58      dst = cv2.fastNlMeansDenoisingColored(
59          src=img,
60          dst=None,
61          h=denoise,
62          hColor=denoise,
63          templateWindowSize=7,
64          searchWindowSize=21)
65
66      # Convert to grayscale
67      grey = cv2.cvtColor(dst, cv2.COLOR_BGR2GRAY)
68
69      cv2.imwrite('./img_grey.png', grey)
70
71      # define a threshold, 128 is the middle of black and white
72      # in grey scale
73      thresh = Threshold #256/2
74
75      # assign blue channel to zeros
76      binary = cv2.threshold(grey, thresh, 256, cv2.THRESH_BINARY)[1]
77
78      cv2.imwrite('./img_binary.png', binary)
79
80  #     # Inverting the colors
81  #     invert = abs(255 - binary)
82
```

```
83      ### IMAGE PROCESSING
84      # perform edge detection, then perform a dilation + erosion
85      # to close gaps in between object edges
86      if invertPimg:
87          edged = cv2.Canny(binary, Threshold, Threshold)
88      else:
89          edged = cv2.Canny(grey, Threshold, Threshold)
90
91      cv2.imwrite('./img_edged.png', edged)
92
93      dilated = cv2.dilate(edged, None, iterations=1)
94      eroded = cv2.erode(dilated, None, iterations=1)
95
96      cv2.imwrite('./img_dilated.png', dilated)
97      cv2.imwrite('./img_eroded.png', eroded)
98
99      if edgeType == "dilated":
100         Pimg = dilated
101     elif edgeType == "eroded":
102         Pimg = eroded
103     else:
104         Pimg = edged
105
106     # Show and save image
107     print()
108     print('Image to Process:')
109     imgname='./img_out.png'
110     cv2.imwrite(imgname,Pimg)
111     display(Image(filename=imgname))
112
113     ### GET IMAGE MEASUREMENTS
114     # find contours in the edge map
115     cnts = cv2.findContours(
116         Pimg.copy(),
117         cv2.RETR_EXTERNAL,
118         cv2.CHAIN_APPROX_SIMPLE)
119     cnts = imutils.grab_contours(cnts)
120
121     # sort the contours from left-to-right and initialize the
122     # 'pixels per metric' calibration variable
123     (cnts, _) = contours.sort_contours(cnts)
124
125     # if the pixels per metric has not been initialized, then
126     # compute it as the ratio of pixels to supplied metric
127     # (in this case, inches) to match the reference object
128     pixelsPerMetric = None
129     i = 0
130     for c in reversed(cnts):
```

```
131         if cv2.contourArea(c) < minObjArea:
132             continue
133 
134         if i == refImg and pixelsPerMetric is None:
135             box = cv2.minAreaRect(c)
136             box = cv2.cv.BoxPoints(box)
137                 if imutils.is_cv2()
138                 else cv2.boxPoints(box)
139             box = np.array(box, dtype="int")
140             box = perspective.order_points(box)
141             (tl, tr, br, bl) = box
142             (tltrX, tltrY) = midpoint(tl, tr)
143             (blbrX, blbrY) = midpoint(bl, br)
144             (tlblX, tlblY) = midpoint(tl, bl)
145             (trbrX, trbrY) = midpoint(tr, br)
146             dA = dist.euclidean((tltrX, tltrY), (blbrX, blbrY))
147             dB = dist.euclidean((tlblX, tlblY), (trbrX, trbrY))
148             if refIsXval:
149                 pixelsPerMetric = dB*(25400000/refVal)
150             else:
151                 pixelsPerMetric = dA*(25400000/refVal)
152         i += 1
153         #print(pixelsPerMetric)
154 
155     # loop over the contours individually
156     i = 0
157     for c in reversed(cnts):
158         # if the contour is not sufficiently large, ignore it
159         if cv2.contourArea(c) < minObjArea:
160             continue
161 
162         # compute the rotated bounding box of the contour
163         orig = orimg.copy()
164         box = cv2.minAreaRect(c)
165         box = cv2.cv.BoxPoints(box)
166             if imutils.is_cv2()
167             else cv2.boxPoints(box)
168         box = np.array(box, dtype="int")
169 
170         # order the points in the contour such that they appear
171         # in top-left, top-right, bottom-right, and bottom-left
172         # order, then draw the outline of the rotated bounding
173         # box
174         box = perspective.order_points(box)
175         cv2.drawContours(
176             orig,
177             [box.astype("int")],
178             -1,
```

```
            (0, 255, 0),
            1)

        # loop over the original points and draw them
        for (x, y) in box:
            cv2.circle(orig, (int(x), int(y)), 2, (0, 0, 255), -1)

        # unpack the ordered bounding box, then compute the
        # midpoint between the top-left and top-right
        # coordinates, followed by the midpoint between
        # bottom-left and bottom-right coordinates
        (tl, tr, br, bl) = box
        (tltrX, tltrY) = midpoint(tl, tr)
        (blbrX, blbrY) = midpoint(bl, br)

        # compute the midpoint between the top-left and
        # top-right points, followed by the midpoint between the
        # top-righ and bottom-right
        (tlblX, tlblY) = midpoint(tl, bl)
        (trbrX, trbrY) = midpoint(tr, br)

        # draw the midpoints on the image
        cv2.circle(orig, (int(tltrX), int(tltrY)),
            2, (255, 0, 0), -1)
        cv2.circle(orig, (int(blbrX), int(blbrY)),
            2, (255, 0, 0), -1)
        cv2.circle(orig, (int(tlblX), int(tlblY)),
            2, (255, 0, 0), -1)
        cv2.circle(orig, (int(trbrX), int(trbrY)),
            2, (255, 0, 0), -1)

        # draw lines between the midpoints
        cv2.line(
            orig,
            (int(tltrX), int(tltrY)),
            (int(blbrX), int(blbrY)),
            (255, 0, 255), 1)
        cv2.line(
            orig,
            (int(tlblX), int(tlblY)),
            (int(trbrX), int(trbrY)),
            (255, 0, 255), 1)

        # compute the Euclidean distance between the midpoints
        dA = dist.euclidean((tltrX, tltrY), (blbrX, blbrY))
        dB = dist.euclidean((tlblX, tlblY), (trbrX, trbrY))

        # compute the size of the object
```

```
227         dimA = dA / pixelsPerMetric
228         dimB = dB / pixelsPerMetric
229 
230         # convert inches to nm
231         dimA = dimA*25400000
232         dimB = dimB*25400000
233 
234         # draw the object sizes on the image
235         txtcolor=(255, 171, 0)
236         cv2.putText(orig, "{:.2f}nm".format(dimB),
237                     (int(tltrX - 15), int(tltrY - 10)),
238                     cv2.FONT_HERSHEY_SIMPLEX,
239                     0.6, txtcolor, 2, 5)
240         cv2.putText(orig, "{:.2f}nm".format(dimA),
241                     (int(trbrX + 10), int(trbrY)),
242                     cv2.FONT_HERSHEY_SIMPLEX,
243                     0.6, txtcolor, 2)
244 
245         # Show and save output image
246         print()
247         print('Measurements in progress ... ' + str(i))
248         print('dimX=' + str(round(dimB,2)) + 'nm;  dimY=' +
249             str(round(dimA,2)) + 'nm;')
250         imgname='./img_out.png'
251         cv2.imwrite(imgname,orig)
252         display(Image(filename=imgname))
253         i += 1
254 
255 help(measureImg);
256 display(Image(filename='./img/UScoinRef.png'));
257 measureImg(
258     './img/example_01.png',
259     './img/example_01.png',
260     True, 5, 24260000,
261     'eroded',
262     100,
263     False,
264     Threshold=150,
265     denoise=15);
```

LISTING F.1: Image Analysis Source Code

Bibliography

[1] Kenry and Chwee Teck Lim. "Nanofiber technology: current status and emerging developments". In: *Progress in Polymer Science* 70 (July 2017), pp. 1–17. ISSN: 00796700. DOI: 10.1016/j.progpolymsci.2017.03.002. URL: http://dx.doi.org/10.1016/j.progpolymsci.2017.03.002%20https://linkinghub.elsevier.com/retrieve/pii/S0079670017300692.

[2] Vega Baudrit J. "Recycling and Elimination of Wastes obtained from Agriculture by using Nanotechnology: Nanosensors". In: *International Journal of Biosensors & Bioelectronics* 3.5 (Dec. 2017), pp. 368–375. ISSN: 25732838. DOI: 10.15406/ijbsbe.2017.03.00084. URL: https://medcraveonline.com/IJBSBE/recycling-and-elimination-of-wastes-obtained-from-agriculture-by-using-nanotechnology-nanosensors.html.

[3] Richard L. McCreery. "Advanced Carbon Electrode Materials for Molecular Electrochemistry". In: *Chemical Reviews* 108.7 (July 2008), pp. 2646–2687. ISSN: 0009-2665. DOI: 10.1021/cr068076m. URL: https://pubs.acs.org/doi/10.1021/cr068076m.

[4] Andre K. Geim. "Random Walk to Graphene (Nobel Lecture)". In: *Angewandte Chemie International Edition* 50.31 (July 2011), pp. 6966–6985. ISSN: 14337851. DOI: 10.1002/anie.201101174. URL: http://doi.wiley.com/10.1002/anie.201101174.

[5] Yanwu Zhu et al. "Graphene and Graphene Oxide: Synthesis, Properties, and Applications". In: *Advanced Materials* 22.35 (Sept. 2010), pp. 3906–3924. ISSN: 09359648. DOI: 10.1002/adma.201001068. URL: http://doi.wiley.com/10.1002/adma.201001068.

[6] M.I Katsnelson and A.K Geim. "Electron scattering on microscopic corrugations in graphene". In: *Philosophical Transactions of the Royal Society A: Mathematical, Physical and Engineering Sciences* 366.1863 (Jan. 2008), pp. 195–204. ISSN: 1364-503X. DOI: 10.1098/rsta.2007.2157. URL: https://royalsocietypublishing.org/doi/10.1098/rsta.2007.2157.

[7] Dan Li and Richard B. Kaner. "MATERIALS SCIENCE: Graphene-Based Materials". In: *Science* 320.5880 (May 2008), pp. 1170–1171. ISSN: 0036-8075. DOI: 10.1126/science.1158180. URL: https://www.sciencemag.org/lookup/doi/10.1126/science.1158180.

[8] A. K. Geim and K. S. Novoselov. "The rise of graphene". In: *Nature Materials* 6.3 (Mar. 2007), pp. 183–191. ISSN: 1476-1122. DOI: 10.1038/nmat1849. URL: http://www.nature.com/articles/nmat1849.

[9] A K Geim. "Graphene: Status and Prospects". In: *Science* 324.5934 (June 2009), pp. 1530–1534. ISSN: 0036-8075. DOI: 10.1126/science.1158877. URL: https://www.sciencemag.org/lookup/doi/10.1126/science.1158877.

[10] M.T.H Siddiqui et al. "Fabrication of advance magnetic carbon nano-materials and their potential applications: A review". In: *Journal of Environmental Chemical Engineering* 7.1 (Feb. 2019), p. 102812. ISSN: 2213-3437. DOI: 10.1016/J.JECE.2018.102812. URL: https://0-www-sciencedirect-com.millenium.itesm.mx/science/article/pii/S2213343718307358%20https://linkinghub.elsevier.com/retrieve/pii/S2213343718307358.

[11] Braulio Cárdenas. "Advanced Manufacturing Techniques for the Fabrication and Surface Modification of Carbon Nanowires". In: (2017), p. 160.

[12] Marc J. Madou et al. "Controlled Continuous Patterning of Polymeric Nanofibers on Three-Dimensional Substrates Using Low-Voltage Near-Field Electrospinning". In: *Nano Letters* 11.4 (2011), pp. 1831–1837. ISSN: 1530-6984. DOI: 10.1021/nl2006164.

[13] Domingo Ricardo Flores. "Role of rheological properties in near field electrospun fibers morphology". In: (2017), p. 130.

[14] Geertruida A. Posthuma-Trumpie et al. "Amorphous carbon nanoparticles: a versatile label for rapid diagnostic (immuno)assays". In: *Analytical and Bioanalytical Chemistry* 402.2 (Jan. 2012), pp. 593–600. ISSN: 1618-2642. DOI: 10.1007/s00216-011-5340-5. URL: http://link.springer.com/10.1007/s00216-011-5340-5.

[15] Lu Zhang et al. "Bamboo and Herringbone Shaped Carbon Nanotubes and Carbon Nanofibres Synthesized in Direct Current-Plasma Enhanced Chemical Vapour Deposition". In: *Journal of Nanoscience and Nanotechnology* 9.7 (July 2009), pp. 4502–4506. ISSN: 15334880. DOI: 10.1166/jnn.2009.M84. URL: http://openurl.ingenta.com/content/xref?genre=article%7B%5C&%7Dissn=1533-4880%7B%5C&%7Dvolume=9%7B%5C&%7Dissue=7%7B%5C&%7Dspage=4502.

[16] Michaël F. L. De Volder et al. "Hierarchical Carbon Nanowire Microarchitectures Made by Plasma-Assisted Pyrolysis of Photoresist". In: *ACS Nano* 5.8 (Aug. 2011), pp. 6593–6600. ISSN: 1936-0851. DOI: 10.1021/nn201976d. URL: https://pubs.acs.org/doi/10.1021/nn201976d.

[17] Xiehong Cao et al. "Graphene Oxide as a Carbon Source for Controlled Growth of Carbon Nanowires". In: *Small* 7.9 (May 2011), pp. 1199–1202. ISSN: 16136810. DOI: 10.1002/smll.201100071. URL: http://doi.wiley.com/10.1002/smll.201100071.

[18] Pierson Hugh. *Handbook of Carbon, Graphite, Diamonds and Fullerenes*. Elsevier, 1994, p. 419. ISBN: 9780815513391.

[19] Hubert B Heersche et al. "Bipolar supercurrent in graphene". In: *Nature* 446.7131 (Mar. 2007), pp. 56–59. ISSN: 0028-0836. DOI: 10.1038/nature05555. URL: http://www.nature.com/articles/nature05555.

[20] R.B. Heimann, S.E. Evsvukov, and Y. Koga. "Carbon allotropes: a suggested classification scheme based on valence orbital hybridization". In: *Carbon* 35.10-11 (1997), pp. 1654–1658. ISSN: 00086223. DOI: 10.1016/S0008-6223(97)82794-7. URL: https://linkinghub.elsevier.com/retrieve/pii/S0008622397827947.

[21] E. A. Belenkov. "Classification of carbon structures". In: *Carbon Nanotubes and Graphene*. Chelyabinsk, Russia: Chelyabinsk State University, 2003, p. 5.

[22] M. Fedel. "Blood compatibility of diamond-like carbon (DLC) coatings". In: *Diamond-Based Materials for Biomedical Applications*. Dlc. Elsevier, 2013, pp. 71–102. ISBN: 9780857093400. DOI: 10.1533/9780857093516.1.71. URL: http://dx.doi.org/10.1533/9780857093516.1.71%20https://linkinghub.elsevier.com/retrieve/pii/B9780857093400500047.

[23] Manijeh Razeghi. *Fundamentals of Solid State Engineering*. Cham: Springer International Publishing, 2019, pp. 1–689. ISBN: 978-3-319-75707-0. DOI: 10.1007/978-3-319-75708-7. URL: http://link.springer.com/10.1007/978-3-319-75708-7.

[24] Keld Alstrup Jensen et al. *Carbon nanotubes - Types, products, market, and provisional assessment of the associated risks to man and the environment*. 1805. The Danish Environmental Protection Agency, 2015, pp. 49–82. ISBN: 978-87-93352-98-8.

[25] Yoong A. Kim et al. "Carbon Nanofibers". In: *Springer Handbook of Nanomaterials*. Ed. by Robert Vajtai. Berlin, Heidelberg: Springer Berlin Heidelberg, 2013, pp. 233–262. ISBN: 978-3-642-20594-1. DOI: 10.1007/978-3-642-20595-8_7. URL: http://link.springer.com/10.1007/978-3-642-20595-8%20http://link.springer.com/10.1007/978-3-642-20595-8%7B%5C_%7D7.

[26] Harry Marsh. *Introduction to Carbon Science*. Vol. 46. 1. Elsevier, Apr. 1989, p. 43. ISBN: 9780408038379. DOI: 10.1016/C2013-0-04111-4. URL: https://linkinghub.elsevier.com/retrieve/pii/C20130041114.

[27] K. S. Novoselov. "Electric Field Effect in Atomically Thin Carbon Films". In: *Science* 306.5696 (Oct. 2004), pp. 666–669. ISSN: 0036-8075. DOI: 10.1126/science.1102896. URL: https://www.sciencemag.org/lookup/doi/10.1126/science.1102896.

[28] F Schedin et al. "Detection of individual gas molecules adsorbed on graphene". In: *Nature Materials* 6.9 (Sept. 2007), pp. 652–655. ISSN: 1476-1122. DOI: 10.1038/nmat1967. URL: http://www.nature.com/articles/nmat1967.

[29] Yasuhide Ohno et al. "Electrolyte-Gated Graphene Field-Effect Transistors for Detecting pH and Protein Adsorption". In: *Nano Letters* 9.9 (Sept. 2009),

pp. 3318–3322. ISSN: 1530-6984. DOI: 10.1021/nl901596m. URL: https://pubs.acs.org/doi/10.1021/nl901596m.

[30] Vinod Kumar Khanna. *Nanosensors*. Vol. 53. 4. CRC Press, Apr. 2016, pp. 391–392. ISBN: 9780429093951. DOI: 10.1201/b11289. URL: http://www.tandfonline.com/doi/abs/10.1080/00107514.2012.689351%20https://www.taylorfrancis.com/books/9781439827130.

[31] Jia Guo et al. "Preparation, characterization, and nonlinear optical properties of hybridized graphene @ gold nanorods nanocomposites". In: *Applied Surface Science* 433 (Mar. 2018), pp. 45–50. ISSN: 01694332. DOI: 10.1016/j.apsusc.2017.10.042. URL: http://dx.doi.org/10.1016/j.apsusc.2017.10.042%20https://linkinghub.elsevier.com/retrieve/pii/S0169433217329653.

[32] Suman Kundu et al. "A planar supercapacitor made of supramolecular nanofibre based solid electrolyte exhibiting 8 V window". In: *Nano Energy* 61.April (July 2019), pp. 259–266. ISSN: 22112855. DOI: 10.1016/j.nanoen.2019.04.054. URL: https://doi.org/10.1016/j.nanoen.2019.04.054%20https://linkinghub.elsevier.com/retrieve/pii/S2211285519303556.

[33] Yasmina Bencheikh et al. "High performance silicon nanowires/ruthenium nanoparticles micro-supercapacitors". In: *Electrochimica Acta* 311 (July 2019), pp. 150–159. ISSN: 00134686. DOI: 10.1016/j.electacta.2019.04.083. URL: https://linkinghub.elsevier.com/retrieve/pii/S0013468619307698.

[34] Mildred Dresselhaus et al. "Nanowires". In: *Springer Handbook of Nanotechnology*. Berlin, Heidelberg: Springer Berlin Heidelberg, 2007, pp. 113–160. DOI: 10.1007/978-3-540-29857-1_4. URL: http://link.springer.com/10.1007/978-3-540-29857-1%7B%5C_%7D4.

[35] Edward D. Weil. "Carbon fibers, 2nd edition by J. B. Donnet and R. C. Bansal, Marcel Dekker, New York (1990), ISBN 470 pp., price $150.00". In: *Polymers for Advanced Technologies* 3.1 (Feb. 1992), pp. 47–47. ISSN: 10427147. DOI: 10.1002/pat.1992.220030109. URL: http://doi.wiley.com/10.1002/pat.1992.220030109.

[36] Xiaosong Huang. "Fabrication and Properties of Carbon Fibers". In: *Materials* 2.4 (Dec. 2009), pp. 2369–2403. ISSN: 1996-1944. DOI: 10.3390/ma2042369. URL: http://www.mdpi.com/1996-1944/2/4/2369.

[37] D.D.L. Chung and D. Chung. *Carbon Fiber Composites*. Elsevier Science, 2012. ISBN: 9780080500737. URL: https://books.google.com.mx/books?id=UYQXAAAAQBAJ.

[38] Shekhar Subramoney. "Science of fullerenes and carbon nanotubes. ByM. S. Dresselhaus,G. Dresselhaus, andP. C. Eklund, XVIII, 965 pp., Academic press, San Diego, CA 1996, hardcover, ISBN 012-221820-5". In: *Advanced Materials* 9.15 (1997), pp. 1193–1193. ISSN: 0935-9648. DOI: 10.1002/adma.19970091518. URL: http://doi.wiley.com/10.1002/adma.19970091518.

[39] M. S. Dresselhaus et al. "Carbon Nanotubes". In: *Electronics*. 1. 2000, pp. 331–379. DOI: 10.1007/978-94-011-4038-6_9. URL: http://link.springer.com/10.1007/978-94-011-4038-6%7B%5C_%7D9.

[40] N.M. Rodriguez. "A review of catalytically grown carbon nanofibers". In: *Journal of Materials Research* 8.12 (Dec. 1993), pp. 3233–3250. ISSN: 0884-2914. DOI: 10.1557/JMR.1993.3233. URL: https://www.cambridge.org/core/product/identifier/S0884291400072551/type/journal%7B%5C_%7Darticle.

[41] Seong-Ho Yoon et al. "KOH activation of carbon nanofibers". In: *Carbon* 42.8-9 (2004), pp. 1723–1729. ISSN: 00086223. DOI: 10.1016/j.carbon.2004.03.006. URL: https://linkinghub.elsevier.com/retrieve/pii/S0008622304001630.

[42] Qingfeng Liu et al. "Semiconducting properties of cup-stacked carbon nanotubes". In: *Carbon* 47.3 (Mar. 2009), pp. 731–736. ISSN: 00086223. DOI: 10.1016/j.carbon.2008.11.005. URL: http://dx.doi.org/10.1016/j.carbon.2008.11.005%20https://linkinghub.elsevier.com/retrieve/pii/S0008622308006003.

[43] Morinobu Endo et al. "Selective and Efficient Impregnation of Metal Nanoparticles on Cup-Stacked-Type Carbon Nanofibers". In: *Nano Letters* 3.6 (June 2003), pp. 723–726. ISSN: 1530-6984. DOI: 10.1021/nl034136h. URL: https://pubs.acs.org/doi/10.1021/nl034136h.

[44] Tomohiro Yokozeki et al. "Fracture toughness improvement of CFRP laminates by dispersion of cup-stacked carbon nanotubes". In: *Composites Science and Technology* 69.14 (Nov. 2009), pp. 2268–2273. ISSN: 02663538. DOI: 10.1016/j.compscitech.2008.12.017. URL: http://dx.doi.org/10.1016/j.compscitech.2008.12.017%20https://linkinghub.elsevier.com/retrieve/pii/S0266353808005265.

[45] Elzbieta Frackowiak and François Béguin. "Electrochemical storage of energy in carbon nanotubes and nanostructured carbons". In: *Carbon* 40.10 (Aug. 2002), pp. 1775–1787. ISSN: 00086223. DOI: 10.1016/S0008-6223(02)00045-3. URL: https://linkinghub.elsevier.com/retrieve/pii/S0008622302000453.

[46] M. Endo et al. "Recent development of carbon materials for Li ion batteries". In: *Carbon* 38.2 (2000), pp. 183–197. ISSN: 00086223. DOI: 10.1016/S0008-6223(99)00141-4. URL: https://linkinghub.elsevier.com/retrieve/pii/S0008622399001414.

[47] Martin Winter et al. "Insertion Electrode Materials for Rechargeable Lithium Batteries". In: *Advanced Materials* 10.10 (July 1998), pp. 725–763. ISSN: 0935-9648. DOI: 10.1002/(SICI)1521-4095(199807)10:10<725::AID-ADMA725>3.0.CO;2-Z. URL: https://onlinelibrary.wiley.com/doi/10.1002/(SICI)1521-4095(199807)10:10%7B%5C%%7D3C725::AID-ADMA725%7B%5C%%7D3E3.0.CO;2-Z.

[48] M. Endo et al. "Capacitance and Pore-Size Distribution in Aqueous and Nonaqueous Electrolytes Using Various Activated Carbon Electrodes". In: *Journal of The Electrochemical Society* 148.8 (2001), A910. ISSN: 00134651. DOI: 10.1149/1.1382589. URL: https://iopscience.iop.org/article/10.1149/1.1382589.

[49] Elzbieta Frackowiak and François Béguin. "Carbon materials for the electrochemical storage of energy in capacitors". In: *Carbon* 39.6 (May 2001), pp. 937–950. ISSN: 00086223. DOI: 10.1016/S0008-6223(00)00183-4. URL: https://linkinghub.elsevier.com/retrieve/pii/S0008622300001834.

[50] A.G. Pandolfo and A.F. Hollenkamp. "Carbon properties and their role in supercapacitors". In: *Journal of Power Sources* 157.1 (June 2006), pp. 11–27. ISSN: 03787753. DOI: 10.1016/j.jpowsour.2006.02.065. URL: https://linkinghub.elsevier.com/retrieve/pii/S0378775306003442.

[51] B. E. Conway. *Electrochemical Supercapacitors*. Vol. 25. 3. Boston, MA: Springer US, 1999, pp. 907–915. ISBN: 978-1-4757-3060-9. DOI: 10.1007/978-1-4757-3058-6. URL: http://link.springer.com/10.1007/978-1-4757-3058-6.

[52] Hee Cheul Choi et al. "Spontaneous Reduction of Metal Ions on the Sidewalls of Carbon Nanotubes". In: *Journal of the American Chemical Society* 124.31 (Aug. 2002), pp. 9058–9059. ISSN: 0002-7863. DOI: 10.1021/ja026824t. URL: https://pubs.acs.org/doi/10.1021/ja026824t.

[53] Wenzhen Li et al. "Carbon nanotubes as support for cathode catalyst of a direct methanol fuel cell". In: *Carbon* 40.5 (Apr. 2002), pp. 791–794. ISSN: 00086223. DOI: 10.1016/S0008-6223(02)00039-8. URL: https://linkinghub.elsevier.com/retrieve/pii/S0008622302000398.

[54] J. M. Planeix et al. "Application of Carbon Nanotubes as Supports in Heterogeneous Catalysis". In: *Journal of the American Chemical Society* 116.17 (Aug. 1994), pp. 7935–7936. ISSN: 0002-7863. DOI: 10.1021/ja00096a076. URL: https://pubs.acs.org/doi/abs/10.1021/ja00096a076.

[55] M.C. Román-Martínez et al. "Metal-support interaction in Pt/C catalysts. Influence of the support surface chemistry and the metal precursor". In: *Carbon* 33.1 (1995), pp. 3–13. ISSN: 00086223. DOI: 10.1016/0008-6223(94)00096-I. URL: https://linkinghub.elsevier.com/retrieve/pii/000862239400096I.

[56] Philippe Serp and Jośe Lúís Figueiredo, eds. *Carbon Materials for Catalysis*. Hoboken, NJ, USA: John Wiley & Sons, Inc., Dec. 2008. ISBN: 9780470403709. DOI: 10.1002/9780470403709. URL: http://doi.wiley.com/10.1002/9780470403709.

[57] F.H. Bach et al. "Uncertainty in xenotransplantation: Individual benefit versus collective risk". In: *Nature Medicine* 4.2 (Feb. 1998), pp. 141–144. ISSN: 1078-8956. DOI: 10.1038/nm0298-141. URL: http://www.nature.com/articles/nm0298-141.

[58] D. Butler et al. "Last chance to stop and think on risks of xenotransplants". In: *Nature* 391.6665 (Jan. 1998), pp. 321–322. ISSN: 0028-0836. DOI: 10.1038/34749. URL: http://www.nature.com/articles/34749.

[59] Frank Delustro et al. "Immune Responses to Allogeneic and Xenogeneic Implants of Collagen and Collagen Derivatives". In: *Clinical Orthopaedics and Related Research* 260 (Nov. 1990), pp. 263–279. ISSN: 0009-921X. DOI: 10.1097/00003086-199011000-00043. URL: http://journals.lww.com/00003086-199011000-00043.

[60] Juan C. Chachques et al. "Myocardial Assistance by Grafting a New Bioartificial Upgraded Myocardium (MAGNUM Trial): Clinical Feasibility Study". In: *The Annals of Thoracic Surgery* 85.3 (Mar. 2008), pp. 901–908. ISSN: 00034975. DOI: 10.1016/j.athoracsur.2007.10.052. URL: https://linkinghub.elsevier.com/retrieve/pii/S0003497507021819.

[61] Anthony Atala et al. "Tissue-engineered autologous bladders for patients needing cystoplasty". In: *The Lancet* 367.9518 (Apr. 2006), pp. 1241–1246. ISSN: 01406736. DOI: 10.1016/S0140-6736(06)68438-9. URL: https://linkinghub.elsevier.com/retrieve/pii/S0140673606684389.

[62] Julie Glowacki and Shuichi Mizuno. "Collagen scaffolds for tissue engineering". In: *Biopolymers* 89.5 (May 2008), pp. 338–344. ISSN: 00063525. DOI: 10.1002/bip.20871. URL: http://doi.wiley.com/10.1002/bip.20871.

[63] Mani T. Valarmathi et al. "The influence of proepicardial cells on the osteogenic potential of marrow stromal cells in a three-dimensional tubular scaffold". In: *Biomaterials* 29.14 (May 2008), pp. 2203–2216. ISSN: 01429612. DOI: 10.1016/j.biomaterials.2008.01.025. URL: https://linkinghub.elsevier.com/retrieve/pii/S0142961208000550.

[64] Kaeuis A. Faraj, Toin H. van Kuppevelt, and Willeke F. Daamen. "Construction of Collagen Scaffolds That Mimic the Three-Dimensional Architecture of Specific Tissues". In: *Tissue Engineering* 13.10 (Oct. 2007), pp. 2387–2394. ISSN: 1076-3279. DOI: 10.1089/ten.2006.0320. URL: https://www.liebertpub.com/doi/10.1089/ten.2006.0320.

[65] Tuomo Visuri, Olli Kiviluoto, and Marja Eskelin. "Carbon fiber for repair of the rotator cuff: A 4-year follow-up of 14 cases". In: *Acta Orthopaedica Scandinavica* 62.4 (Jan. 1991), pp. 356–359. ISSN: 0001-6470. DOI: 10.3109/17453679108994469. URL: http://www.tandfonline.com/doi/full/10.3109/17453679108994469.

[66] John R. Parsons et al. "Long-Term Follow-up of Achilles Tendon Repair with an Absorbable Polymer Carbon Fiber Composite". In: *Foot & Ankle* 9.4 (Feb. 1989), pp. 179–184. ISSN: 0198-0211. DOI: 10.1177/107110078900900406. URL: http://journals.sagepub.com/doi/10.1177/107110078900900406.

[67] Seeram Ramakrishna et al. *An Introduction to Electrospinning and Nanofibers*. WORLD SCIENTIFIC, June 2005, pp. 1–382. ISBN: 978-981-256-415-3. DOI: 10.

1142/5894. URL: https://www.worldscientific.com/worldscibooks/10.1142/5894.

[68] Darrell H. Reneker et al. "Bending instability of electrically charged liquid jets of polymer solutions in electrospinning". In: *Journal of Applied Physics* 87.9 (May 2000), pp. 4531–4547. ISSN: 0021-8979. DOI: 10.1063/1.373532. URL: http://aip.scitation.org/doi/10.1063/1.373532.

[69] Ian D. Norris et al. "Electrostatic fabrication of ultrafine conducting fibers: polyaniline/polyethylene oxide blends". In: *Synthetic Metals* 114.2 (Aug. 2000), pp. 109–114. ISSN: 03796779. DOI: 10.1016/S0379-6779(00)00217-4. URL: https://linkinghub.elsevier.com/retrieve/pii/S0379677900002174.

[70] Giovanni Vozzi et al. "Microfabricated PLGA scaffolds: a comparative study for application to tissue engineering". In: *Materials Science and Engineering: C* 20.1-2 (May 2002), pp. 43–47. ISSN: 09284931. DOI: 10.1016/S0928-4931(02)00011-5. URL: https://linkinghub.elsevier.com/retrieve/pii/S0928493102000115.

[71] C. Kim and K. S. Yang. "Electrochemical properties of carbon nanofiber web as an electrode for supercapacitor prepared by electrospinning". In: *Applied Physics Letters* 83.6 (Aug. 2003), pp. 1216–1218. ISSN: 0003-6951. DOI: 10.1063/1.1599963. URL: http://aip.scitation.org/doi/10.1063/1.1599963.

[72] R. Dersch et al. "Nanoprocessing of polymers: applications in medicine, sensors, catalysis, photonics". In: *Polymers for Advanced Technologies* 16.2-3 (2005), pp. 276–282. ISSN: 1042-7147. DOI: 10.1002/pat.568. URL: http://doi.wiley.com/10.1002/pat.568.

[73] Braulio Cardenas-Benitez et al. "Pyrolysis-induced shrinking of three-dimensional structures fabricated by two-photon polymerization: experiment and theoretical model". In: *Microsystems & Nanoengineering* 5.1 (2019). ISSN: 2055-7434. DOI: 10.1038/s41378-019-0079-9. URL: http://dx.doi.org/10.1038/s41378-019-0079-9.

[74] Bidhan Pramanick et al. "Effect of pyrolysis process parameters on electrical, physical, chemical and electro-chemical properties of SU-8-derived carbon structures fabricated using the C-MEMS process". In: *Materials Today: Proceedings* 5.3 (2018), pp. 9669–9682. ISSN: 22147853. DOI: 10.1016/j.matpr.2017.10.153. URL: www.sciencedirect.comwww.materialstoday.com/proceedings2214-7853.

[75] Shinji Okazaki. "Resolution limits of optical lithography". In: *Journal of Vacuum Science & Technology B: Microelectronics and Nanometer Structures* 9.6 (Nov. 1991), p. 2829. ISSN: 0734211X. DOI: 10.1116/1.585650. URL: http://scitation.aip.org/content/avs/journal/jvstb/9/6/10.1116/1.585650.

[76] Microchem. "SU-8 2000 Series Resists". In: *MicroChem Datenbank* (2012), pp. 2–10. URL: https://louisville.edu/micronano/files/documents/safety-data-sheets-sds/SU82000.pdf.

[77] Jan Boer and Clemens Blitterswijk. *Tissue Engineering*. Ed. by Academic Press of Elsevier AP. 2nd. Safary O Reilly, 2014. URL: https://learning.oreilly.com/library/view/tissue-engineering-2nd/9780124201453/XHTML/B9780124201453000109/B9780124201453000109.xhtml.

[78] Kolin C. Hribar et al. "Light-assisted direct-write of 3D functional biomaterials". In: *Lab Chip* 14.2 (Jan. 2014), pp. 268–275. ISSN: 1473-0197. DOI: 10.1039/C3LC50634G. URL: http://www.ncbi.nlm.nih.gov/pubmed/24257507%20http://xlink.rsc.org/?DOI=C3LC50634G.

[79] Stefan. Landis. *Nano-Lithography*. Ed. by Stefan Landis. Hoboken, NJ USA: John Wiley & Sons, Inc., Feb. 2013, p. 325. ISBN: 9781118622582. DOI: 10.1002/9781118622582. URL: https://learning.oreilly.com/library/view/nano-lithography/9781118621707/%20http://doi.wiley.com/10.1002/9781118622582.

[80] Xiao-Xiao He et al. "Near-Field Electrospinning: Progress and Applications". In: *The Journal of Physical Chemistry C* 121.16 (Apr. 2017), pp. 8663–8678. ISSN: 1932-7447. DOI: 10.1021/acs.jpcc.6b12783. URL: https://pubs.acs.org/doi/10.1021/acs.jpcc.6b12783.

[81] Matthew E. Helgeson and Norman J. Wagner. "A correlation for the diameter of electrospun polymer nanofibers". In: *AIChE Journal* 53.1 (Jan. 2007), pp. 51–55. ISSN: 00011541. DOI: 10.1002/aic.11056. arXiv: arXiv:1402.6991v1. URL: http://doi.wiley.com/10.1002/aic.11056.

[82] Sung Yeun Yang et al. "Fabrication of microgrooved scaffolds using near-field electrospinning-assisted lithography (NFEAL)". In: *Journal of Industrial and Engineering Chemistry* 80 (2019), pp. 471–478. ISSN: 22345957. DOI: 10.1016/j.jiec.2019.08.025. URL: https://doi.org/10.1016/j.jiec.2019.08.025.

[83] Pouria Fattahi, Jordan T. Dover, and Justin L. Brown. "3D Near-Field Electrospinning of Biomaterial Microfibers with Potential for Blended Microfiber-Cell-Loaded Gel Composite Structures". In: *Advanced Healthcare Materials* 6.19 (Oct. 2017), p. 1700456. ISSN: 21922640. DOI: 10.1002/adhm.201700456. URL: https://linkinghub.elsevier.com/retrieve/pii/S0031938416312148%20http://doi.wiley.com/10.1002/adhm.201700456.

[84] Dongwoon Shin et al. "Droplet-jet mode near-field electrospinning for controlled helix patterns with sub-10 μ m coiling diameter". In: *Journal of Micromechanics and Microengineering* 29.4 (Apr. 2019), p. 045004. ISSN: 0960-1317. DOI: 10.1088/1361-6439/ab025e. URL: http://stacks.iop.org/0960-1317/29/i=4/a=045004?key=crossref.9074191901b0e70d0b50dd4c39ae73e4.

[85] Han Wang et al. "Research on Multinozzle Near-Field Electrospinning Patterned Deposition". In: *Journal of Nanomaterials* 2015 (July 2015), pp. 1–8. ISSN: 1687-4110. DOI: 10.1155/2015/529138. URL: http://www.hindawi.com/journals/jnm/2015/529138/.

[86] Deepak Parajuli et al. "Experimental investigation on process parameters of near-field deposition of electrospinning-based rapid prototyping". In: *Virtual and Physical Prototyping* 11.3 (July 2016), pp. 193–207. ISSN: 1745-2759. DOI: 10.1080/17452759.2016.1210314. URL: https://www.tandfonline.com/doi/full/10.1080/17452759.2016.1210314.

[87] Gaofeng Zheng et al. "Precision deposition of a nanofibre by near-field electrospinning". In: *Journal of Physics D: Applied Physics* 43.41 (Oct. 2010), p. 415501. ISSN: 0022-3727. DOI: 10.1088/0022-3727/43/41/415501. URL: http://stacks.iop.org/0022-3727/43/i=41/a=415501?key=crossref.304f8be16661d1ca2c851060187b2845.

[88] Yiin-Kuen Fuh. "Fabrication of monolithic polymer nanofluidic channels via near-field electrospun nanofibers as sacrificial templates". In: *Journal of Micro/Nanolithography, MEMS, and MOEMS* 10.4 (Oct. 2011), p. 043004. ISSN: 1932-5150. DOI: 10.1117/1.3644990. URL: http://nanolithography.spiedigitallibrary.org/article.aspx?doi=10.1117/1.3644990.

[89] Gernot Hochleitner et al. "Additive manufacturing of scaffolds with sub-micron filaments via melt electrospinning writing". In: *Biofabrication* 7.3 (June 2015), p. 035002. ISSN: 1758-5090. DOI: 10.1088/1758-5090/7/3/035002. URL: https://iopscience.iop.org/article/10.1088/1758-5090/7/3/035002/pdf%20https://iopscience.iop.org/article/10.1088/1758-5090/7/3/035002.

[90] Changhai Ru et al. "A novel mathematical model for controllable near-field electrospinning". In: *AIP Advances* 4.1 (Jan. 2014), p. 017108. ISSN: 2158-3226. DOI: 10.1063/1.4861705. URL: http://aip.scitation.org/doi/10.1063/1.4861705.

[91] Niannan Xue et al. "Rapid Patterning of 1-D Collagenous Topography as an ECM Protein Fibril Platform for Image Cytometry". In: *PLoS ONE* 9.4 (Apr. 2014). Ed. by Wei-Chun Chin, e93590. ISSN: 1932-6203. DOI: 10.1371/journal.pone.0093590. URL: https://dx.plos.org/10.1371/journal.pone.0093590.

[92] Zhifeng Wang et al. "Controllable deposition distance of aligned pattern via dual-nozzle near-field electrospinning". In: *AIP Advances* 7.3 (Mar. 2017), p. 035310. ISSN: 2158-3226. DOI: 10.1063/1.4974936. URL: http://aip.scitation.org/doi/10.1063/1.4974936%20http://dx.doi.org/10.1063/1.4974936.

[93] Jiachen Xu et al. "Accuracy Improvement of Nano-fiber Deposition by Near-Field Electrospinning". In: *International Workshop on Microfactories* IWMF2014.9th (2014). URL: http://conf.papercept.net/images/temp/IWMF/media/files/0041.pdf.

[94] Z.H. Liu et al. "Piezoelectric properties of PVDF/MWCNT nanofiber using near-field electrospinning". In: *Sensors and Actuators A: Physical* 193 (Apr. 2013), pp. 13–24. ISSN: 09244247. DOI: 10.1016/j.sna.2013.01.007. URL:

http://dx.doi.org/10.1016/j.sna.2013.01.007%20https://linkinghub.elsevier.com/retrieve/pii/S0924424713000101.

[95] Cheng-Tang Pan et al. *Poly(γ-benzyl α, l-glutamate) in Cylindrical Near-Field Electrospinning Fabrication and Analysis of Piezoelectric Fibers*. Tech. rep. 2. 2014, pp. 63–73. URL: https://myukk.org/SM2017/sm%7B%5C_%7Dpdf/SM971.pdf.

[96] G. Canton et al. "Improved conductivity of suspended carbon fibers through integration of C-MEMS and Electro-Mechanical Spinning technologies". In: *Carbon* 71 (May 2014), pp. 338–342. ISSN: 00086223. DOI: 10.1016/j.carbon.2014.01.009. URL: https://linkinghub.elsevier.com/retrieve/pii/S0008622314000311.

[97] Syandan Chakraborty et al. "Electrohydrodynamics: A facile technique to fabricate drug delivery systems". In: *Advanced Drug Delivery Reviews* 61.12 (Oct. 2009), pp. 1043–1054. ISSN: 0169409X. DOI: 10.1016/j.addr.2009.07.013. URL: https://linkinghub.elsevier.com/retrieve/pii/S0169409X09002269.

[98] Ashish Gupta et al. "Novel Electrohydrodynamic Printing of Nanocomposite Biopolymer Scaffolds". In: *Journal of BIOACTIVE AND COMPATIBLE POLYMERS* 22 (2007). DOI: 10.1177/0883911507078268. URL: https://journals.sagepub.com/doi/pdf/10.1177/0883911507078268.

[99] Feng-Li He et al. "A novel layer-structured scaffold with large pore sizes suitable for 3D cell culture prepared by near-field electrospinning". In: *Materials Science and Engineering: C* 86.September 2017 (May 2018), pp. 18–27. ISSN: 09284931. DOI: 10.1016/j.msec.2017.12.016. URL: https://doi.org/10.1016/j.msec.2017.12.016%20https://linkinghub.elsevier.com/retrieve/pii/S0928493117325390.

[100] Feng-Lei Zhou et al. "Jet deposition in near-field electrospinning of patterned polycaprolactone and sugar-polycaprolactone core–shell fibres". In: *Polymer* 52.16 (July 2011), pp. 3603–3610. ISSN: 00323861. DOI: 10.1016/j.polymer.2011.06.002. URL: http://dx.doi.org/10.1016/j.polymer.2011.06.002%20https://linkinghub.elsevier.com/retrieve/pii/S0032386111004666.

[101] Jie Chen et al. "Mathematical analysis for controllable near-field electrospinning". In: *2013 International Conference on Manipulation, Manufacturing and Measurement on the Nanoscale, 3M-NANO 2013 - Conference Proceedings* August (2013), pp. 207–210. DOI: 10.1109/3M-NANO.2013.6737415.

[102] Gareth R. Williams, Bahijja T. Raimi-Abraham, and C. J. Luo. "Electrospinning fundamentals". In: *Nanofibres in Drug Delivery* (2018), pp. 24–59. DOI: 10.2307/j.ctv550dd1.6.

[103] Woo Seok Choi et al. "Electrospinning onto Insulating Substrates by Controlling Surface Wettability and Humidity". In: *Nanoscale Research Letters* 12 (2017). ISSN: 1556276X. DOI: 10.1186/s11671-017-2380-6.

[104] Yanqiao Pan and Liangcai Zeng. "Simulation and Validation of Droplet Generation Process for Revealing Three Design Constraints in Electrohydrodynamic Jet Printing". In: *Micromachines* 10.2 (Jan. 2019), p. 94. ISSN: 2072-666X. DOI: 10.3390/mi10020094. URL: http://www.mdpi.com/2072-666X/10/2/94.

[105] T. P. Lei, X. Z. Lu, and F. Yang. "Fabrication of various micro/nano structures by modified near-field electrospinning". In: *AIP Advances* 5.4 (Apr. 2015), p. 041301. ISSN: 2158-3226. DOI: 10.1063/1.4901879. URL: http://aip.scitation.org/doi/10.1063/1.4901879.

[106] Kyeorei Lim et al. "Metal oxide patterns of one-dimensional nanofibers: on-demand, direct-write fabrication, and application as a novel platform for gas detection". In: *Journal of Materials Chemistry A* 7.43 (2019), pp. 24919–24928. ISSN: 2050-7488. DOI: 10.1039/C9TA09708B. URL: http://xlink.rsc.org/?DOI=C9TA09708B.

[107] Yang-Seok Park et al. "Near-Field Electrospinning for Three-Dimensional Stacked Nanoarchitectures with High Aspect Ratios". In: *Nano Letters* 20.1 (Jan. 2020), pp. 441–448. ISSN: 1530-6984. DOI: 10.1021/acs.nanolett.9b04162. URL: https://pubs.acs.org/doi/10.1021/acs.nanolett.9b04162.

[108] Yiin-Kuen Fuh, Shengzhan Chen, and Jason S.C. Jang. "Direct-write, Well-aligned Chitosan-Poly(ethylene oxide) Nanofibers Deposited via Near-field Electrospinning". In: *Journal of Macromolecular Science, Part A* 49.10 (Oct. 2012), pp. 845–850. ISSN: 1060-1325. DOI: 10.1080/10601325.2012.714676. URL: http://www.tandfonline.com/doi/abs/10.1080/10601325.2012.714676.

[109] Chieh Chang et al. "Direct-Write Piezoelectric Polymeric Nanogenerator with High Energy Conversion Efficiency". In: *Nano Letters* 10.2 (Feb. 2010), pp. 726–731. ISSN: 1530-6984. DOI: 10.1021/nl9040719. URL: https://pubs.acs.org/doi/10.1021/nl9040719.

[110] Guojie Xu et al. "Accurate fabrication of aligned nanofibers via a double-nozzle near-field electrospinning". In: *Thermal Science* 23.4 (2019), pp. 2143–2150. ISSN: 0354-9836. DOI: 10.2298/TSCI1904143X. URL: http://www.doiserbia.nb.rs/Article.aspx?ID=0354-98361904143X.

[111] Jiarong Zhang et al. "Influence and evaluation of array-nozzle geometry on near- field electrospinning direct writing". In: *Journal of Engineered Fibers and Fabrics* 14 (Jan. 2019), p. 155892501989564. ISSN: 1558-9250. DOI: 10.1177/1558925019895640. URL: http://journals.sagepub.com/doi/10.1177/1558925019895640.

[112] Dongwoon Shin, Jonghyun Kim, and Jiyoung Chang. "Experimental study on jet impact speed in near-field electrospinning for precise patterning of nanofiber". In: *Journal of Manufacturing Processes* 36 (Dec. 2018), pp. 231–237.

ISSN: 1526-6125. DOI: 10.1016/J.JMAPRO.2018.10.011. URL: https://www.sciencedirect.com/science/article/pii/S1526612518315238.

[113] Yiin-Kuen Fuh et al. "Hybrid Energy Harvester Consisting of Piezoelectric Fibers with Largely Enhanced 20 V for Wearable and Muscle-Driven Applications". In: *ACS Applied Materials & Interfaces* 7.31 (Aug. 2015), pp. 16923–16931. ISSN: 1944-8244. DOI: 10.1021/acsami.5b03955. URL: https://pubs.acs.org/doi/10.1021/acsami.5b03955.

[114] Alexander R Nagle et al. "A direct 3D suspension near-field electrospinning technique for the fabrication of polymer nanoarrays". In: *Nanotechnology* 30.19 (May 2019), p. 195301. ISSN: 0957-4484. DOI: 10.1088/1361-6528/ab011b. URL: http://stacks.iop.org/0957-4484/30/i=19/a=195301?key=crossref.f52131109fcde5cb62dca51c37da6e24.

[115] Jie Zheng et al. "Polymer nanofibers prepared by low-voltage near-field electrospinning". In: *Chinese Physics B* 21.4 (2012), pp. 1–6. ISSN: 16741056. DOI: 10.1088/1674-1056/21/4/048102.

[116] Jun Kameoka et al. "A scanning tip electrospinning source for deposition of oriented nanofibres". In: *Nanotechnology* 14.10 (Oct. 2003), pp. 1124–1129. ISSN: 0957-4484. DOI: 10.1088/0957-4484/14/10/310. URL: https://iopscience.iop.org/article/10.1088/0957-4484/14/10/310.

[117] Z H Liu et al. "Direct-write PVDF nonwoven fiber fabric energy harvesters via the hollow cylindrical near-field electrospinning process". In: (2014), pp. 25003–25014. DOI: 10.1088/0964-1726/23/2/025003. URL: http://iopscience.iop.org/0964-1726/23/2/025003.

[118] William E. King et al. "Characterization of Polydioxanone in Near-Field Electrospinning". In: *Polymers* 12.1 (Dec. 2019), p. 1. ISSN: 2073-4360. DOI: 10.3390/polym12010001. URL: https://www.mdpi.com/2073-4360/12/1/1.

[119] Gernot Hochleitner et al. "Melt electrospinning writing of defined scaffolds using polylactide-poly(ethylene glycol) blends with 45S5 bioactive glass particles". In: *Materials Letters* 205 (2017), pp. 257–260. ISSN: 18734979. DOI: 10.1016/j.matlet.2017.06.096.

[120] Jiaxin Jiang et al. "Electrohydrodynamic Direct-Writing Micropatterns with Assisted Airflow". In: *Micromachines* 9.9 (Sept. 2018), p. 456. ISSN: 2072-666X. DOI: 10.3390/mi9090456. URL: http://www.mdpi.com/2072-666X/9/9/456.

[121] O. Husain et al. "Investigating the particle to fibre transition threshold during electrohydrodynamic atomization of a polymer solution". In: *Materials Science and Engineering C* 65 (2016), pp. 240–250. ISSN: 09284931. DOI: 10.1016/j.msec.2016.03.076. URL: http://dx.doi.org/10.1016/j.msec.2016.03.076.

[122] ElectrospinTech. *Advances in Near Field Electrospinning*. 2015. URL: http://electrospintech.com/nearfield.html%7B%5C#%7D.XPqTKFzOmUl.

[123] Toby D. Brown, Paul D. Dalton, and Dietmar W. Hutmacher. "Direct Writing By Way of Melt Electrospinning". In: *Advanced Materials* 23.47 (Dec. 2011),

pp. 5651–5657. ISSN: 09359648. DOI: 10.1002/adma.201103482. URL: http://doi.wiley.com/10.1002/adma.201103482.

[124] Krishna Kolan et al. "Near-field electrospinning of a polymer/bioactive glass composite to fabricate 3D biomimetic structures". In: *International Journal of Bioprinting* 5.1 (Dec. 2018), pp. 0–6. ISSN: 2424-8002. DOI: 10.18063/ijb.v5i1.163. URL: http://ijb.whioce.com/index.php/int-j-bioprinting/article/view/163.

[125] Jiyoung Chang and Liwei Lin. "Large array electrospun PVDF nanogenerators on a flexible substrate". In: *2011 16th International Solid-State Sensors, Actuators and Microsystems Conference*. IEEE, June 2011, pp. 747–750. ISBN: 978-1-4577-0157-3. DOI: 10.1109/TRANSDUCERS.2011.5969865. URL: http://ieeexplore.ieee.org/document/5969865/.

[126] Vince Beachley and Wen Xuejun. "Effect of Electrospinning Parameters on the Nanofibre diameter and length". In: *Material Science and Engineering. C. materials for Biological Applications.* 29.3 (2011), pp. 663–668. DOI: 10.1016/j.msec.2008.10.037.Effect.

[127] Daniela Di Camillo et al. "Near-field electrospinning of conjugated polymer light-emitting nanofibers". In: *Nanoscale* 5 (2013), pp. 11637–11642. DOI: 10.1039/C3NR03094F. URL: https://arxiv.org/ftp/arxiv/papers/1310/1310.5101.pdf.

[128] Jun Kameoka and H. G. Craighead. "Fabrication of oriented polymeric nanofibers on planar surfaces by electrospinning". In: *Applied Physics Letters* 83.2 (July 2003), pp. 371–373. ISSN: 0003-6951. DOI: 10.1063/1.1592638. URL: http://aip.scitation.org/doi/10.1063/1.1592638.

[129] Ningbin Bu et al. "Materials and Manufacturing Processes Continuously Tunable and Oriented Nanofiber Direct-Written by Mechano-Electrospinning Continuously Tunable and Oriented Nanofiber Direct-Written by Mechano-Electrospinning". In: (2012). ISSN: 1532-2475. DOI: 10.1080/10426914.2012.700145. URL: https://www.tandfonline.com/action/journalInformation?journalCode=lmmp20.

[130] Jongwan Lee et al. "Fabrication of Patterned Nanofibrous Mats Using Direct-Write Electrospinning". In: *Langmuir* 28.18 (May 2012), pp. 7267–7275. ISSN: 0743-7463. DOI: 10.1021/la3009249. URL: http://pubs.acs.org/doi/10.1021/la3009249.

[131] YongAn Huang et al. "Versatile, kinetically controlled, high precision electrohydrodynamic writing of micro/nanofibers". In: *Scientific Reports* 4.1 (May 2015), p. 5949. ISSN: 2045-2322. DOI: 10.1038/srep05949. URL: http://www.nature.com/articles/srep05949.

[132] Sara Coppola et al. "Layered 3D Printing by Tethered Pyro-Electrospinning". In: *Advances in Polymer Technology* 2020 (Jan. 2020), pp. 1–9. ISSN: 0730-6679. DOI: 10.1155/2020/1252960. URL: https://www.hindawi.com/journals/apt/2020/1252960/.

[133] Albert Cisquella-Serra et al. "Study of the electrostatic jet initiation in near-field electrospinning". In: *Journal of Colloid and Interface Science* 543 (May 2019), pp. 106–113. ISSN: 0021-9797. DOI: 10.1016/J.JCIS.2019.02.041. URL: https://www.sciencedirect.com/science/article/pii/S0021979719302152.

[134] F. Ruggieri et al. "Preparation of nitrogen doped TiO2 nanofibers by near field electrospinning (NFES) technique for NO2 sensing". In: *Sensors and Actuators B: Chemical* 179 (Mar. 2013), pp. 107–113. ISSN: 09254005. DOI: 10.1016/j.snb.2012.10.094. URL: http://dx.doi.org/10.1016/j.snb.2012.10.094%20https://linkinghub.elsevier.com/retrieve/pii/S0925400512011306.

[135] Gernot Hochleitner et al. "High definition fibrous poly(2-ethyl-2-oxazoline) scaffolds through melt electrospinning writing". In: *Polymer* 55.20 (Sept. 2014), pp. 5017–5023. ISSN: 00323861. DOI: 10.1016/j.polymer.2014.08.024. URL: http://dx.doi.org/10.1016/j.polymer.2014.08.024%20https://linkinghub.elsevier.com/retrieve/pii/S0032386114007162.

[136] Ziming Zhu et al. "Fabricated Wavy Micro/Nanofiber via Auxiliary Electrodes in Near-Field Electrospinning". In: *Materials and Manufacturing Processes* 31.6 (2016), pp. 707–712. ISSN: 15322475. DOI: 10.1080/10426914.2015.1048464. URL: http://dx.doi.org/10.1080/10426914.2015.1048464.

[137] Toby D. Brown et al. "Melt electrospinning of poly(ϵ-caprolactone) scaffolds: Phenomenological observations associated with collection and direct writing". In: *Materials Science and Engineering: C* 45 (Dec. 2014), pp. 698–708. ISSN: 09284931. DOI: 10.1016/j.msec.2014.07.034. URL: http://dx.doi.org/10.1016/j.msec.2014.07.034%20https://linkinghub.elsevier.com/retrieve/pii/S092849311400441X.

[138] Chieh Chang, Kevin Limkrailassiri, and Liwei Lin. "Continuous near-field electrospinning for large area deposition of orderly nanofiber patterns". In: *Appl Phys Lett* 93.12 (2008), p. 3. ISSN: 00036951. DOI: 10.1063/1.2975834. URL: http://www-bsac.eecs.berkeley.edu/publications/search/send%7B%5C_%7Dpublication%7B%5C_%7Dpdf2client.php?pubID=1217995664.

[139] Maximilian Sonntag et al. "Improved control over polymer nanofiber deposition with a programmable 3-axis electrospinning apparatus". In: *Journal of Electrostatics* 103.November 2019 (Jan. 2020), p. 103406. ISSN: 03043886. DOI: 10.1016/j.elstat.2019.103406. URL: https://doi.org/10.1016/j.elstat.2019.103406%20https://linkinghub.elsevier.com/retrieve/pii/S0304388619302463.

[140] Jinseong Kim, Bohee Maeng, and Jungyul Park. "Characterization of 3D electrospinning on inkjet printed conductive pattern on paper". In: *Micro and Nano Systems Letters* 6.1 (Dec. 2018), p. 12. ISSN: 2213-9621. DOI: 10.1186/s40486-018-0074-1. URL: https://mnsl-journal.springeropen.com/articles/10.1186/s40486-018-0074-1.

[141] Jufeng Deng, Chong Liu, and Marc Madou. "Ultra-thin carbon nanofibers based on graphitization of near-field electrospun polyacrylonitrile". In: *Nanoscale* (2020). ISSN: 2040-3364. DOI: 10.1039/D0NR00031K. URL: http://xlink.rsc.org/?DOI=D0NR00031K.

[142] Daewoo Han and Andrew J. Steckl. "Coaxial Electrospinning Formation of Complex Polymer Fibers and their Applications". In: *ChemPlusChem* 84.10 (Oct. 2019), pp. 1453–1497. ISSN: 2192-6506. DOI: 10.1002/cplu.201900281. URL: https://onlinelibrary.wiley.com/doi/abs/10.1002/cplu.201900281.

[143] Derosh George et al. "Fabrication of patterned graphitized carbon wires using low voltage near-field electrospinning, pyrolysis, electrodeposition, and chemical vapor deposition". In: *Microsystems & Nanoengineering* 6.1 (Dec. 2020), p. 7. ISSN: 2055-7434. DOI: 10.1038/s41378-019-0117-7. URL: http://dx.doi.org/10.1038/s41378-019-0117-7%20http://www.nature.com/articles/s41378-019-0117-7.

[144] Daoheng Sun et al. "Near-Field Electrospinning". In: *Nano Letters* 6.4 (Apr. 2006), pp. 839–842. ISSN: 1530-6984. DOI: 10.1021/nl0602701. URL: https://pubs.acs.org/doi/10.1021/nl0602701.

[145] Cheng-Tang Pan et al. "Near-field electrospinning enhances the energy harvesting of hollow PVDF piezoelectric fibers". In: *RSC Advances* 5.103 (2015), pp. 85073–85081. ISSN: 2046-2069. DOI: 10.1039/C5RA16604G. URL: http://xlink.rsc.org/?DOI=C5RA16604G.

[146] Caiwei Shen et al. "Direct-write polymeric strain sensors with arbitary contours on flexible substrates". In: *2016 IEEE 29th International Conference on Micro Electro Mechanical Systems (MEMS)*. January. IEEE, Jan. 2016, pp. 869–872. ISBN: 978-1-5090-1973-1. DOI: 10.1109/MEMSYS.2016.7421768. URL: http://ieeexplore.ieee.org/document/7421768/.

[147] Michael J Strauss et al. "Cooperative Self-Assembly of Pyridine-2,6-Diimine-Linked Macrocycles into Mechanically Robust Nanotubes". In: *Angewandte Chemie International Edition* 58.41 (Oct. 2019), pp. 14708–14714. ISSN: 1433-7851. DOI: 10.1002/anie.201907668. URL: https://onlinelibrary.wiley.com/doi/abs/10.1002/anie.201907668.

[148] Yiin Fuh, Sheng Chen, and Zhe He. "Direct-write, highly aligned chitosan-poly(ethylene oxide) nanofiber patterns for cell morphology and spreading control". In: *Nanoscale Research Letters* 8.1 (2013), p. 97. ISSN: 1556-276X. DOI: 10.1186/1556-276X-8-97. URL: http://nanoscalereslett.springeropen.com/articles/10.1186/1556-276X-8-97.

[149] Soumayajit Sarkar, Seetharama Deevi, and Gary Tepper. "Biased AC electrospinning of aligned polymer nanofibers". In: *Macromolecular Rapid Communications* 28.9 (2007), pp. 1034–1039. ISSN: 10221336. DOI: 10.1002/marc.200700053.

[150] Xiangyu You, Chengcong Ye, and Ping Guo. "Electric field manipulation for deposition control in near-field electrospinning". In: *Journal of Manufacturing Processes* 30 (Dec. 2017), pp. 431–438. ISSN: 15266125. DOI: 10.1016/j.jmapro.2017.10.005. URL: http://dx.doi.org/10.1016/j.jmapro.2017.10.005%20https://linkinghub.elsevier.com/retrieve/pii/S1526612517303018.

[151] Zhifeng Wang et al. "Fabrication and evaluation of controllable deposition distance for aligned pattern by multi-nozzle near-field electrospinning". In: *AIP Advances* 8.7 (July 2018), p. 075111. ISSN: 2158-3226. DOI: 10.1063/1.5032082. URL: http://aip.scitation.org/doi/10.1063/1.5032082.

[152] Jiang-Yi Zheng et al. "Electrohydrodynamic Direct-Write Orderly Micro/Nanofibrous Structure on Flexible Insulating Substrate". In: *Journal of Nanomaterials* 2014 (May 2014), pp. 1–7. ISSN: 1687-4110. DOI: 10.1155/2014/708186. URL: http://www.hindawi.com/journals/jnm/2014/708186/.

[153] Chiho Song et al. "Patterned polydiacetylene-embedded polystyrene nanofibers based on electrohydrodynamic jet printing". In: *Macromolecular Research* 23.1 (Jan. 2015), pp. 118–123. ISSN: 1598-5032. DOI: 10.1007/s13233-015-3024-2. URL: http://link.springer.com/10.1007/s13233-015-3024-2.

[154] Gaofeng Zheng et al. "Experiment and simulation of coiled nanofiber deposition behavior from near-field electrospinning". In: *2010 IEEE 5th International Conference on Nano/Micro Engineered and Molecular Systems*. IEEE, Jan. 2010, pp. 284–288. ISBN: 978-1-4244-6543-9. DOI: 10.1109/NEMS.2010.5592216. URL: http://ieeexplore.ieee.org/document/5592216/.

[155] Z.H. Liu et al. "Crystallization and mechanical behavior of the ferroelectric polymer nonwoven fiber fabrics for highly durable wearable sensor applications". In: *Applied Surface Science* 346 (Aug. 2015), pp. 291–301. ISSN: 01694332. DOI: 10.1016/j.apsusc.2015.03.173. URL: https://linkinghub.elsevier.com/retrieve/pii/S0169433215007898.

[156] Sung-Yong Min et al. "Large-scale organic nanowire lithography and electronics". In: *Nature Communications* 4.1 (June 2013), p. 1773. ISSN: 2041-1723. DOI: 10.1038/ncomms2785. URL: http://www.nature.com/articles/ncomms2785.

[157] Guoxi Luo et al. "High aspect-ratio 3D microstructures via near-field electrospinning for energy storage applications". In: *2016 IEEE 29th International Conference on Micro Electro Mechanical Systems (MEMS)*. January. IEEE, Jan. 2016, pp. 29–32. ISBN: 978-1-5090-1973-1. DOI: 10.1109/MEMSYS.2016.7421549. URL: http://ieeexplore.ieee.org/document/7421549/.

[158] A.A. Yousefi et al. "Uniaxially aligned microwire networks for flexible transparent electrodes using a novel electrospinning set-up". In: *Solar Energy* 188.July (Aug. 2019), pp. 1111–1117. ISSN: 0038092X. DOI: 10.1016/j.solener.2019.07.007. URL: https://linkinghub.elsevier.com/retrieve/pii/S0038092X19306619.

[159] Sara Coppola et al. "Tethered Pyro-Electrohydrodynamic Spinning for Patterning Well-Ordered Structures at Micro-and Nanoscale". In: *Chem. Mater* 26 (2014), p. 3360. DOI: 10.1021/cm501265j. URL: https://pubs.acs.org/doi/10.1021/cm501265j..

[160] Formhals Anton. *Process and apparatus for preparing artificial threads*. 1930. DOI: https://patents.google.com/?q=D01D5\%2f0076.

[161] Zheng-Ming Huang et al. "A review on polymer nanofibers by electrospinning and their applications in nanocomposites". In: *Composites Science and Technology* 63.15 (Nov. 2003), pp. 2223–2253. DOI: 10.1016/S0266-3538(03)00178-7.

[162] Darrell H. Reneker and Alexander L. Yarin. "Electrospinning jets and polymer nanofibers". In: *Polymer* 49.10 (May 2008), pp. 2387–2425. DOI: 10.1016/J.POLYMER.2008.02.002.

[163] Jessica D. Schiffman and Caroline L. Schauer. "A Review: Electrospinning of Biopolymer Nanofibers and their Applications". In: *Polymer Reviews* 48.2 (May 2008), pp. 317–352. DOI: 10.1080/15583720802022182.

[164] Quan Li. *Chapter 7: Liquid Crystal-Functionalized Nano- and Microfibers Produced by Electrospinning - Liquid Crystals Beyond Displays: Chemistry, Physics, and Applications*. John Wiley & Sons, 2012. DOI: 9781118078617.

[165] Leilei Zhang et al. "Coaxial electrospray of ranibizumab-loaded microparticles for sustained release of anti-VEGF therapies". In: *PLoS ONE* 10.8 (2015), pp. 1–16. DOI: 10.1371/journal.pone.0135608.

[166] Geoffrey Ingram Taylor. "Disintegration of water drops in an electric field". In: *Proceedings of the Royal Society of London. Series A. Mathematical and Physical Sciences* 280.1382 (July 1964), pp. 383–397. DOI: 10.1098/rspa.1964.0151.

[167] Jayesh Doshi and Darrell H Reneker. "Electrospinning process and applications of electrospun fibers". In: *Journal of Electrostatics* 35.2-3 (Aug. 1995), pp. 151–160. DOI: 10.1016/0304-3886(95)00041-8.

[168] Albert Cisquella-Serra et al. "Study of the electrostatic jet initiation in near-field electrospinning". In: *Journal of Colloid and Interface Science* 543 (May 2019), pp. 106–113. DOI: 10.1016/J.JCIS.2019.02.041.

[169] Y. M. Shin et al. "Electrospinning: A whipping fluid jet generates submicron polymer fibers". In: *Applied Physics Letters* 78.8 (Feb. 2001), pp. 1149–1151. DOI: 10.1063/1.1345798.

[170] Royal Kessick, John Fenn, and Gary Tepper. "The use of AC potentials in electrospraying and electrospinning processes". In: *Polymer* 45.9 (Apr. 2004), pp. 2981–2984. DOI: 10.1016/j.polymer.2004.02.056.

[171] Gareth R. Williams, Bahijja T. Raimi-Abraham, and C. J. Luo. "Alternative nanofibre fabrication approaches". In: *Nanofibres in Drug Delivery* (2018), pp. 160–186. DOI: 10.2307/j.ctv550dd1.10.

[172] Soumayajit Sarkar, Seetharama Deevi, and Gary Tepper. "Biased AC electrospinning of aligned polymer nanofibers". In: *Macromolecular Rapid Communications* 28.9 (2007), pp. 1034–1039. DOI: 10.1002/marc.200700053.

[173] Cselko Attila et al. "Alternating current electrospinning for preparation of fibrous drug delivery systems". In: *International Journal of Pharmaceutics* 495.1 (2015). Alternating current electrospinning,Dissolution enhancement,Electrospinning,Poorly water-soluble drugs. Solid dispersion, pp. 75–80. DOI: 10.1016/j.ijpharm.2015.08.069. URL: http://dx.doi.org/10.1016/j.ijpharm.2015.08.069.

[174] Kamal Sarkar et al. "Electrospinning to Forcespinning™". In: *Materials Today* 13.11 (2010), pp. 12–14. DOI: 10.1016/S1369-7021(10)70199-1.

[175] Suntharavathanan Mahalingam and Mohan Edirisinghe. "Forming of polymer nanofibers by a pressurised gyration process". In: *Macromolecular Rapid Communications* 34.14 (2013), pp. 1134–1139. DOI: 10.1002/marc.201300339.

[176] Mohammad Reza Badrossamay et al. "Nanofiber Assembly by Rotary Jet-Spinning". In: *Nano Letters* 10.6 (June 2010), pp. 2257–2261. DOI: 10.1021/nl101355x.

[177] Nicole E. Zander. "Formation of melt and solution spun polycaprolactone fibers by centrifugal spinning". In: *Journal of Applied Polymer Science* 132.2 (2015), pp. 1–9. DOI: 10.1002/app.41269.

[178] L. Amalorpava Mary et al. "Centrifugal spun ultrafine fibrous web as a potential drug delivery vehicle". In: *Express Polymer Letters* 7.3 (2012), pp. 238–248. DOI: 10.3144/expresspolymlett.2013.22.

[179] Xiangwu Zhang and Yao Lu. "Centrifugal spinning: An alternative approach to fabricate nanofibers at high speed and low cost". In: *Polymer Reviews* 54.4 (2014), pp. 677–701. DOI: 10.1080/15583724.2014.935858.

[180] O O Dosunmu et al. "Electrospinning of polymer nanofibres from multiple jets on a porous tubular surface". In: *Nanotechnology* 17.4 (Feb. 2006), pp. 1123–1127. DOI: 10.1088/0957-4484/17/4/046.

[181] Mariya Kancheva et al. "Advanced centrifugal electrospinning setup". In: *Materials Letters* 136 (2014), pp. 150–152. DOI: 10.1016/j.matlet.2014.08.045.

[182] Ariane E. Erickson et al. "High-throughput and high-yield fabrication of uniaxially-aligned chitosan-based nanofibers by centrifugal electrospinning". In: *Carbohydrate Polymers* 134 (2015), pp. 467–474. DOI: 10.1016/j.carbpol.2015.07.097.

[183] Chia Chun Liao et al. "Electrospinning fabrication of partially crystalline bisphenol A polycarbonate nanofibers: Effects on conformation, crystallinity, and mechanical properties". In: *European Polymer Journal* 47.5 (2011), pp. 911–924. DOI: 10.1016/j.eurpolymj.2011.01.006.

[184] Dennis Edmondson et al. "Centrifugal electrospinning of highly aligned polymer nanofibers over a large area". In: *Journal of Materials Chemistry* 22.35 (Aug. 2012), p. 18646. DOI: 10.1039/c2jm33877g.

[185] Michelle Andrade Souza, Karine Yamamura Sakamoto, and Luiz Henrique Capparelli Mattoso. "Release of the diclofenac sodium by nanofibers of poly(3-hydroxybutyrate- co -3-hydroxyvalerate) obtained from electrospinning and solution blow spinning". In: *Journal of Nanomaterials* 2014 (2014). DOI: 10.1155/2014/129035.

[186] Juliano Elvis Oliveira et al. "Development of poly(lactic acid) nanostructured membranes for the controlled delivery of progesterone to livestock animals". In: *Materials Science and Engineering C* 33.2 (2013), pp. 844–849. DOI: 10.1016/j.msec.2012.10.032.

[187] T Ondarçuhu and C Joachim. "Drawing a single nanofibre over hundreds of microns". In: *Europhysics Letters (EPL)* 42.2 (Apr. 1998), pp. 215–220. DOI: 10.1209/epl/i1998-00233-9.

[188] Amrinder S. Nain et al. "Drawing suspended polymer micro-/nanofibers using glass micropipettes". In: *Applied Physics Letters* 89.18 (2006). DOI: 10.1063/1.2372694.

[189] Alexander Tokarev et al. "Touch- and Brush-Spinning of Nanofibers". In: *Advanced Materials* 27.41 (2015), pp. 6526–6532. DOI: 10.1002/adma.201502768.

[190] Jie Cheng et al. "Electrospinning versus microfluidic spinning of functional fibers for biomedical applications". In: *Biomaterials* 114 (2017), pp. 121–143. DOI: 10.1016/j.biomaterials.2016.10.040.

[191] Edward Kang et al. "Digitally tunable physicochemical coding of material composition and topography in continuous microfibres". In: *Nature Materials* 10.11 (2011), pp. 877–883. DOI: 10.1038/nmat3108.

[192] Juan Estehan Dıaz et al. "Controlled encapsulation of hydrophobic liquids in hydrophilic polymer nanofibers by co-electrospinning". In: *Advanced Functional Materials* 16.16 (2006), pp. 2110–2116. DOI: 10.1002/adfm.200600204.

[193] I. G. Loscertales et al. "Micro/nano encapsulation via electrified coaxial liquid jets". In: *Science* 295.5560 (2002), pp. 1695–1698. DOI: 10.1126/science.1067595.

[194] Zaicheng Sun et al. "Compound Core-Shell Polymer Nanofibers by Co-Electrospinning". In: *Advanced Materials* 15.22 (2003), pp. 1929–1932. DOI: 10.1002/adma.200305136.

[195] Panagiotis Sofokleous et al. "The effect of needle tip displacement in co-axial electrohydrodynamic processing". In: *RSC Advances* 6.79 (2016), pp. 75258–75268. DOI: 10.1039/c6ra08877e.

[196] Z. Ahmad et al. "Generation of multilayered structures for biomedical applications using a novel tri-needle coaxial device and

electrohydrodynamic flow". In: *Journal of the Royal Society Interface* 5.27 (2008), pp. 1255–1261. DOI: 10.1098/rsif.2008.0247.

[197] Z. Ahmad et al. "Generation of multilayered structures for biomedical applications using a novel tri-needle coaxial device and electrohydrodynamic flow". In: *Journal of the Royal Society Interface* 5.27 (2008), pp. 1255–1261. DOI: 10.1098/rsif.2008.0247.

[198] Toby D. Brown, Paul D. Dalton, and Dietmar W. Hutmacher. "Melt electrospinning today: An opportune time for an emerging polymer process". In: *Progress in Polymer Science* 56 (2016), pp. 116–166. DOI: 10.1016/j.progpolymsci.2016.01.001.

[199] Zsombor Kristóf Nagy et al. "Solvent-Free Melt Electrospinning for Preparation of Fast Dissolving Drug Delivery System and Comparison with Solvent-Based Electrospun and Melt Extruded Systems". In: *Journal of Pharmaceutical Sciences* 102.2 (Feb. 2013), pp. 508–517. DOI: 10.1002/jps.23374.

[200] Attila Balogh et al. "Plasticized drug-loaded melt electrospun polymer mats: Characterization, thermal degradation, and release kinetics". In: *Journal of Pharmaceutical Sciences* 103.4 (2014), pp. 1278–1287. DOI: 10.1002/jps.23904.

[201] He Lian and Zhaoxu Meng. "Melt electrospinning vs. solution electrospinning: A comparative study of drug-loaded poly ($ε$-caprolactone) fibres". In: *Materials Science and Engineering C* 74 (2017), pp. 117–123. DOI: 10.1016/j.msec.2017.02.024.

[202] Gernot Hochleitner et al. "Melt electrospinning writing of defined scaffolds using polylactide-poly(ethylene glycol) blends with 45S5 bioactive glass particles". In: *Materials Letters* 205 (2017), pp. 257–260. DOI: 10.1016/j.matlet.2017.06.096.

[203] † Jesse T. McCann et al. "Melt Coaxial Electrospinning: A Versatile Method for the Encapsulation of Solid Materials and Fabrication of Phase Change Nanofibers". In: (2006). DOI: 10.1021/NL0620839.

[204] Chieh Chang, Kevin Limkrailassiri, and Liwei Lin. "Continuous near-field electrospinning for large area deposition of orderly nanofiber patterns". In: *Appl Phys Lett* (2008), p. 3. DOI: 10.1063/1.2975834.

[205] Jie Zheng et al. "Polymer nanofibers prepared by low-voltage near-field electrospinning". In: *Chinese Physics B* 21.4 (2012), pp. 1–6. DOI: 10.1088/1674-1056/21/4/048102.

[206] Syandan Chakraborty et al. "Electrohydrodynamics: A facile technique to fabricate drug delivery systems". In: *Advanced Drug Delivery Reviews* 61.12 (Oct. 2009), pp. 1043–1054. DOI: 10.1016/j.addr.2009.07.013.

[207] Jiajia Xue et al. "Electrospinning and Electrospun Nanofibers: Methods, Materials, and Applications". In: *Chemical Reviews* 119.8 (Apr. 2019), pp. 5298–5415. DOI: 10.1021/acs.chemrev.8b00593.

[208] Gareth R. Williams, Bahijja T. Raimi-Abraham, and C. J. Luo. "Monoaxial electrospinning". In: *Nanofibres in Drug Delivery* (2018), pp. 60–105. DOI: 10.2307/j.ctv550dd1.7.

[209] Konstantinos Alexandros G. Katsogiannis, Goran T. Vladisavljević, and Stella Georgiadou. "Porous electrospun polycaprolactone (PCL) fibres by phase separation". In: *European Polymer Journal* 69 (2015), pp. 284–295. DOI: 10.1016/j.eurpolymj.2015.01.028.

[210] Filippos Tourlomousis et al. "Melt Electrospinning Writing Process Guided by a "Printability Number"". In: *Journal of Manufacturing Science and Engineering* 139.8 (Aug. 2017). ISSN: 1087-1357. DOI: 10.1115/1.4036348. URL: https://asmedigitalcollection.asme.org/manufacturingscience/article/doi/10.1115/1.4036348/376362/Melt-Electrospinning-Writing-Process-Guided-by-a.

[211] Gobind S. Bisht et al. "Controlled Continuous Patterning of Polymeric Nanofibers on Three-Dimensional Substrates Using Low-Voltage Near-Field Electrospinning". In: *Nano Letters* 11.4 (Apr. 2011), pp. 1831–1837. DOI: 10.1021/nl2006164.

[212] Jinseong Kim, Bohee Maeng, and Jungyul Park. "Characterization of 3D electrospinning on inkjet printed conductive pattern on paper". In: *Micro and Nano Systems Letters* 6.1 (Dec. 2018), p. 12. DOI: 10.1186/s40486-018-0074-1.

[213] Ashish Gupta et al. "Novel Electrohydrodynamic Printing of Nanocomposite Biopolymer Scaffolds". In: *Journal of BIOACTIVE AND COMPATIBLE POLYMERS* 22 (2007). DOI: 10.1177/0883911507078268.

[214] Han Wang et al. "Research on Multinozzle Near-Field Electrospinning Patterned Deposition". In: *Journal of Nanomaterials* 2015 (July 2015), pp. 1–8. DOI: 10.1155/2015/529138.

[215] Zhifeng Wang et al. "Controllable deposition distance of aligned pattern via dual-nozzle near-field electrospinning". In: *AIP Advances* 7.3 (Mar. 2017), p. 035310. DOI: 10.1063/1.4974936.

[216] Zhifeng Wang et al. "Fabrication and evaluation of controllable deposition distance for aligned pattern by multi-nozzle near-field electrospinning". In: *AIP Advances* 8.7 (July 2018), p. 075111. DOI: 10.1063/1.5032082.

[217] YongAn Huang et al. "Versatile, kinetically controlled, high precision electrohydrodynamic writing of micro/nanofibers". In: *Scientific Reports* 4.1 (May 2015), p. 5949. DOI: 10.1038/srep05949.

[218] Ningbin Bu et al. "Materials and Manufacturing Processes Continuously Tunable and Oriented Nanofiber Direct-Written by Mechano-Electrospinning Continuously Tunable and Oriented Nanofiber Direct-Written by Mechano-Electrospinning". In: (2012). DOI: 10.1080/10426914.2012.700145.

[219] Alexander R Nagle et al. "A direct 3D suspension near-field electrospinning technique for the fabrication of polymer nanoarrays". In: *Nanotechnology* 30.19 (May 2019), p. 195301. DOI: 10.1088/1361-6528/ab011b.

[220] Jun Kameoka and H. G. Craighead. "Fabrication of oriented polymeric nanofibers on planar surfaces by electrospinning". In: *Applied Physics Letters* 83.2 (July 2003), pp. 371–373. DOI: 10.1063/1.1592638.

[221] Daoheng Sun et al. "Near-Field Electrospinning". In: (2006). DOI: 10.1021/nl0602701.

[222] Niannan Xue et al. "Rapid Patterning of 1-D Collagenous Topography as an ECM Protein Fibril Platform for Image Cytometry". In: *PLoS ONE* 9.4 (Apr. 2014). Ed. by Wei-Chun Chin, e93590. DOI: 10.1371/journal.pone.0093590.

[223] Sara Coppola et al. "Tethered Pyro-Electrohydrodynamic Spinning for Patterning Well-Ordered Structures at Micro-and Nanoscale". In: *Chem. Mater* 26 (2014), p. 3360. DOI: 10.1021/cm501265j.

[224] Daniela Di Camillo et al. "Near-field electrospinning of conjugated polymer light-emitting nanofibers". In: *Nanoscale* 5 (2013), pp. 11637–11642. DOI: 10.1039/C3NR03094F.

[225] Qian Xiang et al. "Electrospinning using a Teflon-coated spinneret". In: *Applied Surface Science* 284 (Nov. 2013), pp. 889–893. DOI: 10.1016/j.apsusc.2013.08.030.

[226] Qing Wang et al. "Electrospun amorphous medicated nanocomposites fabricated using a Teflon-based concentric spinneret". In: *E-Polymers* 18.1 (2018), pp. 3–11. DOI: 10.1515/epoly-2017-0110.

[227] Chiho Song et al. "Patterned polydiacetylene-embedded polystyrene nanofibers based on electrohydrodynamic jet printing". In: *Macromolecular Research* 23.1 (Jan. 2015), pp. 118–123. DOI: 10.1007/s13233-015-3024-2.

[228] Geoffrey Taylor. "Electrically Driven Jets". In: *Proceedings of the Royal Society A: Mathematical, Physical and Engineering Sciences* 313.1515 (Dec. 1969), pp. 453–475. DOI: 10.1098/rspa.1969.0205.

[229] J. J. Feng. "The stretching of an electrified non-Newtonian jet: A model for electrospinning". In: *Physics of Fluids* 14.11 (Nov. 2002), pp. 3912–3926. DOI: 10.1063/1.1510664.

[230] Gaofeng Zheng et al. "Precision deposition of a nanofibre by near-field electrospinning". In: *Journal of Physics D: Applied Physics* 43.41 (Oct. 2010), p. 415501. DOI: 10.1088/0022-3727/43/41/415501.

[231] Kamal Sarkar et al. "A neural network model for the numerical prediction of the diameter of electro-spun polyethylene oxide nanofibers". In: *Journal of Materials Processing Technology* 209.7 (Apr. 2009), pp. 3156–3165. ISSN: 09240136. DOI: 10.1016/j.jmatprotec.2008.07.032. URL: https://linkinghub.elsevier.com/retrieve/pii/S0924013608005827.

[232] Yunshen Cai and Michael Gevelber. "The effect of relative humidity and evaporation rate on electrospinning: fiber diameter and measurement for control implications". In: *Journal of Materials Science* 48.22 (Nov. 2013), pp. 7812–7826. ISSN: 0022-2461. DOI: 10.1007/s10853-013-7544-x. URL: http://link.springer.com/10.1007/s10853-013-7544-x.

[233] Chi Wang, Chia-Hung Hsu, and I.-Hwe Hwang. "Scaling laws and internal structure for characterizing electrospun poly[(R)-3-hydroxybutyrate] fibers". In: *Polymer* 49.19 (Sept. 2008), pp. 4188–4195. ISSN: 00323861. DOI: 10.1016/j.polymer.2008.07.033. URL: https://linkinghub.elsevier.com/retrieve/pii/S0032386108006162.

[234] P. M. Widartiningsih et al. "The Influence of Solvent Parameters along Terminal Jet Radius and Fiber Diameter in Electrospinning". In: *Journal of Physics: Conference Series* 1445.1 (Jan. 2020), p. 012025. ISSN: 1742-6588. DOI: 10.1088/1742-6596/1445/1/012025. URL: https://iopscience.iop.org/article/10.1088/1742-6596/1445/1/012025.

[235] Wei-Min Chang, Cheng-Chien Wang, and Chuh-Yung Chen. "The combination of electrospinning and forcespinning: Effects on a viscoelastic jet and a single nanofiber". In: *Chemical Engineering Journal* 244.1 (May 2014), pp. 540–551. ISSN: 13858947. DOI: 10.1016/j.cej.2014.02.001. URL: http://dx.doi.org/10.1016/j.cej.2014.02.001%20https://linkinghub.elsevier.com/retrieve/pii/S1385894714001284.

[236] Hadley Brooks and Nick Tucker. "Electrospinning predictions using artificial neural networks". In: *Polymer* 58 (Feb. 2015), pp. 22–29. ISSN: 00323861. DOI: 10.1016/j.polymer.2014.12.046. URL: http://dx.doi.org/10.1016/j.polymer.2014.12.046%20https://linkinghub.elsevier.com/retrieve/pii/S003238611401146X.

[237] Matthew E. Helgeson et al. "Theory and kinematic measurements of the mechanics of stable electrospun polymer jets". In: *Polymer* 49.12 (June 2008), pp. 2924–2936. ISSN: 00323861. DOI: 10.1016/j.polymer.2008.04.025. URL: https://www.sciencedirect.com/science/article/pii/S0032386108003522%20https://linkinghub.elsevier.com/retrieve/pii/S0032386108003522.

[238] Siddharth B. Gadkari. "Scaling analysis for electrospinning". In: *SpringerPlus* 3.1 (Dec. 2014), p. 705. ISSN: 2193-1801. DOI: 10.1186/2193-1801-3-705. URL: https://springerplus.springeropen.com/articles/10.1186/2193-1801-3-705.

[239] Z H Liu et al. "Direct-write PVDF nonwoven fiber fabric energy harvesters via the hollow cylindrical near-field electrospinning process". In: (2014), pp. 25003–25014. DOI: 10.1088/0964-1726/23/2/025003.

[240] Woo Seok Choi et al. "Electrospinning onto Insulating Substrates by Controlling Surface Wettability and Humidity". In: *Nanoscale Research Letters* 12 (2017). DOI: 10.1186/s11671-017-2380-6.

[241] Yongqing Duan et al. "Helix Electrohydrodynamic Printing of Highly Aligned Serpentine Micro/Nanofibers." In: *Polymers* 9.9 (Sept. 2017). DOI: 10.3390/polym9090434.

[242] Chunxue Zhang et al. "Study on morphology of electrospun poly(vinyl alcohol) mats". In: *European Polymer Journal* 41.3 (Mar. 2005), pp. 423–432.

ISSN: 00143057. DOI: 10.1016/j.eurpolymj.2004.10.027. URL: https://linkinghub.elsevier.com/retrieve/pii/S0014305704003945.

[243] Darrell H Reneker and Iksoo Chun. "Nanometre diameter fibres of polymer, produced by electrospinning". In: *Nanotechnology* 7.3 (Sept. 1996), pp. 216–223. ISSN: 0957-4484. DOI: 10.1088/0957-4484/7/3/009. URL: http://stacks.iop.org/0957-4484/7/i=3/a=009?key=crossref.b62a3c509c723c5a2561f1e345fc1706%20https://iopscience.iop.org/article/10.1088/0957-4484/7/3/009.

[244] O.S. Yördem, M. Papila, and Y.Z. Menceloğlu. "Effects of electrospinning parameters on polyacrylonitrile nanofiber diameter: An investigation by response surface methodology". In: *Materials & Design* 29.1 (Jan. 2008), pp. 34–44. ISSN: 02613069. DOI: 10.1016/j.matdes.2006.12.013. URL: https://linkinghub.elsevier.com/retrieve/pii/S0261306906003967.

[245] Feng-Cheng Chang, Kei-Kei Chan, and Chia-Yuan Chang. "The Effect of Processing Parameters on Formation of Lignosulfonate Fibers Produced using Electrospinning Technology". In: *BioResources* 11.2 (Apr. 2016), pp. 4705–4717. ISSN: 1930-2126. DOI: 10.15376/biores.11.2.4705-4717. URL: http://ojs.cnr.ncsu.edu/index.php/BioRes/article/view/9253.

[246] Yana Bagbi, Arvind Pandey, and Pratima R. Solanki. "Electrospun Nanofibrous Filtration Membranes for Heavy Metals and Dye Removal". In: *Nanoscale Materials in Water Purification*. Elsevier, 2019, pp. 275–288. ISBN: 9780128139271. DOI: 10.1016/B978-0-12-813926-4.00015-X. URL: http://dx.doi.org/10.1016/B978-0-12-813926-4.00015-X%20https://linkinghub.elsevier.com/retrieve/pii/B978012813926400015X.

[247] Afeesh Rajan Unnithan, R.S. Arathyram, and Cheol Sang Kim. "Electrospinning of Polymers for Tissue Engineering". In: *Nanotechnology Applications for Tissue Engineering*. Elsevier, 2015, pp. 45–55. ISBN: 9780323353038. DOI: 10.1016/B978-0-323-32889-0.00003-0. URL: http://dx.doi.org/10.1016/B978-0-323-32889-0.00003-0%20https://linkinghub.elsevier.com/retrieve/pii/B9780323328890000030.

[248] Moses M. Hohman et al. "Electrospinning and electrically forced jets. I. Stability theory". In: *Physics of Fluids* 13.8 (Aug. 2001), pp. 2201–2220. ISSN: 1070-6631. DOI: 10.1063/1.1383791. URL: http://aip.scitation.org/doi/10.1063/1.1383791.

[249] J. J. Feng. "The stretching of an electrified non-Newtonian jet: A model for electrospinning". In: *Physics of Fluids* 14.11 (Nov. 2002), pp. 3912–3926. ISSN: 1070-6631. DOI: 10.1063/1.1510664. URL: http://aip.scitation.org/doi/10.1063/1.1510664.

[250] A. Greiner and J. H. Wendorff. "Functional Self-Assembled Nanofibers by Electrospinning". In: *Self-Assembled Nanomaterials I*. Vol. 219. 1. Berlin, Heidelberg: Springer Berlin Heidelberg, 2008, pp. 107–171. ISBN:

9783540851028. DOI: 10.1007/12_2008_146. URL: http://link.springer.com/10.1007/12%7B%5C_%7D2008%7B%5C_%7D146.

[251] J.M Deitzel et al. "The effect of processing variables on the morphology of electrospun nanofibers and textiles". In: *Polymer* 42.1 (Jan. 2001), pp. 261–272. ISSN: 00323861. DOI: 10.1016/S0032-3861(00)00250-0. URL: https://linkinghub.elsevier.com/retrieve/pii/S0032386100002500.

[252] Wenguo Cui et al. "Investigation on process parameters of electrospinning system through orthogonal experimental design". In: *Journal of Applied Polymer Science* 103.5 (Mar. 2007), pp. 3105–3112. ISSN: 00218995. DOI: 10.1002/app.25464. URL: http://doi.wiley.com/10.1002/app.25464.

[253] Chi Wang, Chia-Hung Hsu, and I.-Hwe Hwang. "Scaling laws and internal structure for characterizing electrospun poly[(R)-3-hydroxybutyrate] fibers". In: *Polymer* 49.19 (Sept. 2008), pp. 4188–4195. ISSN: 00323861. DOI: 10.1016/j.polymer.2008.07.033. URL: https://linkinghub.elsevier.com/retrieve/pii/S0032386108006162.

[254] Matthew G. McKee et al. "Correlations of Solution Rheology with Electrospun Fiber Formation of Linear and Branched Polyesters". In: *Macromolecules* 37.5 (Mar. 2004), pp. 1760–1767. ISSN: 0024-9297. DOI: 10.1021/ma035689h. URL: https://pubs.acs.org/doi/10.1021/ma035689h.

[255] Pankaj Gupta et al. "Electrospinning of linear homopolymers of poly(methyl methacrylate): exploring relationships between fiber formation, viscosity, molecular weight and concentration in a good solvent". In: *Polymer* 46.13 (June 2005), pp. 4799–4810. ISSN: 00323861. DOI: 10.1016/j.polymer.2005.04.021. URL: https://linkinghub.elsevier.com/retrieve/pii/S0032386105004167.

[256] Xiaoyan Yuan et al. "Morphology of ultrafine polysulfone fibers prepared by electrospinning". In: *Polymer International* 53.11 (Nov. 2004), pp. 1704–1710. ISSN: 0959-8103. DOI: 10.1002/pi.1538. URL: http://doi.wiley.com/10.1002/pi.1538.

[257] C. Wang et al. "Investigation of fundamental parameters affecting electrospun PVA/CuS composite nanofibres". In: *Pigment & Resin Technology* 38.1 (Jan. 2009), pp. 25–32. ISSN: 0369-9420. DOI: 10.1108/03699420910923544. URL: https://www.emerald.com/insight/content/doi/10.1108/03699420910923544/full/html.

[258] C.J. Thompson et al. "Effects of parameters on nanofiber diameter determined from electrospinning model". In: *Polymer* 48.23 (Nov. 2007), pp. 6913–6922. ISSN: 00323861. DOI: 10.1016/j.polymer.2007.09.017. URL: https://linkinghub.elsevier.com/retrieve/pii/S0032386107009275.

[259] U. S. Sajeev et al. "Control of nanostructures in PVA, PVA/chitosan blends and PCL through electrospinning". In: *Bulletin of Materials Science* 31.3 (June 2008), pp. 343–351. ISSN: 0250-4707. DOI: 10.1007/s12034-008-0054-9. URL: http://link.springer.com/10.1007/s12034-008-0054-9.

[260] T. Mazoochi and V. Jabbari. "Chitosan Nanofibrous Scaffold Fabricated via Electrospinning: The Effect of Processing Parameters on the Nanofiber Morphology". In: *International Journal of Polymer Analysis and Characterization* 16.5 (July 2011), pp. 277–289. ISSN: 1023-666X. DOI: 10.1080/1023666X.2011.587943. URL: http://www.tandfonline.com/doi/abs/10.1080/1023666X.2011.587943.

[261] A. MATARAM et al. "A REVIEW OF ASSEMBLED POLYACRYLONITRILE-BASED CARBON NANOFIBER PREPARED ELECTROSPINNING PROCESS". In: *International Journal of Nanoscience* 10.03 (June 2011), pp. 455–469. ISSN: 0219-581X. DOI: 10.1142/S0219581X11008228. URL: https://www.worldscientific.com/doi/abs/10.1142/S0219581X11008228.

[262] Yong Liu et al. "Preparation of novel ultrafine fibers based on DNA and poly(ethylene oxide) by electrospinning from aqueous solutions". In: *Reactive and Functional Polymers* 67.5 (May 2007), pp. 461–467. ISSN: 13815148. DOI: 10.1016/j.reactfunctpolym.2007.02.008. URL: https://linkinghub.elsevier.com/retrieve/pii/S1381514807000405.

[263] Homa Homayoni, Seyed Abdolkarim Hosseini Ravandi, and Masoumeh Valizadeh. "Electrospinning of chitosan nanofibers: Processing optimization". In: *Carbohydrate Polymers* 77.3 (July 2009), pp. 656–661. ISSN: 01448617. DOI: 10.1016/j.carbpol.2009.02.008. URL: http://dx.doi.org/10.1016/j.carbpol.2009.02.008%20https://linkinghub.elsevier.com/retrieve/pii/S0144861709000988.

[264] Orlando J. Rojas, Gerardo A. Montero, and Youssef Habibi. "Electrospun nanocomposites from polystyrene loaded with cellulose nanowhiskers". In: *Journal of Applied Polymer Science* 113.2 (July 2009), pp. 927–935. ISSN: 00218995. DOI: 10.1002/app.30011. URL: http://doi.wiley.com/10.1002/app.30011.

[265] Joon-pyo Jeun et al. "Electrospinning of Poly (L-lactide- co -D , L-lactide)". In: 13.4 (2007), pp. 592–596.

[266] Abhay Mohan. "Formation and Characterization of Electrospun Nonwoven Webs". PhD thesis. 2002. URL: https://www.mendeley.com/viewer/?fileId=789cf426-0a97-dd89-4e13-fa027cfe584a%7B%5C&%7DdocumentId=c2902bde-2e32-39df-80cd-8f3b76838cea.

[267] Bumsu Kim et al. "Poly(acrylic acid) nanofibers by electrospinning". In: *Materials Letters* 59.7 (Mar. 2005), pp. 829–832. ISSN: 0167577X. DOI: 10.1016/j.matlet.2004.11.032. URL: https://linkinghub.elsevier.com/retrieve/pii/S0167577X0400878X.

[268] Chidchanok Mit-uppatham, Manit Nithitanakul, and Pitt Supaphol. "Ultrafine Electrospun Polyamide-6 Fibers: Effect of Solution Conditions on Morphology and Average Fiber Diameter". In: *Macromolecular Chemistry and*

Physics 205.17 (Nov. 2004), pp. 2327–2338. ISSN: 1022-1352. DOI: 10.1002/macp.200400225. URL: http://doi.wiley.com/10.1002/macp.200400225.

[269] Hao Fong and Darrell H. Reneker. "Elastomeric nanofibers of styrene-butadiene-styrene triblock copolymer". In: *Journal of Polymer Science, Part B: Polymer Physics* 37.24 (1999), pp. 3488–3493. ISSN: 08876266. DOI: 10.1002/(SICI)1099-0488(19991215)37:24<3488::AID-POLB9>3.0.CO;2-M.

[270] Suresh L. Shenoy et al. "Role of chain entanglements on fiber formation during electrospinning of polymer solutions: good solvent, non-specific polymer–polymer interaction limit". In: *Polymer* 46.10 (Apr. 2005), pp. 3372–3384. ISSN: 00323861. DOI: 10.1016/j.polymer.2005.03.011. URL: https://linkinghub.elsevier.com/retrieve/pii/S0032386105002867.

[271] Teodor Burghelea. *Transport Phenomena in Complex Fluids*. Ed. by Teodor Burghelea and Volfango Bertola. Vol. 598. CISM International Centre for Mechanical Sciences. Cham: Springer International Publishing, 2020. ISBN: 978-3-030-35557-9. DOI: 10.1007/978-3-030-35558-6. URL: http://link.springer.com/10.1007/978-3-030-35558-6.

[272] Bird R. Byron, Armstrong Robert C., and Hassager Ole. *Dynamics of Polymeric Liquids, Volume 1: Fluid Mechanics*. 2nd. Wiley, 1987, p. 672. ISBN: 978-0-471-80245-7. URL: https://www.wiley.com/en-us/Dynamics+of+Polymeric+Liquids%7B%5C%%7D2C+Volume+1%7B%5C%%7D3A+Fluid+Mechanics%7B%5C%%7D2C+2nd+Edition-p-9780471802457.

[273] Christopher W. Macosko. *Rheology: Principles, Measurements, and Applications*. Wiley, 1994, p. 568. URL: https://www.wiley.com/en-us/Rheology%7B%5C%%7D3A+Principles%7B%5C%%7D2C+Measurements%7B%5C%%7D2C+and+Applications-p-9780471185758.

[274] R. W. Connelly and J. Greener. "High-Shear Viscometry with a Rotational Parallel-Disk Device". In: *Journal of Rheology* 29.2 (1985), pp. 209–226. ISSN: 0148-6055. DOI: 10.1122/1.549828.

[275] Christopher J Pipe, Trushant S Majmudar, and Gareth H. McKinley. "High shear rate viscometry". In: *Rheologica Acta* 47.5-6 (July 2008), pp. 621–642. ISSN: 0035-4511. DOI: 10.1007/s00397-008-0268-1. URL: http://link.springer.com/10.1007/s00397-008-0268-1.

[276] Domingo R Flores-hernandez et al. "Tailoring the Diameters of Electro-Mechanically Spun Fibers by Controlling Their Deborah Numbers". In: (2020). DOI: 10.3390/polym12061358.

[277] Vu Anh Doan et al. "Interphase transfer of tackifier between poly(butadiene) and poly(styrene-co-butadiene)". In: *Journal of Materials Science* 48.5 (Mar. 2013), pp. 2046–2052. ISSN: 0022-2461. DOI: 10.1007/s10853-012-6974-1. URL: http://link.springer.com/10.1007/s10853-012-6974-1.

[278] Ralph H. Colby, Lewis J. Fetters, and William W. Graessley. "The melt viscosity-molecular weight relationship for linear polymers". In:

Macromolecules 20.9 (Sept. 1987), pp. 2226–2237. ISSN: 0024-9297. DOI: 10.1021/ma00175a030. URL: https://pubs.acs.org/doi/abs/10.1021/ma00175a030.

[279] A. Bateni et al. "Effect of electric fields on contact angle and surface tension of drops". In: *Journal of Colloid and Interface Science* 283.1 (2005), pp. 215–222. ISSN: 00219797. DOI: 10.1016/j.jcis.2004.08.134.

[280] *International Chemical Safety Cards (ICSCs)*. URL: https://www.ilo.org/dyn/icsc/showcard.home (visited on 11/20/2020).